

**This dissertation has been  
microfilmed exactly as received**

**66-10,381**

**STOW, Stephen Harrington, 1940-  
THE DISTRIBUTION OF ELEMENTS AMONG THE  
COEXISTING PHASES OF THE PRE-CAMBRIAN  
META-SEDIMENTS OF WEST TEXAS.**

**Rice University, Ph.D., 1966  
Geology**

**University Microfilms, Inc., Ann Arbor, Michigan**

RICE UNIVERSITY

THE DISTRIBUTION OF ELEMENTS AMONG THE  
COEXISTING PHASES OF THE PRE-CAMBRIAN  
META-SEDIMENTS OF WEST TEXAS

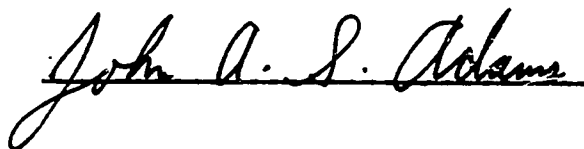
by

Stephen H. Stow

A THESIS SUBMITTED  
IN PARTIAL FULFILLMENT OF THE  
REQUIREMENTS FOR THE DEGREE OF

Doctor of Philosophy

Thesis Director's signature:

A handwritten signature in cursive script, reading "John A. S. Adams", written over a horizontal line.

Houston, Texas

May, 1966

# TABLE OF CONTENTS

	<u>Page</u>
ACKNOWLEDGMENTS.....	1
INTRODUCTION.....	2
Mineralogic Occurrence of Trace Elements.....	2
Metamorphic Reactions.....	3
Ideals of the Investigation.....	4
GEOLOGIC SETTING AND GEOLOGY OF THE VAN HORN AREA.	6
PREVIOUS WORK.....	10
SAMPLE PREPARATION AND CHEMICAL ANALYSIS.....	13
PETROGRAPHY OF THE VAN HORN SAMPLES.....	13
The Mica Schists.....	13
The Hornblende-bearing Amphibolites.....	16
Hornblende-plagioclase group.....	17
Hornblende-plagioclase-epidote group....	17
Hornblende-plagioclase-almandine group..	18
Plagioclase-anthophyllite group.....	18
MINERAL STRUCTURES AND CHEMISTRY.....	19
The Micas.....	19
Hornblende.....	20
Plagioclase.....	21
Epidote.....	22
Garnet.....	22
SOME THEORETICAL CONSIDERATIONS OF METAMORPHIC ELEMENTAL DISTRIBUTIONS.....	23
Explanation of the Distribution Coefficient, $K_D$	24
Influence of Pressure and Temperature on $K_D$ ..	29
RESULTS.....	30
EXPLANATION AND SIGNIFICANCE OF RESULTS.....	31
Element Distribution between Muscovite and Biotite.....	31
Distribution in the Oc <sub>2</sub> sites.....	31
Distribution in the Oc <sub>1</sub> sites.....	34
Distribution in the large cation sites..	39
Element Distribution between Plagioclase and Hornblende.....	42
Distribution between the Oc <sub>2</sub> site of hornblende and the Al site of plagioclase.....	42

	<u>Page</u>
Distributions between the $Oc_1$ site of hornblende and the Na-Ca site of plagioclase.....	44
Distribution between the large cation site of hornblende and the Na-Ca site of plagioclase.....	47
Element Distribution between Hornblende and Epidote.....	49
Distribution between the $Oc_2$ site of hornblende and the Al-Fe <sup>+3</sup> site of epidote.....	49
Distribution between the $Oc_1$ site of hornblende and the Mg-Fe <sup>+2</sup> site of epidote.....	51
Distribution between the Ca site of hornblende and the Oc Ca site of epidote.....	53
Element Distribution between Epidote and Plagioclase.....	54
Distribution between the Al site of plagioclase and the Al-Fe <sup>+3</sup> site of epidote.....	54
Distribution between the Ca site of plagioclase and the Mg-Fe <sup>+2</sup> site of epidote.....	55
Distribution between the Ca sites.....	55
Distributions between Garnet and Hornblende..	56
SUMMARY AND CONCLUSIONS.....	57
BIBLIOGRAPHY.....	79
APPENDIX.....	86
Sample Preparation.....	86
Chemical Preparation, Precision, Sensitivity, and Analysis.....	91
Geochronological Considerations.....	112

TABLES

<u>Table</u>	<u>Description</u>	<u>Page</u>
1	Mineral assemblages of Mica Mine and Wylie Mountain samples	14
2	Crystal field stabilization energies	34
3	Summary of distributions, $K_D$ 's	59
4	Sample weights	88
5	Dilution ranges for analyses	95
6	Precision and sensitivity of analyses	96
7	Chemical analyses	97
8	Distribution of Al between the octahedral and tetrahedral sites of the micas	111

## ILLUSTRATIONS

<u>Figure</u>	<u>Description</u>	<u>Page</u>
1	Map of the Van Horn area	7
2	Detailed map of the Mica Mine area	8
3,4	Ti distribution between muscovite and biotite	61
5	Ti distribution between muscovite and biotite	62
6	Fe <sup>+3</sup> distribution between muscovite and biotite	62
7	Cr distribution between muscovite and biotite	62
8	Fe <sup>+2</sup> distribution between muscovite and biotite	63
9	Mg distribution between muscovite and biotite	63
10	Mn distribution between muscovite and biotite	64
11	Zn distribution between muscovite and biotite	64
12	Co distribution between muscovite and biotite	65
13	Ni distribution between muscovite and biotite	65
14	Cu distribution between muscovite and biotite	65
15	Li distribution between muscovite and biotite	66
16	Na distribution between muscovite and biotite	66
17	Rb distribution between muscovite and biotite	67

<u>Figure</u>	<u>Description</u>	<u>Page</u>
18	Sr distribution between muscovite and biotite	67
19	Ba distribution between muscovite and biotite	67
20	Pb distribution between muscovite and biotite	68
21	Ti distribution between plagioclase and hornblende	68
22	Fe <sup>+3</sup> distribution between plagioclase and hornblende	69
23	Cr distribution between plagioclase and hornblende	69
24	Mg distribution between plagioclase and hornblende	70
25	Mn distribution between plagioclase and hornblende	70
26	Zn distribution between plagioclase and hornblende	71
27	Co distribution between plagioclase and hornblende	71
28	Cu distribution between plagioclase and hornblende	72
29	Li distribution between plagioclase and hornblende	72
30	K distribution between plagioclase and hornblende	73
31	Sr distribution between plagioclase and hornblende	73
32	Ti distribution between epidote and hornblende	74
33	Fe <sup>+3</sup> distribution between epidote and hornblende	74
34	Cr distribution between epidote and hornblende	74

<u>Figure</u>	<u>Description</u>	<u>Page</u>
35	Fe <sup>+2</sup> distribution between epidote and hornblende	74
36	Mg distribution between epidote and hornblende	74
37	Mn distribution between epidote and hornblende	75
38	Zn distribution between epidote and hornblende	75
39	Co distribution between epidote and hornblende	75
40	Cu distribution between epidote and hornblende	75
41	K distribution between epidote and hornblende	76
42	Na distribution between epidote and hornblende	76
43	Sr distribution between epidote and hornblende	76
44	Pb distribution between epidote and hornblende	76
45	Fe <sup>+3</sup> distribution between plagioclase and epidote	77
46	Mg distribution between plagioclase and epidote	77
47	Zn distribution between plagioclase and epidote	77
48	Co distribution between plagioclase and epidote	77
49	Ni distribution between plagioclase and epidote	77
50	K distribution between plagioclase and epidote	77
51	Mn distribution between garnet and hornblende	78



<u>Figure</u>	<u>Description</u>	<u>Page</u>
52	Mg distribution between garnet and hornblende	78
53	Fe distribution between garnet and hornblende	78
54	Flow diagram for sample preparation	87

#### ACKNOWLEDGMENTS

This study was supported by the Robert A. Welch Foundation Grant C-009 to Drs. John A.S. Adams and John J. W. Rogers. The use of material and equipment belonging to the Geology Department of Rice University is greatly appreciated.

The writer wishes to express his sincere gratitude to Dr. Adams, the thesis advisor, Dr. Rogers, Dr. T.W. Leland, Dr. P.T. Flawn, Dr. D.S. McKay and Mr. Glenn Fryer for their critical review of the manuscript and helpful discussions involving interpretation of the data and analytical procedures. Some of the rock standards used were loaned by Mr. Willis Brimhall and these were greatly appreciated.

Special thanks are extended to Drs. Robert Harriss and Ernst Bolter who assisted in the gathering of the samples and to the residents of the Van Horn region who were more than helpful in making their property and facilities available to the writer. Without their generous cooperation this project could not have been completed.

## INTRODUCTION

The study of metamorphic rocks provides the scientist with an opportunity to investigate complex multi-component equilibria in natural systems. The thermodynamic methods of examining element distributions and associated equilibria are becoming well established and of great practical application throughout the geologic sciences, and it is anticipated that the present investigation will contribute meaningful data toward the establishment of these principles.

### Mineralogic Occurrence of Trace Elements

Trace elements may occur in a host mineral in three ways:

- a) Occlusion. This mode is dominant where mineral growth has been rapid, and ions, foreign solid phases and liquid phases may be included in the rapidly growing crystal lattice.
- b) Surface adsorption. This mode is important where the carrier mineral phase has a large surface area and foreign ions are bonded by unsatisfied surface charges.
- c) Solid solution. This method involves the substitution of a trace element ion for a major element in a lattice position of the carrier mineral.

Although the first two cases are certainly important and are considered by some (Devore, 1955a) to be the principal

modes of trace element occurrence in minerals, this research will deal only with the solid solution approach. Occlusion and surface adsorption are relatively random, involve unknown variables, do not necessarily represent equilibrium and cannot be treated thermodynamically. By contrast, the solid solution approach is more definable.

The concentration of a trace element in the host mineral is partially dependent upon the ionic radius, valency, electronegativity, and coordination number of the trace element in comparison to those properties exhibited by the host and its lattice sites. In the case of the transition elements the crystal field stabilization energy of the cation and the size of the incorporating structural site are the chief controlling factors.

#### Metamorphic Reactions

A concise discussion of the reactions which proceed under a closed metamorphic environment is presented by McKay (1964). Briefly, these involve formation of new minerals, phase changes, distribution and ordering of major and minor elements, and textural and lattice rearrangements. Each type of reaction may proceed independently and should lower the free energy of the system. While equilibrium may be achieved with respect to one type of reaction, i.e., textural, disequilibrium may be the case when other variables, i.e., site distributions of trace elements, are considered. This work is concerned chiefly with the distribution of elements among

newly formed minerals and within the lattice sites of a given mineral.

### Ideals of the Investigation

The writer intends to present data which will facilitate understanding of the following problems of metamorphism:

- a) The distribution of elements among coexisting metamorphic phases of isofacial rocks.
- b) The relationships of the elemental distributions to pressure and temperature.
- c) Equilibrium - To what degree is equilibrium achieved, what criteria can be presented for the recognition of equilibrium, and in what volume of sample is equilibrium attained?
- d) The distributions of major and trace elements with respect to lattice sites in different coexisting phases.
- e) The geochemistry of various elements under metamorphic conditions.

The minerals examined during this study - muscovite, biotite, hornblende, plagioclase, and epidote - were chosen for their universal occurrence in metamorphic rocks, especially in the Van Horn samples under consideration. Muscovite and biotite are of similar structure and chemistry, and, with the exception of McKay's (1964) paper, are unstudied with respect to partition coefficients. Thus, it was hypothesized that significant elemental distributions might be observed.

Hornblende and plagioclase, although dissimilar in structure, are common coexisting phases in a wide variety of metamorphic and igneous systems. Perhaps data arrived at from this investigation coupled with similar studies in the future will illuminate distribution trends for differing pressure and temperature conditions of formation. Research is actively progressing concerning the stability relationships of epidotes (Strens, 1966). The analyses of the seven epidotes and their coexisting phases presented in this paper may contribute to this area of research.

The pre-Cambrian Van Horn area of west Texas was chosen for its proximity to the writer, for the excellent mapping which has been done in the area (King and Flawn, 1953), and in the expectation that some inherent problems of pre-Cambrian metamorphism might be investigated. The pre-Cambrian basement is presently being explored in detail to determine its age and structural relationships with the overlying sediments and the surrounding oceanic bodies.

Throughout the report certain symbols are used to represent the mineral phases studied. These are: muscovite (Ms), biotite (Bi), hornblende (Hb), plagioclase (Pc), epidote (Ep), almandine garnet (G), and anthophyllite (At). The letters "MM" with the number and mineral designation indicate that the sample was collected at the Mica Mine. Others include: Wylie Mountains (WM), and Carrizo Mountains (CM).

## GEOLOGIC SETTING AND GEOLOGY OF THE VAN HORN AREA

The distribution of the pre-Cambrian rocks of the Van Horn area may be seen in Figure 1. Exact sampling localities are indicated in Figure 2, which represents the Mica Mine area. Treatment of the partition distribution data involves only samples from the Mica Mine with the exception of one muscovite-biotite schist from the Wylie Mountains (WM 5).

Mineralogically and texturally the investigated samples may be divided into two groups: 1) medium-grain, medium-grade amphibolites of the Mica Mine, and 2) the medium- to coarse-grained muscovite-biotite schists from the Mica Mine and Wylie Mountains. A detailed petrographic description of these is presented under the section on petrography.

Structurally, genetically, and historically the amphibolites and schists from the Van Horn area may be considered as two distinct groups. The first includes the meta-igneous amphibolites of the Carrizo, Wylie, and Eagle Mountains which have been subjected to regional metamorphism and later, in the Carrizo Mountains, to a cataclastic and retrogressive metamorphism. The second group includes the amphibolite facies, meta-sedimentary rocks of the Mica Mine region which are the subject of this investigation.

In the Carrizo Mountains the meta-dioritic amphibolites occur as highly tilted northeast striking conformable sills and discordant plugs which have intruded the pre-Cambrian quartzofeldspathics and meta-rhyolites of the Carrizo Mountain

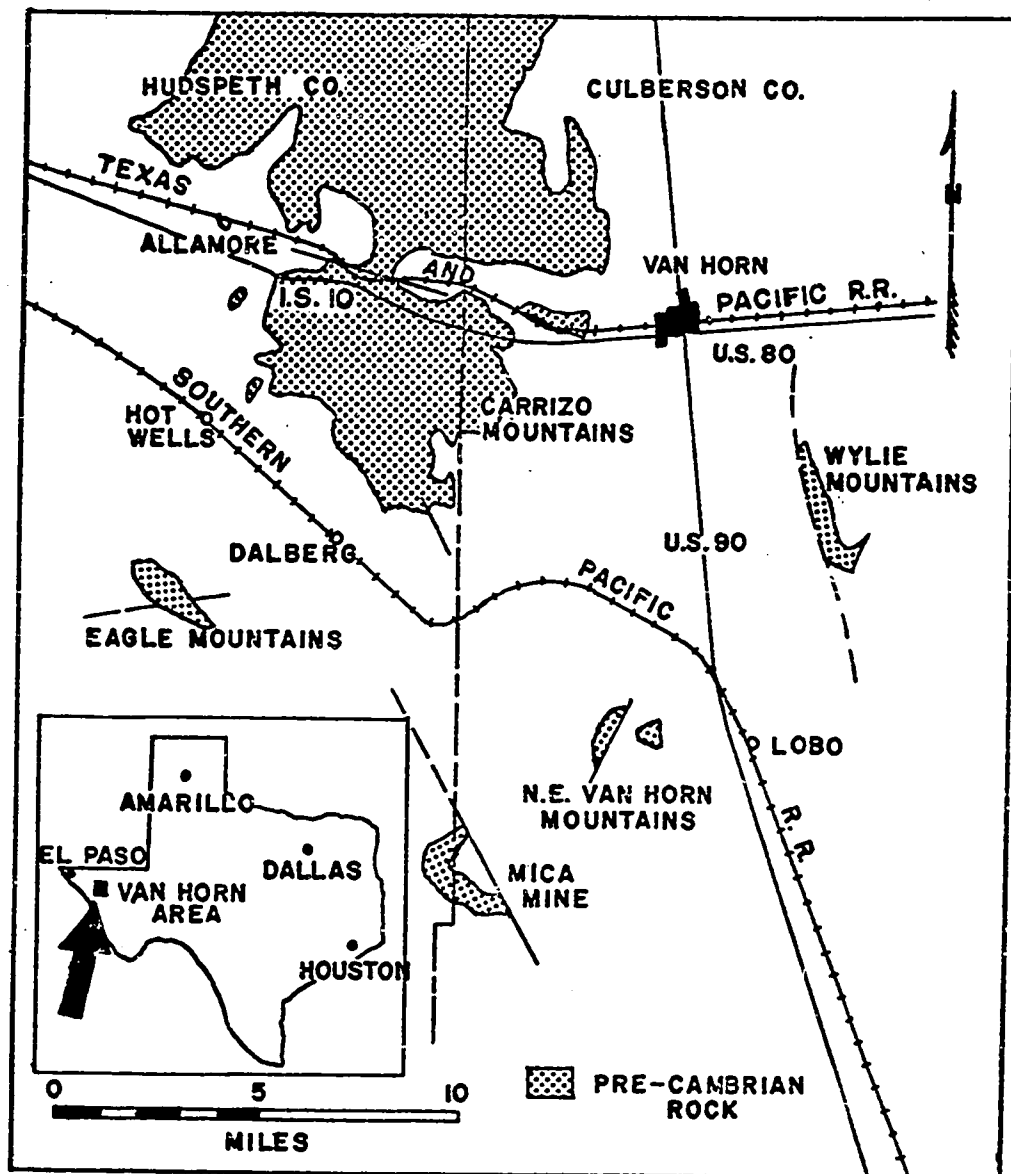
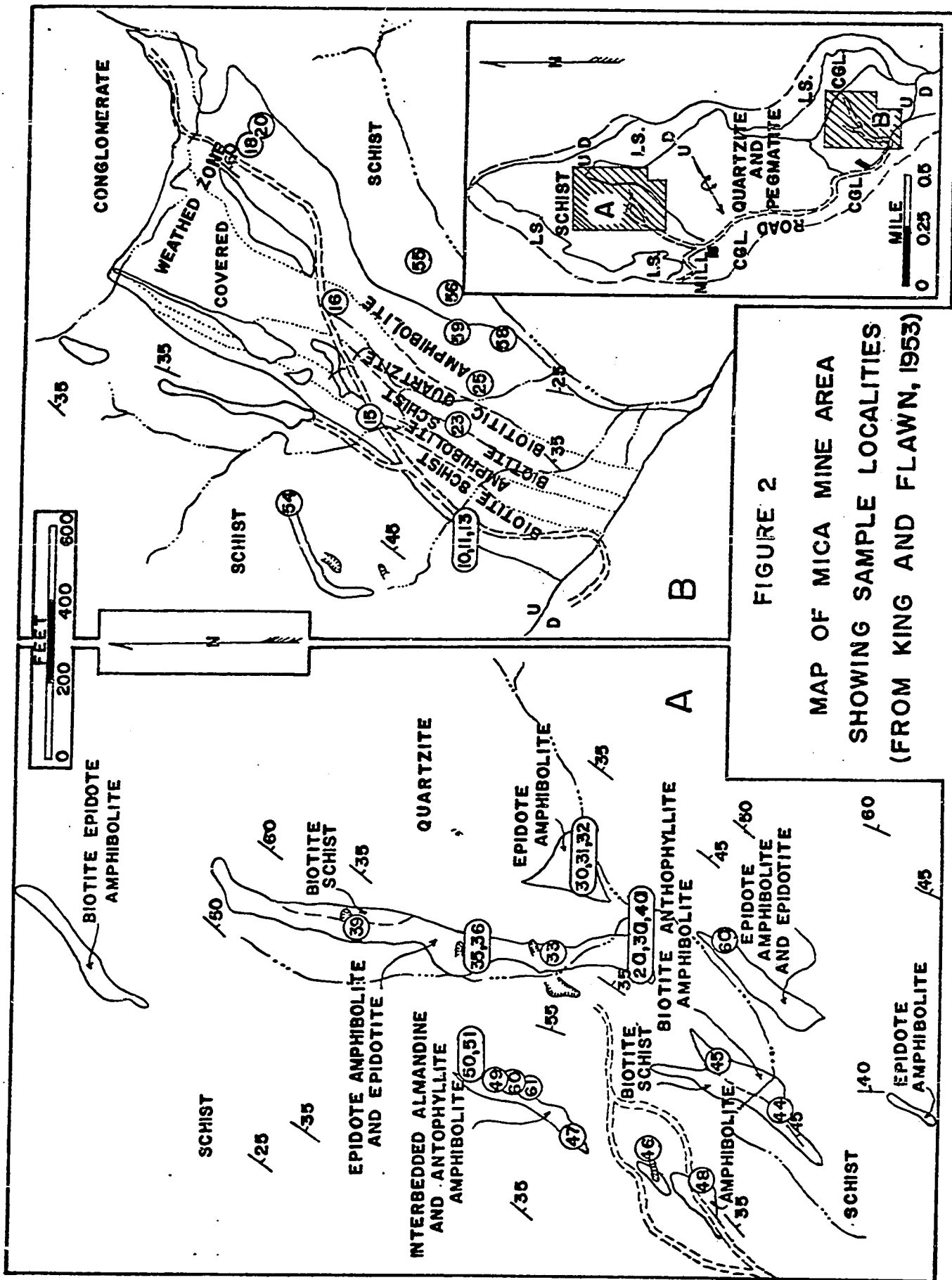


FIGURE 1  
MAP OF VAN HORN AREA WITH  
PRE-CAMBRIAN OUTCROPS  
(MODIFIED FROM KING AND FLAWN, 1953)





Group. Some relic igneous structures can still be observed. The pre-Cambrian mountain block was thrust to the north over the Cambrian Allamore and Hazel formations, and the northern extremity of the block is today marked by the Steeruwitz Overthrust which lies just north of the Texas and Pacific Railroad line. Associated with this thrusting was intrusion of the dioritic sills and a retrogressive and cataclastic metamorphism which was superimposed on the regional metamorphism. The degree of metamorphism observed today increases toward the south until the highest grade in the area is found in the Mica Mine region. Metamorphism at the thrust is principally retrogressive and cataclastic, having advanced just to the biotite stage of progressive metamorphism.

In the Mica Mine area the only igneous activity appears to have been intrusion of numerous pegmatites, many of which have been mined for their mica contents (Flawn, 1951b), and a small epidiorite sill. The amphibolites and schists are, in contrast to those described above, of sedimentary origin. Although no sedimentary structures exist owing to the metamorphism, the field relationships, mineralogy, and chemical composition support this hypothesis. King and Flawn (1953) point out that the chemical analyses of these rocks fall in the sedimentary field of Vogt's ACF diagrams. The dimensions of the sampled area at the Mica Mine are about one-half by two miles. Therefore similar temperature and pressure conditions of formation for all samples should be expected.

The structure of the Mica Mine involves principally an overturned anticline plunging to the southwest with meta-quartzite in the center, and muscovite-biotite schists and amphibolites occurring stratigraphically higher and toward the limbs of the fold (see Fig. 2). The wide mineralogic variability in the para-amphibolites appears to be attributable to variations in the chemical composition of the original sediments, and not to local gradations in temperature and pressure conditions over the relatively small area of the Mica Mine.

King and Flawn (1953) present an excellent discussion of the possible parent materials for the amphibolites of the Van Horn region and the gross mineral relationships at the Mica Mine locality.

#### PREVIOUS WORK

No attempt will here be made to cover in detail previous geochemical and petrologic investigations of metamorphic equilibrium and elemental distributions. The basis for much of the field work and geologic discussions in this paper may be found in the publication by King and Flawn (1953) in which the pre-Cambrian rocks of the Van Horn area are examined in detail and their relationship to the regional geology is investigated. Continuous references have been, and will be made to this excellent publication.

There has long been interest in the formulations which

describe the distribution of elements among different physical-chemical phases. In 1891 Nernst derived the well known Nernst distribution law and for years investigations in this field centered only around studies of partitioning of elements between solvent phases and liquid and gas phases. It was not until 1937 that Goldschmidt set forth the principles of distributions of chemical elements in minerals and rocks. In 1955 DeVore published two papers on the distribution of elements during crystal growth and fractionation as governed by adsorption, but it was not until 1959 that Kretz derived a thermodynamic approach to explain the distributions of elements between minerals. In this paper and later ones (Kretz, 1960, 1961, 1964) Kretz expands the thermodynamic theory and examines the distributions of elements among the minerals garnet, biotite, hornblende, plagioclase, orthopyroxene, and clinopyroxene.

Numerous other authors have studied the distributions of elements between metamorphic minerals. Mueller (1961) reported on the distributions of Mg, Mn, and Fe among actinolite, cummingtonite, Ca-pyroxene, and orthopyroxene, and in 1962 Frost published on the Fe-Mg distribution between garnet-biotite and garnet-hornblende pairs. Turekian and Phinney (1962) studied the partitioning of Ni, Co, Cr, Cu, Ba, and Sr between biotite-garnet pairs from St. Paul's Island, Nova Scotia, following this up in 1963 with a report on phase equilibria between the same biotite-garnet pairs as determined by their major element chemistry. Ernst (1964) examined the

distribution of Mg, Mn, Fe, and Al among blueschist facies white micas, amphiboles, sodic pyroxenes, chlorites, garnets, and epidotes. To the writer's knowledge the only previous thermodynamic study of partitioning of elements between coexisting micas is that by McKay (1964). Albee (1965a, 1965b) investigated the distributions of Fe, Mg, and Mn in a suite of garnet-biotite pairs with data collected from the literature, and among various phases from kyanite-zone pelitic schists from central Vermont. McIntire (1963) presents a literature review of distribution data published up to that time.

Extensive work has been carried out on the distribution of elements during fractional crystallization of magmas. Nockolds and Mitchell (1948), Wager and Mitchell (1951), Neumann, Mead, and Vitaliano (1954), Ringwood (1955), Solodov (1960), Carter (1965), and Nockolds (1966) are a few of these to which the reader is referred.

The use of trace element distributions in other geologic fields has been realized. Bethke and Barton (1959) have employed distribution principles in determining the pressure and temperature of ore formation. Fredrickson (1962) and McIntire (1963) review a number of the possibilities.

Engel and Engel (1960, 1962) have examined the migration of elements in amphibolites under metamorphic conditions. Evans and Leake (1960), Edwards (1957), and Francis (1958) discuss the compositions, origins, and metamorphisms of amphibolites from Ireland, Australia, and Sutherland, respectively.

## SAMPLE PREPARATION AND CHEMICAL ANALYSIS

Mineral separates were prepared by crushing the rock and purifying the mineral phases by means of a Frantz Isodynamic Separator and heavy liquids. All samples were minus-97 mesh and plus-200 mesh in size and were in excess of 99.5% pure.

All analyses except those for  $\text{Fe}^{+2}$  were carried out on a solution prepared by a standard  $\text{HF-HNO}_3$  opening with appropriate dilutions. The atomic absorption flame photometer was employed for all analyses with the exception of Ti and  $\text{Fe}^{+2}$  which were examined by the methods described by Shapiro and Brannock (1962) and Shapiro (1960), respectively. A full description of these procedures is given in the Appendix.

## PETROGRAPHY OF THE VAN HORN SAMPLES

Samples from the Mica Mine area (MM) and the one sample from the Wylie Mountains (WM 5) may be divided into two equilibrium groups on the basis of their mineralogy: 1) the mica schists, and 2) the hornblende-bearing amphibolites. A complete list of the mineral assemblages is presented in Table 1.

### The Mica Schists

All mica schists from which mineral separates were prepared in this investigation contained both muscovite and

Table 1  
Mineral Assemblages

Sample	quartz	plagioclase	microcline	hornblende	anthophyllite	epidote	almandine	biotite	muscovite	magnetite	ilmenite	hematite	sphene	zircon
MM 2a	X	X	X	X	-	-	-	X	-	-	X	-	X	-
MM 3a	-	X	X	X	-	X	-	X	-	-	X	X	X	-
MM 4a	-	X	-	X	-	X	-	X	-	-	X	-	X	-
MM 6a	X	X	-	X	-	-	-	X	-	-	X	-	-	-
MM 4	X	X	X	-	-	-	-	X	X	-	X	-	-	X
MM 10	X	X	X	-	-	-	-	X	X	-	-	-	-	X
MM 11	X	X	-	-	-	-	-	X	X	-	-	-	-	-
MM 13	X	X	-	-	-	-	-	X	X	-	-	-	-	X
MM 15	X	X	-	-	-	-	-	X	X	-	-	-	-	-
MM 16	X	X	-	-	-	-	-	X	X	-	-	-	-	-
MM 18	X	X	-	X	-	-	-	X	-	X	-	-	-	-
MM 20	-	X	-	X	-	-	-	-	-	-	X	-	-	X
MM 23	-	X	-	X	-	-	-	X	-	X	X	-	X	-
MM 25h	X	X	-	X	-	-	-	-	-	-	X	-	-	-
MM 25p	-	X	-	X	-	-	-	X	-	-	X	-	-	-
MM 30	X	X	-	X	-	X	-	-	-	X	X	-	X	-
MM 31	X	X	-	X	-	-	-	-	-	-	X	-	-	-
MM 32	X	X	-	X	-	-	-	X	-	-	X	-	-	-
MM 33	-	X	-	X	-	-	-	X	-	-	X	-	X	-
MM 35	X	X	-	X	-	X	-	X	-	-	X	-	X	-
MM 36	-	X	X	X	-	X	-	X	-	-	X	-	X	-
MM 39	-	X	-	X	-	X	-	X	-	-	X	-	X	-
MM 44	X	X	-	-	-	-	-	X	X	-	-	-	-	X
MM 45	X	X	-	-	X	-	-	X	-	-	-	-	X	-
MM 46	X	X	?	X	-	-	-	X	-	-	X	X	-	-
MM 47	-	X	-	X	-	-	X	-	-	-	X	X	-	X
MM 49	?	X	-	X	-	-	-	-	-	-	X	-	X	-
MM 50	-	X	-	X	X	-	-	-	-	-	X	-	X	-
MM 51	X	X	X	-	X	-	-	-	-	-	X	X	X	-
MM 54	X	X	X	-	-	-	-	X	X	-	-	-	-	X
MM 55	X	X	-	X	-	-	-	X	-	X	X	-	-	-
MM 56	X	X	-	-	-	-	-	X	X	-	-	-	-	X
MM 58	-	X	-	X	-	X	-	-	-	-	-	-	X	-
MM 59	-	X	X	X	-	-	-	X	-	-	X	-	-	X
MM 60	?	X	-	X	-	-	X	-	-	-	X	-	-	X
MM 61	?	X	-	X	X	-	-	-	-	-	X	-	-	-
WM 5	X	X	-	-	-	-	-	X	X	-	-	-	-	X

X : Mineral present  
- : Mineral absent

biotite in separable quantities. Three mineral assemblages are recognized in the schists:

- 1) plagioclase-quartz-muscovite-biotite
- 2) plagioclase-quartz-microcline-muscovite-biotite
- 3) plagioclase-quartz-microcline-ilmenite-muscovite-biotite

Zircon is commonly present in the above assemblages.

The range of mineral percentages in the 11 samples from which muscovite-biotite pairs were prepared is considerable. The sample, MM 44, represents a feldspathic muscovite schist containing 30% muscovite and only 1-2 % biotite with an average grain size of 0.5 mm. In contrast, MM 11, MM 13, and MM 54 represent samples containing up to 50% biotite and only 2% muscovite. Specimens were observed which contained muscovite (up to 40%) and no biotite, or biotite (up to 80%) and no muscovite. Average grain size tends to increase with the biotite content. The biotite in all samples is red brown to olive green in color and appears in quite fresh laths ranging up to 2 mm. in length as seen in a thin section. Muscovite is always of smaller grain size. Plagioclase, microcline, and quartz occur as a mosaic with the microcline exhibiting the characteristic grid twinning. Plagioclase shows slight sericitization, rare twinning and zoning. MM 6 is obviously of a different origin than the other 10 mica samples. It is in conformable contact with a small pegmatitic vein and probably formed as a result of intrusion of the pegmatitic magma.



The intimate field association of the biotite-rich schists with amphibolites suggests that the biotite schist might represent a transition from the feldspathic muscovite-bearing rocks to the hornblende-plagioclase amphibolites (King and Flawn, 1953).

#### The Hornblende-bearing Amphibolites

A wide variety of mineral assemblages may be recognized for this group and all contain hornblende except one anthophyllite-bearing sample (MM 51).

- 1) plagioclase-hornblende-ilmenite
- 2) plagioclase-hornblende-biotite-ilmenite (or magnetite)
- 3) plagioclase-quartz-hornblende-biotite-ilmenite  
(or magnetite)
- 4) plagioclase-microcline-quartz-hornblende-biotite-ilmenite
- 5) plagioclase-hornblende-epidote
- 6) plagioclase-hornblende-epidote-biotite-ilmenite
- 7) plagioclase-quartz-hornblende-epidote-magnetite  
(possibly a trace of biotite)
- 8) plagioclase-microcline-hornblende-epidote-biotite-ilmenite
- 9) plagioclase-hornblende-almandine-ilmenite
- 10) plagioclase-quartz-biotite-anthophyllite (no hornblende)
- 11) plagioclase-hornblende-ilmenite-anthophyllite-  
(quartz?)

Sphene is generally present in all assemblages.

These 11 mineral assemblages may be subdivided and considered as four distinct groups:

- 1) the hornblende-plagioclase samples
- 2) the hornblende-plagioclase-epidote samples
- 3) the hornblende-plagioclase-almandine samples
- 4) the plagioclase-anthophyllite group, with hornblende  
or biotite

The petrography of each of these groups will be discussed separately.

Hornblende-plagioclase group: These are black, slabby, shiny rocks which may have a lineation and always have a foliation to some degree as defined by the hornblende prisms which range up to six mm. in length and comprise as much as 75% of the rock. In thin section the hornblende appears as fresh blue-green prisms exhibiting strong pleochroism, and the plagioclase occurs as unzoned, untwinned, fairly equant grains, often slightly sericitized. Average grain size is about 0.5 mm. Quartz, biotite, and microcline may be present in small amounts.

Hornblende-plagioclase-epidote group: These samples appear as a mottled mixture of light green epidote grains in a mass of black hornblende prisms. A foliation is generally present as exhibited by hornblende-rich and epidote-rich bands ranging up to  $\frac{1}{2}$  inch thick. Epidote commonly occurs in local patches where it may constitute 90% of the rock, but normally it is in a lesser amount than hornblende. Hornblende may compose as much as 35% of the rock and occurs as small blue-green prisms in the thin section. Epidote is

observed as very small equant grains, and plagioclase occurs as untwinned, unzoned grains in abundance of about 25%. Sphene is invariably present, and quartz, microcline, and biotite may be present.

Hornblende-plagioclase-almandine group: In the hand specimen the samples consist of dark red garnet euhedra varying in size up to 1.5 cm. in diameter and composing 20% of the rock in a groundmass of black hornblende prisms which average 0.5 mm. in length and small plagioclase grains. The thin section reveals that the hornblende is highly concentrated around the almandine crystals which contain ilmenite grains paralleling the lineation of the rock fabric. The rock consists of about 40% hornblende, 35% slightly altered plagioclase, and 5% ilmenite.

Plagioclase-anthophyllite group with hornblende or biotite: The biotite-rich sample (MM 45) is gray in color with 10% biotite 20% anthophyllite porphyroblasts lying in the plane of foliation. The porphyroblasts average 0.5 cm. in diameter. Slightly sericitized, untwinned plagioclase comprises the remaining 70% of the rock with the exception of 1-2% quartz.

Anthophyllite-rich specimens containing hornblende are quite different. Golden anthophyllite blades ranging in length to 4 cm. lie in a dark groundmass of 1 mm.-long hornblende prisms and plagioclase grains. No lineation or foliation is observed in the hand specimen or thin section. The pleochroic

hornblende is blue-green in transmitted light and the plagioclase is slightly altered and untwinned. Mineral percentages are: hornblende - 30%, plagioclase - 15%, anthophyllite - 50%, and ilmenite - 5%.

## MINERAL STRUCTURES AND CHEMISTRY

### The Micas

Biotite:  $(K,Ca,Na)(Fe,Mg,Mn,Ti,Al)_3(Al,Si)_4O_{10}(OH,F,Cl)_2$

Muscovite:  $(K,Ca,Na)(Fe,Mg,Mn,Ti,Al)_2(Al,Si)_4O_{10}(OH,F,Cl)_2$

The basic structure of the micas consists of a layer of octahedrally coordinated cations (Fe,Mg,Mn,Al) between two identical layers of (Si,Al)O<sub>4</sub> tetrahedra. This unit of three layers is bonded to an identical unit by a layer of large cations (K,Ca,Na) in 12-fold coordination with the bonding oxygens of the (Si,Al)O<sub>4</sub> tetrahedral layer.

The octahedral layer in the case of biotite, a trioctahedral mica, consists of an octahedral configuration of two OH groups and four oxygens in six-fold coordination around a central Mg ion. The Mg ions form a pattern of interlocking hexagonal rings with a Mg ion at the center of each ring. Anions are shared between rings so there are three Mg ions for each octahedron of anions (OH+O). Since all cation positions are filled, micas containing this sheet are termed trioctahedral micas.

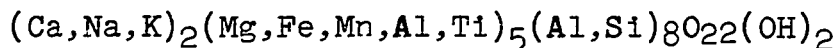
In the case of muscovite, a dioctahedral mica, the octahedral layer is formed by a series of four oxygens and

two OH groups in octahedral coordination around a central Al ion. Owing to the charge difference (Mg in the trioctahedral layer has a +2 charge) there is a ratio of only two Al ions to each octahedron of anions. There remains one position unfilled. Hence, the dioctahedral term is derived.

The tetrahedral (Si,Al) $O_4$  layers on both sides of the octahedral layer are bonded to the oxygen of the octahedrally coordinated Mg and Al. Substitution of one Al for every fourth Si in the tetrahedral layer leaves a charge deficiency so that large cations occur in 12-fold coordination between the tetrahedral-octahedral-tetrahedral units and bind these units together. These large cations are principally K. If one-half of the Si ions are replaced by Al ions, then Ca can enter the structure.

Principal substitutions and solid solutions can be noted in the above formulas for biotite and muscovite.

#### Hornblende



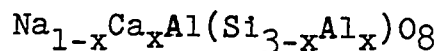
The structure of hornblende consists of a series of  $Si_4O_{11}$  double chains of infinite extent which are bound together by ionic bonds of two different varieties, the bond depending on the type of cation site filled. Cation type X refers to those cations which are large, weakly charged, and in eight-fold coordination with oxygen. These are chiefly Na, K, and Ca. The second type of cation, type Y, is smaller, more highly charged, and in six-fold coordination

with oxygen. These consist of Mg,  $\text{Fe}^{+2}$ ,  $\text{Fe}^{+3}$ , Al, Mn, Ti, and occasionally Li. Hydroxyl groups are found in voids between single chains of the pyroxene type. A generalized formula might be written for hornbländes:  $\text{X}_{0-7}\text{Y}_{7-14}\text{Z}_{16}\text{O}_{44}(\text{OH})_4$ .

There is complete ionic substitution between Na and Ca, and Mg, Fe and Mn, but limited substitution between  $\text{Fe}^{+3}$  and Al, and Ti and other Y type ions. Partial substitution of Al for Si is observed.

The structure of anthophyllite is similar. The unit cell is doubled owing to the occupation of both X and Y sites by small cations ( $\text{Mg}$ ,  $\text{Fe}^{+2}$ ) (Deer, Howie, Zussman, 1964b).

### Plagioclase

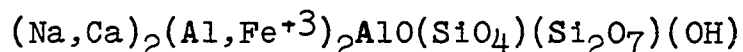


The crystal structure of plagioclase is quite simple and well studied. Al and Si are in similar tetrahedral coordination with oxygen. The two kinds of tetrahedra are ionically linked by sharing oxygens to form a three dimensional network. As Al substitutes for Si, the charge is balanced by substitution of one monovalent cation per  $\text{AlO}_4$  tetrahedra, or one divalent cation per two tetrahedra. These cations occupy voids in the tetrahedral framework, and, as seen from the formula above, the total of them must equal one (Na and Ca in most cases).

The chemistry of the plagioclases is simple since there exists only one cation site into which elements may enter. K and Ba are the two most common substitutions in the feldspar

solid solution series, but  $\text{Fe}^{+2}$ , Mg, Mn, and Sr are often found in significant amounts.  $\text{Fe}^{+3}$  and Ti may substitute for Al to a very minor extent.

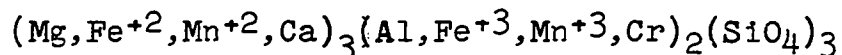
### Epidote



The structure of epidote is rather complex. It may be described as a series of chains of  $\text{AlO}_6$  and  $\text{AlO}_4(\text{OH})_2$  octahedra extending in the direction of the y-axis with O and OH groups sharing the edges of the octahedra. Tetrahedra of  $\text{SiO}_4$  and double tetrahedra of  $\text{Si}_2\text{O}_7$  bridge the chains and are bonded to the oxygens of the Al octahedra. Al, Fe, and Ca occur in octahedral coordination outside the chains.  $\text{Fe}^{+3}$  probably replaces Al outside the chains rather than the octahedrally coordinated chain Al.

Na, Sr,  $\text{Mn}^{+2}$ , and occasionally Pb are readily substituted for Ca in its irregular octahedral coordination, and  $\text{Mn}^{+3}$  and Cr ions are found in the Al-Fe octahedral site. Those ions replacing Ca are generally large and weakly charged while those replacing Al and Fe are smaller and of a higher charge.

### Garnet



The garnet structure is relatively simple and consists of  $\text{SiO}_4$  tetrahedral bonded to octahedra formed around the trivalent ions. The divalent ions lie in voids in the lattice

framework and are in 8-fold coordination with the surrounding oxygens. There is complete substitution and interchange of the divalent ions with the exception of Ca which substitutes with more difficulty. Limited solution is observed in the trivalent sites.

#### SOME THEORETICAL CONSIDERATIONS OF METAMORPHIC ELEMENTAL DISTRIBUTIONS

Metamorphic reactions tend toward equilibrium by decreasing the free energy of the system and the establishment of stable equilibrium mineral assemblages. Metamorphic rocks at the surface of the earth today are, however, in a metastable state with respect to the original physical conditions of formation. With increasing temperature the free energy will decrease at a rate proportional to the entropy, and will increase with increasing pressure at a rate proportional to the volume. Therefore, at metamorphic temperatures and pressures, the smallest volume and greatest entropy phases are favored, and, since entropy increases with temperature, metamorphic reactions are endothermic. Owing to the great entropy of the gaseous phase, water vapor, dehydration is favored by a rise in temperature.

It is obvious that temperature and pressure tend toward counteracting each other with increasing temperature and pressure with respect to the free energy consideration. Although entropy changes are generally small for the majority of metamorphic reactions, volume changes are negligible in



most cases, and temperature is the principal controlling variable in metamorphism. It follows also that free energy changes are small for metamorphic reactions. With increasing temperature a fewer number of phases are favored, these phases being those which have a high potential for substitution and solid solution, but ionic ordering and partitioning are more pronounced at high pressure and low temperature than at low pressure and high temperature owing to the reduction of the entropy and the increased selectivity of the high pressure crystal lattice because of low ionic thermal activity and decrease in site size at low temperatures and high pressures.

The rate of a metamorphic reaction is controlled by the slowest step which may be diffusion, nucleation, or catalysis by water.

#### Explanation of the Distribution Coefficient, $K_D$

The derivation and explanation of the distribution coefficient has been adequately covered by a number of writers including Kretz (1959, 1960, 1961, 1964), Mueller (1961), McIntire (1963), Albee (1965), Ernst (1964), and Trumbore, Isenberg, and Porbansky (1958). Most of the following material is extracted from these works.

It is a well established observation that  $\mu$ , the chemical potential, of any component is the same in all phases in which it exists in a system at equilibrium. The chemical potential of a component is independent of the presence of

other phases and of the amount of these phases and in the case of major components is only very slightly changed by a variation of small amounts of other components in the system. The chemical potential of a component is equivalent to the partial Gibbs free energy which is the potential for attainment of equilibrium of a component between phases, even though the component may be of low concentration. Each rock may be considered as a series of subsystems consisting of two or more mineral phases each, and each phase may in turn be considered as a member of two or more subsystems and participate in an equilibrium in each subsystem. Thus, there may be numerous equilibria within a given system.

Let us consider an ion exchange reaction for the systems (A,B)Z and (A,B)Y, designated "1" and "2", respectively:



where A and B are components, and 1 and 2 refer to the phases, respectively. The relationship of the Gibbs free energy change for the ion exchange reaction,  $\Delta G$ , the standard state Gibbs free energy,  $\Delta G^0$ , and the activities,  $a$ , of the components may be shown in van't Hoff's equation:

$$\Delta G = \Delta G^0 + RT \ln \frac{a_B^1 a_A^2}{a_A^1 a_B^2}, \quad (2)$$

where  $a_A^1$  refers to the activity of component A in phase 1, R is the gas constant, and T is the absolute temperature. At equilibrium,  $\Delta G$  equals zero and the activity term is a constant, K. Therefore,

$$\Delta G = -RT \ln K + RT \ln \frac{a_B^1 a_A^2}{a_A^1 a_B^2}, \quad (3)$$

and  $a_A^1$  is equal to  $X_A^1 \gamma_A^1$  where  $X_A^1$  is the composition ratio A/A+B in phase 1,  $\gamma_A^1$  is the activity coefficient of A in phase 1, and  $X_B^1 = 1 - X_A^1$ . Therefore, equation 3 now becomes

$$\exp \frac{\Delta G}{RT} = \frac{(1-X_A^1) X_A^2}{X_A^1 (1-X_A^2)} \cdot \frac{\gamma_B^1 \gamma_A^2}{\gamma_A^1 \gamma_B^2}. \quad (4)$$

At a specified temperature and pressure the left-hand side of equation 4 is a constant, K. Therefore, making the assumption of ideal solutions (Henry's Law), the activity coefficient term is equal to unity, and equation 4 may be rewritten:

$$K_D = \frac{(1-X_A^1) X_A^2}{X_A^1 (1-X_A^2)}, \quad (5)$$

where  $K_D$  is termed the distribution coefficient of the component in phases 1 and 2. This equation holds true when component A is present in small amounts in the phases. At dilute concentrations,

$$\frac{(1-X_A^1) X_A^2}{X_A^1 (1-X_A^2)} \approx \frac{X_A^2}{X_A^1}, \quad (6)$$

which is the familiar Nernst distribution equation and may be used for trace elements with the assumption of adherence to Henry's Law. If, however,  $\gamma$  does not equal unity, it can still be constant if:

1) the  $\gamma$ 's are constant through the range of compositions under consideration, or,

2) the  $\gamma$ 's are not constant but deviate such that the ratios of  $\frac{\gamma_B^2}{\gamma_B^1}$  and  $\frac{\gamma_A^1}{\gamma_A^2}$  are constant.

Therefore, for major elements,  $K_D = \frac{x_A^2/1-x_A^2}{x_A^1/1-x_A^1}$ , and will

be constant with the above specifications. For trace elements,

$K_D = \frac{x_A^2}{x_A^1}$  with the same specifications. Ideality is normal-

ly the case for trace elements, and, in this respect, the free energy of the reaction must not be influenced by the presence and variation in concentration of components other than A and B in the phases under consideration.

In order to treat the data arrived at from the analysis of a mineral phase one must consider the number of atoms of an element per total number of coordination positions open to that element. The elemental components are considered to be end members of a solid solution series. For example, consider the mineral phase hornblende,  $(Ca,Na,K)_2-(Mg,Fe,Mn,Al,Ti)_5(Al,Si)_8O_{22}(OH)_2$ , and the partitioning of Mg between it and a coexisting phase.  $x_{Mg}^{Hb}$  = atoms Mg/atoms  $Mg+Fe+Mn+Ti+Al$  only if complete solid solution exists among all five of these components and only if all octahedrally coordinated positions are open to Mg. If the distribution of Mg when defined in this manner is not regular, one might conclude that all positions are not available for Mg.

Perhaps only the divalent ion positions can be occupied by Mg and the distribution will involve  $X_{Mg}^{Hb} = \text{atoms Mg/atoms Mg+Fe}^{+2}\text{+Mn}$ . If this distribution is regular, then this is the choice which should be examined. The ideal solution thus depends upon the variability of charge and the size of the coordinating ions which compete for the octahedral positions and all positions are not open to all ions. Often in the case of a trace element the exact coordination position is not known and an examination of weight percent of the trace element between phases is sufficient to indicate a distribution.

Let us consider briefly this more complex situation where two phases, 1 and 2, coexist, with formulas (A,B,C)Z and (A,B,C)Y, respectively. Equation 6 remains valid if phases 1 and 2 are ideal solutions with respect to A, B, and C. In this case  $X_A^1 = A/A+B+C$ . The distribution of A between 1 and 2 may in fact be a function of the B:C ratio in either phase if ideal mixing is the case. If, however, the phases are not ideal mixtures, the distribution of A between the two may be a function of the distribution of C between the phases. The principle of the influence of the concentration of one component on the distribution of another has been realized by Kretz (1959, 1960) and Ernst (1964).

If one is not able to arrive at a significant distribution, one or more of the following explanations should be considered:

- 1) Inclusions and foreign phases have been included in the analyzed minerals.
- 2) Elements not examined exert a profound influence on the distribution of the element under consideration.
- 3) Variables which have not been considered or complexity of variables cause deviations from a regular distribution.
- 4) Temperature and pressure conditions have varied from sample to sample and the distribution coefficient is of course not the same value for all samples.
- 5) Chemical equilibrium was not reached in the system, or, if it was reached, it was not retained. The question arises concerning the size sample which is considered to represent an equilibrium assemblage and complete chemical communication. In general, this is thought to be a hand-size specimen, but recently Phinney (1963) has shown that the Fe/Mg ratio in metamorphic biotite grains coexisting within millimeters of each other, as well as those ratios within a single grain, are significantly variable. This indicates lack of chemical mobility.

#### Influence of Pressure and Temperature on $K_D$

From equation 3,  $K_D = K = \exp - \Delta G^\circ / RT$ , where  $\Delta G^\circ$  is the Gibb's free energy change at a given temperature and pressure with all phases in their standard states. Therefore,  $K$  and  $K_D$  for a distribution are a function of tempera-

ture and pressure, and

$$\frac{\partial \ln K}{\partial T}_p \frac{\Delta H^\circ}{RT^2}, \text{ and } \frac{\partial \ln K}{\partial P} \frac{\Delta V^\circ}{RT}.$$

In general,  $\Delta H^\circ$  approaches zero as the temperature increases, and, as pointed out earlier, less fractionation is observed with higher temperature. Owing to the fact that  $\Delta V^\circ$  is extremely small in most metamorphic reactions, the pressure effect on  $K_D$  can be essentially neglected.

## RESULTS

Complete chemical analyses of the mineral phases are found in Table 7. For the major elements both the percent of the metallic oxide and percent of the elemental metal are included for ease in calculating the mole fractions. Although water was not determined in this investigation an ideal percentage of water has been included for the hydrous phases in order that  $\text{SiO}_2$  might be determined by subtracting the total weight percent of the major element oxides from 100 percent. The water percentages chosen are: biotite - 4.0%, muscovite - 4.5%, hornblende - 2.0%, epidote - 2.0%, and anthophyllite - 2.0%. It is noted that these percentages are often lower than the theoretical water content of the phases, but if actual mineral analyses are examined from the literature (Deer, Howie, and Zussman, 1963), one notices that actual water content is generally considerably lower than the theoretical content expected from the structural formula.

Aluminum distribution between the octahedral and tetrahedral layers for the micas has been calculated according to the method suggested by Stevens (1946) and the results are presented in Table 8.

Throughout the discussion of the results,  $K_D$ 's are derived so that a  $K_D$  value in excess of unity indicates a concentration of the element under consideration in the more acidic (higher  $\text{SiO}_2$ ) phase. Likewise, a  $K_D$  value less than unity indicates enrichment in the more basic mineral of the pair. The distribution lines for the mica pairs are drawn employing the least squares calculation.

#### EXPLANATION AND SIGNIFICANCE OF RESULTS

##### Element Distribution between Muscovite and Biotite

Distribution in the  $\text{Oc}_2$  sites: Radoslovich (1963a,b) proposes the existence of two distinct subsites within the octahedral layers of the micas. He finds ordering in the octahedral biotite sites with one site containing the smaller highly charged ions ( $\text{Al}^{+3}$ ,  $\text{Fe}^{+3}$ ,  $\text{Ti}^{+4}$ , and  $\text{Cr}^{+3}$ ) and the remaining two sites containing the larger divalent octahedrally coordinated ions.

In the case of muscovite, Radoslovich proposes that the trivalent and tetravalent cations occur in the smaller  $\text{Al}$  sites and the larger divalent cations are found in a larger vacant octahedral site. Sites containing the smaller highly charged cations will be referred to as  $\text{Oc}_2$  sites and those



containing the divalent ions will be  $Oc_1$  sites.

Figures 3, 4, and 5 represent the distribution of Ti between muscovite and biotite employing three different mole fractions. Figure 3 is constructed assuming Ti to be located in the  $Oc_1$  site, and no relationship is apparent. This mole fraction  $Ti/Ti+Mg+Mn+Fe^{+2}$  has been used by Kretz and others in their examinations of biotite-hornblende partitioning, but apparently is not applicable in this study. Figure 4 represents the mole fraction,  $Ti/Ti+Fe^{+3}+Al_{Oc}$ , and, as above, no relationship is observed indicating that all  $Oc_2$  sites are not open to titanium. If the mole fraction  $Ti/Ti+Fe^{+3}$  is chosen (Fig. 5) scatter is reduced and a  $K_D$  of 0.56 can be defined ( $K_D = \frac{X_{Ti}^{Ms}}{X_{Ti}^{Bi}}$ ) for the linear portion of the curve below  $X_{Ti}^{Bi}=0.45$ . Above this point the curve should tend toward higher  $X_{Ti}^{Ms}$  values as nonideality is encountered with high mole fraction values and the curved portion has been dashed in to indicate its probable existence. The analytical accuracy for Ti is poor and accounts for a considerable amount of the scatter. As indicated by McKay (1964) highly charged cations are distributed preferentially into the  $Oc_2$  sites of biotite owing to the configuration of six  $Oc_1$  sites around each  $Oc_2$  site in the biotite lattice as contrasted with muscovite which has three  $Oc_1$  and three  $Oc_2$  positions around each  $Oc_2$  site. The concentration of  $Ti^{+4}$  in biotite is observed and indicated by the  $K_D$  of 0.56.

The distribution of  $Fe^{+3}$  between muscovite and biotite is seen in Figure 6 where the mole fraction is  $Fe^{+3}/Fe^{+3}+Ti+Al_{Oc}$ .

The  $K_D$ , defined by the relationship  $x_{Fe^{+3}}^{Ms}/x_{Fe^{+3}}^{Bi}$ , is 0.32 indicating a tendency for ferric ion to be concentrated in the  $Oc_2$  site of biotite relative to muscovite. This distribution of  $Fe^{+3}$  and that of  $Fe^{+2}$ , which will be discussed shortly, support Ramberg's (1952) model in which he states that the substitution of Al for Si in the biotite tetrahedral layers imparts a tendency for more electronegative cations to be attracted into the  $Oc_2$  sites. Ferric ion should partition similarly to Ti in light of the explanation advanced above concerning the configuration of  $Oc_1$  and  $Oc_2$  sites. The sum total of these two effects thus gives a  $K_D$  of 0.32 indicating the preferential concentration in the biotite.

No significant distribution could be found for  $Al_{Oc}$  using the mole fraction  $Al_{Oc}/Al_{Oc}+Ti+Fe^{+3}$ . There is very little variability in the octahedral Al of the muscovite and analytical techniques are not of the highest quality so any distribution that might exist was not observed. One should expect a predominance of  $Al_{Oc}$  in muscovite (McKay, 1964).

Chromium is the last cation to be considered in the  $Oc_2$  position. Figure 7 indicates a definite relationship with a  $K_D = x_{Cr}^{Ms}/x_{Cr}^{Bi} = 0.28$  employing the mole fraction,  $Cr/Cr+Fe^{+3}+Ti+Al_{Oc}$ . In accordance with the  $Oc_1$ - $Oc_2$  configuration theory advanced above one would expect Cr to be found in the  $Oc_2$  site of biotite. A straight line defines the relationship and ideality should be the case owing to the small mole fractions involved ( $\times 10^{-4}$ ).

Distribution in the  $Oc_1$  sites: The distribution of elements between the  $Oc_1$  sites of muscovite and biotite may be more thoroughly explained by use of the crystal field stabilization energy theory. Cotton and Wilkinson (1962) and Curtis (1964) present an adequate discussion of this. In general, the element with the greatest crystal field stabilization energy will concentrate in the smaller site. The  $Oc_1$  site of muscovite is smaller than the  $Oc_1$  site in biotite (Radoslovich, 1963a). Table 2 is a presentation of octahedral stabilization energies of elements considered in this report, the values taken from McClure (1957).

Table 2  
Crystal Field Stabilization Energies  
(McClure, 1957)

Cation	Octahedral Stabilization (kcal/mole)
$Cr^{+3}$	60.0
$Ni^{+2}$	29.3
$Cu^{+2}$	22.2
$Co^{+2}$	17.1
$Fe^{+2}$	11.4
$Fe^{+3}$	0.0
$Mn^{+2}$	0.0
$Zn^{+2}$	0.0

It might be pointed out that the distribution of

$K_D$  = 0.28) is not in accord with this stabilization energy theory and the  $Oc_1$ - $Oc_2$  configuration effect appears to be predominant. Curtis (1964) feels that the stabilization energy effect is the principal factor controlling the distributions of the transition elements and the data presented in this investigation tend to support this conclusion in general.

The three principal cations found in the  $Oc_1$  sites in the micas are  $Fe^{+2}$ , Mg, and Mn, and most substitutions involve divalent ions of similar size (0.60-0.80 Å). One exception is Li which is of similar size but is univalent.

Figure 8 represents the partitioning of  $Fe^{+2}$  between biotite and muscovite. The mole fraction,  $Fe^{+2}/Fe^{+2}+Mg+Mn$ , yields a  $K_D$  of 0.59 for the linear portion of the curve below  $x_{Fe^{+2}}^{Bi} = 0.35$ . Above this point mole fractions become too great for strict adherence to Henry's Law and Nernst's Distribution Law. One notes that two points (6 and 56) lie rather far from the proposed line. Sample 6 represents a pegmatitic muscovite-biotite pair which no doubt formed under different conditions than the remainder of the samples. No reason is apparent for the deviation of sample 56 from the line. As mentioned under the discussion for  $Fe^{+3}$ , Ramberg's model is supported by the low  $K_D$  for  $Fe^{+2}$ .

The distribution of Mg between the  $Oc_1$  sites of the micas is shown in Figure 9.  $K_D$  is defined by the equation  $x_{Mg}^{Ms}(1-x_{Mg}^{Bi})/(1-x_{Mg}^{Ms})x_{Mg}^{Bi} = 2.25$ , when the mole fraction,  $Mg/Mg+Fe^{+2}+Mn$ , is considered. The distribution of Mg (and  $Fe^{+2}$ )

in sample 56 may be controlled by variation in the concentration of another element or variation in the ratio of other elements not considered in this investigation. It would be difficult to assign the deviations of sample 56 from the  $K_D$  lines to temperature and pressure differences as it was collected in close proximity (300 feet) to other muscovite-biotite samples. The large  $K_D$  value of 2.25 indicates preferential concentration of Mg in muscovite which may be explained by a consideration of the size of the  $Mg^{+2}$  ion. The cation is small (0.65Å) and would tend to be incorporated in the  $Oc_1$  site of the muscovite which is smaller than the  $Oc_1$  biotite site.

Manganese is quite well distributed between the mica pairs as can be seen in Figure 10 where the  $K_D$  is defined by the equation  $x_{Mn}^{Ms}/x_{Mn}^{Bi} = 0.62$ . The mole fraction,  $Mn/(Mn+Mg+Fe^{+2})$ , was chosen in accordance with Radoslovich's model of subsites within the octahedral layer of the micas. The radius of  $Mn^{+2}$  is fairly large (0.80Å) and thus it would be expected to enter the  $Oc_1$  site in biotite rather than muscovite. Divalent manganese has no crystal field stabilization energy and therefore should be found in the larger  $Oc_1$  site of biotite. The combined effect of these yields the  $K_D$  of 0.62. It is interesting to note that both samples 6 and 56 lie on the proposed  $K_D$  line.

Zinc should be incorporated into the  $Oc_1$  sites of the micas owing to its charge and size, and the excellent distribution shown in Figure 11 indicates that this is the case.

The mole fraction considered is  $Zn/(Zn+Mn+Mg+Fe^{+2})$ , and the  $K_D$  is 0.76 indicating the preference of zinc for the  $Oc_1$  site in biotite. Since zinc has no crystal field stabilization energy, the controlling factor for its distribution should be its size ( $0.74\text{\AA}$ ). This size prohibits zinc from readily entering the  $Oc_1$  site in muscovite where smaller ions, such as  $Mg^{+2}$  and  $Li^{+1}$ , are easily incorporated.

Although considerable scatter is observed in Figure 12, representing the distribution of Co between the mica pairs, a line may be constructed which represents the equation  $x_{Co}^{Ms}/x_{Co}^{Bt} = 7.5$ . The large value of the  $K_D$  is explained by use of the crystal field theory which indicates that crystal field stabilization energy is the dominant factor controlling the distributions of the transition elements. Considering only the radius of Co, one would expect it to enter the biotite site preferentially to the muscovite, an expectation which is obviously not the case. When one considers the high stabilization energy of Co in octahedral coordination (17.1 kcal/mole) and the fact that the  $Oc_1$  site of muscovite is smaller than that of biotite, it is apparent why the  $K_D$  is of such magnitude. The large amount of scatter is most likely due to poor analytical data, and sample 6 (pegmatitic) was not considered in construction of the  $K_D$  line.

The distribution of Ni is similar to that of Co and is shown in Figure 13. A  $K_D$  of 6.9 is defined by the line representing the relationship,  $x_{Ni}^{Ms}/x_{Ni}^{Bt}$ , with X equal to

$\text{Ni}/\text{Ni}+\text{Mg}+\text{Mn}+\text{Fe}^{+2}$ . The explanation of the large  $K_D$  is similar to that for Co, and although scatter is quite serious, the general relationship is apparent. It is noted that one point, sample WM 5, lies far from the  $K_D$  line. This is most readily explained by the fact that its geographical location in the Wylie Mountains is about eight miles from the Mica Mine area where the other ten samples were collected and the physical conditions of metamorphism may have varied considerably over this distance. If equilibrium was attained with respect to Ni in sample WM 5 then it is of a different magnitude than the Mica Mine samples, reflecting the different physical conditions.

Figure 14 represents the distribution of Cu between the  $\text{Oc}_1$  sites of the micas with  $X = \text{Cu}/\text{Cu}+\text{Mg}+\text{Mn}+\text{Fe}^{+2}$ . Deviation from the proposed  $K_D$  line is considerable in the case of the samples 6, 16, 54, and 56, but a relationship on the order of  $K_D = 11$  is apparent. The interpretation of this is similar to that for Co and Ni. No correlation between the deviating samples and varying concentrations of elements other than Cu could be found.

Lithium is distinctive in its  $\text{Oc}_1$  distribution in the micas in that it is univalent and has a smaller radius than any of the other common elements occurring in this site. Although the data are extremely scattered, a  $K_D$  on the order of 2.1 is observed when the mole fraction,  $\text{Li}/\text{Li}+\text{Mg}+\text{Mn}+\text{Fe}^{+2}$ , is chosen (Fig. 15). Other mole fractions give graphs with considerably more scatter. In spite of the poor quality of

the relationship it does appear that Li is concentrated in the  $Oc_1$  position of muscovite. This is obvious when one considers the size of the Li ion ( $0.60\text{\AA}$ ) and its univalent nature. The small cation should tend to enter the smaller  $Oc_1$  site of muscovite, which, in contrast to the  $Oc_1$  site of biotite, is surrounded by six trivalent  $Oc_2$  sites. An ion of small charge would be favored in this case. The distribution of Li between the micas may represent a disequilibrium situation.

The data concerning element distribution in the octahedral sites appear to substantiate the structural models of Radoslovich and the crystal field stabilization energy observations of Curtis (1964). With the exception of Cr and  $Fe^{+2}$ , elements with high octahedral stabilization energies (Co, Cu, and Ni) are highly concentrated in the muscovite, while those with low energies ( $Fe^{+3}$ , Mn, and Zn) are concentrated in the biotite.

Distribution in the large cation sites: Elements to be considered in the large cation sites include K, Na, Rb, Ca, Sr, and Ba. The writer has included Pb in this group also owing to its charge and size.

No relationship was found for K when the mole fraction  $K/(K+Na+Ca+Ba)$  was considered. The addition of Ba and Ca to this mole fraction has little effect on the value of the fraction since K is present in such overwhelming amounts. Therefore, no matter which mole fraction is chosen, its value



will approach unity and a partitioning of K cannot be observed in this case.

Figure 16 represents the partitioning of Na between the large cation sites of biotite and muscovite. The data are scattered but appear to represent a distribution defined by the equation,  $K_D = X_{Na}^{Ms}/X_{Na}^{Bi} = 2.9$ , where  $X = Na/(Na+K+Ca+Ba)$ . When one considers other mole fractions the scatter is of greater magnitude. The  $K_D$  of 2.9 is easily explained by a consideration of the size of the Na cation ( $0.95\text{\AA}$ ), and of the fact that the large cation site of muscovite has been observed to be smaller than that of biotite (Radoslovich, 1963a). Sodium is the smallest of the cations which readily substitute into this site and therefore it would be expected to concentrate in the muscovite lattice.

The distribution of Rb between the micas is well defined as may be seen in Figure 17. The ratio,  $Rb/(Rb+K+Na+Ca+Ba)$ , is considered and the  $K_D$  is equal to 0.41, indicating a preference of Rb for biotite. Rubidium is the largest of the large cations being considered and thus will be incorporated in the larger biotite site. One point, sample WM 5, lies far above the  $K_D$  line. As pointed out in the discussion of Ni, WM 5 is from a different geographical locality and may represent a different equilibrium, or no equilibrium at all.

No distribution was observed for Ca owing chiefly to the analytical quality of the data and the extremely low abundances of Ca in the muscovites, often below the limit of detection.

The interference of Ba with Ca in the flame photometric analysis hindered the detection of trace amounts of Ca. One would expect Ca to enter the muscovite large cation site but this is apparently not the case.

When the mole fraction,  $\text{Sr}/(\text{Sr}+\text{K}+\text{Na}+\text{Ca}+\text{Ba})$ , is considered no distribution of Sr is observed (see Fig. 18). A possible explanation for this apparent "disequilibrium" might involve the inclusion of submicroscopic inclusions of apatite. McKay (1964) observed Sr (ionic radius equal to  $1.13\text{\AA}$ ) to be incorporated in the muscovite with a  $K_D$  of 4.1.

Barium (Fig. 19) yields a poor but recognizable distribution with a  $K_D$  defined by the equation,  $x_{\text{Ba}}^{\text{Ms}}/x_{\text{Ba}}^{\text{Bi}} = 1.33$ , where  $X = \text{Ba}/(\text{Ba}+\text{K}+\text{Na}+\text{Ca})$ . The scatter is definitely attributed in part to poor analytical data. When the ionic radius of  $1.35\text{\AA}$  for Ba is compared to that of Sr, the other divalent cation for which a distribution has been found, it becomes apparent that, although Ba is concentrated in muscovite, it should have a lower  $K_D$  than that of Sr. This is in fact the case.

Lead has a divalent radius of  $1.20\text{\AA}$  and should enter the mica structure incorporated in the large cation site. A plot of  $\text{Pb}/(\text{Pb}+\text{K}+\text{Na}+\text{Ca}+\text{Ba})$  for muscovite versus that for biotite produces no relationship (Fig. 20). Possibly the mole fraction chosen is not the correct one, or the Pb content may be a function of the original uranium and thorium distribution between the minerals. It would be difficult to hypothesize as to the site in which the original uranium and thorium were

concentrated since it is not known whether they actually substituted in the lattice or were incorporated as accessory minerals. If the radioactive elements were present in accessory minerals, there is no reason to expect a systematic relationship today among the Pb contents of the various mica pairs.

It can be seen from these distribution data that the partitioning of an element between the large cation sites of muscovite and biotite is controlled chiefly by the ionic radius.

#### Element Distribution between Plagioclase and Hornblende

The structure of hornblende may be considered similar to those of the micas in that there is a large cation position in eight-fold coordination and the two octahedral sites which will be termed  $Oc_1$  and  $Oc_2$  during this discussion for the sake of brevity.

The model used for plagioclase assumes that all univalent and divalent ions enter the Ca-Na site and trivalent and tetravalent ions substitute for Al (Deer, Howie, and Zussman, 1963d).

Distribution between the  $Oc_2$  site of hornblende and the Al site of plagioclase: Elements included in this group include Al, Ti,  $Fe^{+3}$ , and Cr. No good relationships are observed in this group and a number of explanations may be offered: 1) lack of knowledge about the exact distribution of Al within sites in the plagioclase and hornblende

structures, 2) dissimilarity in the plagioclase and hornblende structures, 3) poor analytical data for Ti and Cr, 4) slight alteration of the plagioclase, and 5) idealized mole fractions.

No distribution was determined for Al between the two minerals owing to the fact that the Al substituting for Si and the octahedrally coordinated Al in the hornblendes are not distinguished.

Figure 21 represents a plot of the mole fraction,  $Ti/Ti+Al+Fe^{+3}$ , for hornblende versus plagioclase. No relationship is apparent, and the cause may be attributed to the analytical data and Al distribution. It is noted also that other mole fractions ( $Ti/Ti+Fe^{+3}$ ,  $Ti/Ti+Al$ , and  $Ti/Ti+Mg+Mn+Fe$ ) indicate no significant distribution either. It is obvious from the analyses that Ti is dominant in the hornblende ( $K_D$  less than unity).

The partitioning of  $Fe^{+3}$  is represented in Figure 22 and a line may be tentatively drawn through the points defining a  $K_D = X_{Fe^{+3}}^{Pc}/X_{Fe^{+3}}^{Hb} = 0.002$  indicating the predominance of  $Fe^{+3}$  in the hornblende phase. Similar arguments as those advanced above may be used in explaining the scatter. The mole fraction used is  $Fe^{+3}/Fe^{+3}+Ti+Al$ .

Chromium appears to be distributed according to a  $K_D$  of 0.05 when a mole fraction of  $Cr/Cr+Al+Ti+Fe^{+3}$  is considered (Fig. 23). If the distribution of Cr is controlled by the crystal field stabilization energy (60.0 kcal/mole) this would indicate the Al site in hornblende to be smaller than

the equivalent site in plagioclase. This observation is not supported by the distribution of  $\text{Fe}^{+3}$  (stabilization energy = 0 kcal/mole). One notes that similar discrepancies were observed in the  $\text{Fe}^{+3}$  and Cr distributions between muscovite and biotite.

Distribution between  $\text{Oc}_1$  site of hornblende and the Na-Ca site of plagioclase: The three chief cations found in the  $\text{Oc}_1$  site of hornblende are Mg, Mn, and  $\text{Fe}^{+2}$ , and, as with the micas, the transition elements and Li substitute into this position. The Na-Ca site in plagioclase is the only major position where univalent and divalent cations may enter the structure and no evidence of subsites within this position has been reported.

No distribution for  $\text{Fe}^{+2}$  can be observed owing to the relative nonexistence of  $\text{Fe}^{+2}$  in the plagioclase structure.

Figure 24 represents the distribution of Mg between hornblende and plagioclase. Although a curve is drawn through the points, no simple equation can be derived to fit the points and no unique distribution constant,  $K_D$ , can be assigned. It is apparent that the distribution of Mg changes with the concentration of the element and nonideality is the case. It has been observed that Mg substitutes in the  $\text{Oc}_1$  site in hornblende in an ideal manner up to about  $x_{\text{Mg}}^{\text{Hb}} = 0.7$ , where  $X = \text{Mg}/\text{Mg}+\text{Mn}+\text{Fe}^{+2}+\text{Ti}$  (Kretz, 1959). The mole fraction considered in this investigation,  $\text{Mg}/\text{Mg}+\text{Mn}+\text{Fe}^{+2}$ , is essentially equal to that of Kretz, so ideality might be assumed for Mg

in hornblende. In this case the non-ideal nature of the distribution is attributed to the Mg in plagioclase. Poor distributions are generally observed where an element is considered which is a major component in one phase and a trace component in the other. It should be noted that the mole fractions are not the same for hornblende and plagioclase. The mole fraction of Mg in the plagioclase site is, by definition,  $Mg/Mg+Na+K+Ca$ , and it is with these ions (and other trace ions) that Mg competes for its position in plagioclase. Therefore, it would not be a valid representation of the mole fraction to consider the ratio,  $Mg/Mg+Mn+Fe^{+2}$ , when examining plagioclase.

The distribution of Mn is represented in Figure 25. The situation is similar to that for Mg in that no distribution can be assigned to the curve. Manganese has been observed to be quite non-ideal above the point  $x_{Mn}^{Hb} = 0.01$  (Kretz, 1959, 1960). This fact, coupled with the lack of knowledge of the behavior of Mn in plagioclase, may help to explain the absence of a distribution. One notes again the difference in mole fractions for the two minerals. The possibility that the distributions of Mg and Mn are controlled by variations in the mole fraction of another component was examined but no conclusive observations could be made.

When the mole fraction for zinc in hornblende,  $Zn/Zn+Mg+Mn+Fe^{+2}$ , is plotted against the mole fraction for plagioclase,  $Zn/Zn+Na+K+Ca$ , no relationship is observed (Fig. 26). Upon examination of the mole fraction of Mn in hornblende, however,

it becomes apparent that as  $X_{Mn}^{Hb}$  decreases, the  $K_D$  for the ratio  $X_{Zn}^{Pc}/X_{Zn}^{Hb}$  increases. Although the distribution of Zn appears to be controlled by  $X_{Mn}^{Hb}$ , a general statement can be made that the large cation site of plagioclase favors the incorporation of zinc since all  $K_D$ 's for the points in Figure 26 are greater than unity. The crystal field stabilization energy theory predicts this if it is recalled that the  $Oc_1$  site in hornblende is smaller than the Ca-Na site in plagioclase and that the stabilization energy of Zn is zero kcal/mole.

Figure 27 indicates the distribution of Co between hornblende and plagioclase. Although the data are poor, a  $K_D$  of 0.77 is defined by the straight line passing through the origin. Considering the stabilization energy of Co (17.1 kcal/mole), it is expected to concentrate in the hornblende phase.

No distribution can be observed for Ni and no correlation between the mole fraction of Ni in either phase and variations in the mole fraction of a second component is obvious.

Copper is irregularly distributed between hornblende and plagioclase as observed in Figure 28. The dashed line indicates a  $K_D = X_{Cu}^{Pc}/X_{Cu}^{Hb} = 0.94$ . Different mole fractions are again chosen for the two minerals, these being  $Cu/(Cu+Mg+Mn+Fe^{+2})$  and  $Cu/(Cu+Na+K+Ca)$  for hornblende and plagioclase, respectively. Copper is only slightly concentrated in the basic hornblende phase. One notices that sample 47

consistently lies far from the  $K_D$  line. The reason for this is not apparent. Both samples 47 and 60 contain almandine garnet and this abnormal assemblage might be advanced as an explanation, but sample 60 generally does not deviate significantly from the distribution line, and both samples were collected within ten feet of each other so temperature and pressure variations cannot be suggested.

Lithium should substitute in the  $Oc_1$  position of hornblende according to its ionic radius ( $0.60\overset{O}{\text{\AA}}$ ), similarly to its behavior in biotite. The mole fraction,  $Li/Li+Mg+Mn+Fe^{+2}$ , in hornblende plotted against the mole fraction,  $Li/Li+Na+K+Ca$ , for plagioclase describes a line with slope of 0.28 which is the  $K_D$  for Li (Fig. 29). Owing to the small size of the Li ion the tendency should be for Li to predominate in hornblende. The low  $K_D$  indicates this to be the case. Samples 47 and 60 both lie far from the  $K_D$  line in this case due to the high Li content of the hornblende in each pair. A partial explanation for this may lie in the fact that both samples contain garnet and lack biotite, a Li-rich phase. In this respect the hornblende would be expected to incorporate slightly more Li than if biotite were present. Two other biotite-free samples contain hornblendes which are of average Li content so this hypothesis may be an oversimplification.

Distribution between the large cation site of hornblende and the Ca-Na site of plagioclase: Elements under consideration



in this section include K, Na, Rb, Ca, Sr, and Pb. No analyses were made for Ba.

Figure 30 represents the distribution of K between hornblende and plagioclase where the mole fraction,  $K/(K+Na+Ca)$ , is chosen for both minerals. The proposed  $K_D$  line does not intersect the origin and there seems to be little justification for constructing a curved line, so the value of the  $K_D$  (0.61) is questionable, but its order of magnitude is probably significant. A possible interpretation for the fact that the line does not intersect the origin involves the presence of potassium feldspar in an exsolved state in the feldspar samples or as an occasional contaminating grain. Most of the plagioclase samples showed slight sericitization and this might account for the high potassium values. It is interesting to note that the distribution of K is in part controlled by the mole fraction,  $Rb/(Rb+Na+K+Ca)$ , for plagioclase. The five points representing the five highest values of  $X_K^{Pc}$  represent the five greatest values of  $X_{Rb}^{Pc}$  in regular order. A plot using the mole fraction,  $K/(K+Na)$ , for hornblende yields a somewhat similar distribution but with more scatter.

No distribution was found for Na. The mole fractions,  $Na/(Na+K+Ca)$  and  $Na/(Na+K)$ , were examined but no relationship could be observed. The abundance of Rb in the hornblendes was below the limit of detection so no distribution can be proposed.

The Ca content of the hornblendes is essentially invariable so the mole fraction,  $\text{Ca}/\text{Ca}+\text{Na}+\text{K}$ , is quite a constant value and partitioning of Ca between hornblende and plagioclase has little meaning.

A distribution is observed for Sr (Fig. 31) when the mole fraction,  $\text{Sr}/\text{Sr}+\text{Ca}+\text{Na}+\text{K}$ , is considered for both minerals.  $K_D$  is defined by the equation,  $X_{\text{Sr}}^{\text{Pc}}/X_{\text{Sr}}^{\text{Hb}} = 13.3$ , indicating a very marked enrichment of Sr in plagioclase. It may be concluded from the extreme concentration of Sr and Rb in the plagioclase lattice that the Ca-Na site of plagioclase is considerably larger than the large cation site of hornblende.

No systematic partitioning of Pb is observed when the mole fraction,  $\text{Pb}/\text{Pb}+\text{Na}+\text{K}+\text{Ca}$ , is chosen. The lack of a distribution may be caused by an incorrectly selected mole fraction or, more likely, as with the micas, variations in the original thorium and uranium contents.

It is observed from these hornblende-plagioclase distributions that partitioning between the pair is generally poor, owing chiefly to the significant differences in the structures and chemistry of the minerals. The list of causes listed at the first of this section may in fact be applied to all hornblende-plagioclase distributions.

#### Element Distribution between Hornblende and Epidote

Distribution between the  $\text{Oc}_2$  site of hornblende and the  $\text{Al-Fe}^{+3}$  site of epidote: Figure 32 represents the distribution

of Ti between hornblende and epidote with  $X_{Ti} = Ti/Ti+Al+Fe^{+3}$ . It is difficult to draw a  $K_D$  line through the seven points, but it is obvious that Ti predominates in the hornblende. The scatter is attributed chiefly to the Ti analytical error. It should be pointed out that there is little need to distinguish between the Al distribution between positions in the epidote structure as essentially all Al occurs in the octahedrally coordinated site (see discussion of crystal structures). A plot for Ti using the mole fraction,  $Ti/Ti+Fe^{+3}$ , yields similar results.

A  $K_D$  of 0.80 is defined by the line in Figure 33 which represents the  $Fe^{+3}$  distribution with  $Fe^{+3}/Fe^{+3}+Al+Ti$  chosen as a mole fraction. If the crystal field stabilization energy theory applies to the partitioning of  $Fe^{+3}$ , the  $K_D$  would imply that the  $Oc_2$  site of hornblende is larger than the equivalent site in epidote since  $Fe^{+3}$  has no stabilization energy. It should be remembered, however, that the  $Fe^{+3}$  (and Cr) distributions between micas, and plagioclase and hornblende are not controlled by the stabilization energy.

No Al distribution is found owing to the site problem of Al in hornblende and the small variability in the abundance of Al. The fact that only seven epidote-hornblende pairs were studied limits the accuracy of any  $K_D$  lines that might be proposed for distributions but the general distribution trend should be significant.

Chromium is slightly concentrated in the epidote phase as seen in Figure 34. The  $K_D$  for the mole fraction,

$\text{Cr}/\text{Cr}+\text{Al}+\text{Ti}+\text{Fe}^{+3}$ , is 1.2. The implication that the  $\text{Oc}_2$  site of hornblende is small is supported by the distribution of Cr.

Distribution between the  $\text{Oc}_1$  site of hornblende and the  $\text{Oc}-(\text{Mg}-\text{Fe}^{+2})$  site of epidote: Figure 35 represents an interesting relationship. Two different  $K_D$ 's are proposed for the partitioning of  $\text{Fe}^{+2}$  between hornblende and epidote for the mole fraction,  $\text{Fe}^{+2}/\text{Fe}^{+2}+\text{Mn}+\text{Mg}$ . The one  $K_D$  indicates that  $\text{Fe}^{+2}$  occurs equally distributed between the phases while the second represents a noticeable preference of  $\text{Fe}^{+2}$  for epidote, implying that the Oc site of epidote is smaller than the  $\text{Oc}_1$  site of hornblende. The possibility exists that the points are merely scattered and represent a  $K_D$  somewhere between 1.00 and 1.43. No conclusive correlation can be made between the two distributions and variations in a second component with the available data.

Magnesium is preferentially incorporated in hornblende (Fig. 36). The mole fraction is  $\text{Mg}/\text{Mg}+\text{Fe}^{+2}$  and the  $K_D$  defined by the ratio,  $x_{\text{Mg}}^{\text{Ep}}(1-x_{\text{Mg}}^{\text{Hb}})/x_{\text{Mg}}^{\text{Hb}}(1-x_{\text{Mg}}^{\text{Ep}})$ , is 0.32. It is interesting to note that in this instance more scatter is observed when the mole fraction,  $\text{Mg}/\text{Mg}+\text{Fe}^{+2}+\text{Mn}$ , is chosen. Apparently the presence of Mn effects the Mg distribution to a small extent.

Manganese is distributed according to the equation,  $x_{\text{Mn}}^{\text{Ep}}/x_{\text{Mn}}^{\text{Hb}} = 1.74 = K_D$ , with  $\text{Mn}/\text{Mn}+\text{Mg}+\text{Fe}^{+2}$  as the mole fraction (Fig. 37). According to the stabilization energy of Mn

(zero kcal/mole), Mn will enter the larger site, which, reasoning from the  $K_D$ , is in epidote. This observation is in opposition to the one drawn from the  $Fe^{+2}$  distribution, and other factors apparently affect the partitioning.

Figure 38 indicates that the distribution of Zn is controlled by  $X_{Fe^{+2}}^{Hb}$ . The implication of this control is admittedly not too strong but it should be mentioned. In the case of zinc scatter cannot be attributed to analytical inaccuracies and there is little reason for doubting the mole fraction,  $Zn/Zn+Mg+Mn+Fe^{+2}$ , so either disequilibrium or control by another element should be suspected. It does appear that Zn is slightly concentrated in epidote.

The extreme enrichment of Co in the epidote site is indicated by the  $K_D$  of 24 when the mole fraction,  $Co/Co+Mg+Mn+Fe^{+2}$ , is considered in Figure 39. The  $K_D$ 's of Co, and Ni and Cu, the discussions of which follow, all are quite large and indicate that the Oc site of epidote is definitely smaller than the  $Oc_1$  site of hornblende.

No unique  $K_D$  distribution line can be defined from the data representing the distribution of Ni, but it can be stated that Ni is incorporated in the epidote site in an amount of about 30 times that which enters the equivalent hornblende site when  $Ni/Ni+Mg+Mn+Fe^{+2}$  is examined as the mole fraction.

The data for Cu are poor and the distribution line is questionable (Fig. 40). Sample 58 is far from the  $K_D$  line in this figure and invariably is anomalous in one way or

another in all epidote-hornblende distributions. The chemistry of Ep58 is the obvious reason for this (see Table 7). The data do suggest, however, a  $K_D$  of about 45, indicating the extreme preference of Cu for epidote.

No significant distribution of Li is observed in the seven mineral pairs analyzed with the mole fraction  $Li/Li+Mg+Mn+Fe^{+2}$ . This may be attributed to some lack of knowledge as to the exact distribution of Li within the epidote lattice, or simply to a lack of equilibrium.

Distribution between the Ca site of hornblende and the Oc Ca site of epidote: A  $K_D$  of 1.5 is suggested for the distribution of K between the phases when  $K/K+Na$  is chosen as a mole fraction (Fig. 4), but if  $K/K+Na+Ca$  is used no  $K_D$  can be observed.

A  $K_D$  of 0.79 is found for Na when the mole fraction  $Na/Na+K$  is considered (Fig. 42), but no significant distribution is observed with  $Na/Na+K+Ca$  chosen as the fraction. This distribution and that observed for K may be caused by the overwhelming amount of Ca and the poor analytical quality of the Ca data. No distribution of Ca is observed owing to the small variation in its abundance in hornblende and its pre-dominance over other cations in the site.

The data for the Sr distribution indicate a  $K_D$  on the order of 20, representing a strong enrichment of Sr in epidote (Fig. 43). The two points, 36 and 58, indicate epidote samples with high Ca contents, and therefore lower

$X_{Sr}^{Ep}$  values when  $X = Sr/Sr+Ca+Na+K$ .

Lead exhibits no meaningful distribution when the mole fraction  $Pb/Pb+Na+Ca+K$  is used, but the data indicate a general preference of Pb for epidote (Fig. 44).

Few generalizations can be made about the distributions between the Ca sites since only two  $K_D$ 's could be observed, but it appears that the larger divalent cations favor epidote and the smaller univalent cations enter the hornblende.

#### Element Distribution between Epidote and Plagioclase

Only five epidote-plagioclase pairs were analyzed in this investigation so distributions are generally poorly defined and admittedly of quite dubious value. When two minerals are being examined which have structures and chemistry of radically different types, a large number of pairs (at least 20) should be considered in order to obtain meaningful distributions.

Distribution between the Al site of plagioclase and the Al-Fe<sup>+3</sup> site of epidote: The distribution of Ti shows no systematic trend when either  $Ti/Ti+Al+Fe^{+3}$  or  $Ti/Ti+Fe^{+3}$  is chosen as the mole fraction. Aside from the possibility of disequilibrium, the poor analytical data for Ti and the question about the distribution of Al within plagioclase may be cited as causes.

Ferric ion is represented in Figure 45 where a  $K_D$  of 0.02 may be defined by the line,  $X_{Fe^{+3}}^{Pc}/X_{Fe^{+3}}^{Ep}$ , with a mole

fraction of  $\text{Fe}^{+3}/\text{Fe}^{+3}+\text{Al}+\text{Ti}$ . The  $\text{Fe}^{+3}$  cation is greatly concentrated in epidote. No distribution was found for Al. Only three of the five plagioclase samples contained detectable amounts of Cr, so only three points could be considered and these showed no relationship.

Distribution between the Ca site of plagioclase and the Mg-Fe<sup>+2</sup> site of epidote: Figure 46 represents the data for Mg. A  $K_D$  of 0.025 is observed with the mole fractions,  $\text{Mg}/\text{Mg}+\text{Mn}+\text{Fe}^{+2}$  and  $\text{Mg}/\text{Mg}+\text{Na}+\text{K}+\text{Ca}$ , signifying the abundance of Mg in epidote. No significant distribution is observed for Mn, but Mn is concentrated in the Mg-Fe site of epidote over the Ca site of plagioclase.

Similar distributions are exhibited by Zn, Co, and Ni as seen in Figures 47, 48, and 49. All  $K_D$ 's are of the same order of magnitude (0.018-0.030), indicating the preference of these transition elements for epidote. Copper and Li show no distributions. In all these cases it is necessary to consider two different mole fractions for the two different minerals, these being, in the case of Zn,  $\text{Zn}/\text{Zn}+\text{Mg}+\text{Mn}+\text{Fe}^{+2}$  and  $\text{Zn}/\text{Zn}+\text{Na}+\text{K}+\text{Ca}$  for epidote and plagioclase, respectively.

Distribution between the Ca sites: The predominance of K in plagioclase is seen in Figure 50 where a  $K_D$  of 35 is defined when  $\text{K}/\text{K}+\text{Na}+\text{Ca}$  is chosen for the mole fraction. The  $K_D$  for Na is essentially meaningless as it represents a high-Na phase, plagioclase, and a phase in which Na occurs as a minor constituent. No significant distribution is noted



for Sr or Ca. Rubidium occurs in epidote in amounts below the limit of detection so no distribution can be made.

#### Distributions between Garnet and Hornblende

Since only two garnet-hornblende pairs were analyzed for this investigation, no significant distributions can be derived on the basis of these alone. In Figures 51, 52, and 53 the distributions of Mn, Mg, and Fe, respectively, are superimposed on figures taken from a paper by Kretz (1959) in which he examines distributions between hornblende and garnet from the Grenville gneisses of Quebec. The data for the two samples, 47 and 60, in general agree well with the published relationships of Kretz, especially in the case of Mn where a  $K_D$  of about 0.1 is defined by the relationship,  $X_{Mn}^{Hb}/X_{Mn}^G$ , in the region below  $X_{Mn}^G = 0.08$ . Kretz does not suggest a  $K_D$  in his publication owing to lack of data in the field of high  $X_{Mn}^G$  values.

The two garnet-hornblende samples do not ideally fit into Kretz's Mg distribution diagram (Fig. 52) in which he relates the distribution of Mg to the mole fraction of Mn in garnet. This mole fraction for both samples from this investigation lies in the 0.03-0.11, or "B" range of Kretz, but only one of the samples falls into the "B" region on the diagram.

Kretz suggests no value for the distribution of Fe between garnet and hornblende on the basis of his data (Fig. 53). The two mineral pairs from this study add little to the

situation but do conform fairly well with the published data.

### SUMMARY AND CONCLUSIONS

The distributions examined indicate that in general the rocks of the Mica Mine area have either approached or achieved chemical equilibrium with respect to most elements. Evidence of this is more marked in the mica schists than in the amphibolites although both have certainly been subjected to similar temperature and pressure conditions of metamorphism. Several elements adhere closely to the Nernst distribution equation and exhibit ideal solution behavior throughout the limited range of concentration considered. Most notable among these are: Mg, Mn, Zn, and Rb distributions between the micas.

Scatter in the distribution diagrams is in general attributed to several factors: 1) disequilibrium with respect to an element, 2) influence of the mole fraction of another element on the distribution being examined - more data are needed in order to examine complex relationships, 3) lack of knowledge concerning the distribution of Al within a mineral, 4) alter-valency of Cr, Ti and Mn, 5) poor analytical data in the case of Ti, Ca, Ba, and some of the transition elements, and 6) slight alteration of plagioclase. When one mineral of a pair consistently contains more of a given element, but no significant distribution is observed, equilibrium is probably approached but not fully achieved.

A summary of the distributions is presented in Table 3 for the four mineral pairs examined. It is observed that as the chemical and structural nature of the paired minerals becomes more dissimilar, fewer and poorer distributions are observed. The pair, muscovite-biotite, exhibits the greatest number of and most significant distributions while distributions for the other three groups are less well defined and less abundant.

Observed elemental distributions can be explained with consideration of such factors as similarities in crystal structures between minerals, the valency and radius of ions competing for a structural site, the size of the structural site into which an element enters, and the crystal field stabilization energy of the transition elements.

It is interesting to note that apparent chemical equilibrium is attained in hand specimen size samples. This observation is not in accord with that of Turekian and Phinney (1962) who conclude that: "rarely in samples of hand specimen size are equilibrium distributions of trace elements between co-existing phases observed in metamorphic sequences."

The data presented in this investigation cannot be directly applied to the problem of determining the temperature and pressure conditions of formation in light of the fact that little if any experimental work has been pursued and published concerning the distribution of trace elements between phases at a known temperature and pressure. In the

Table 3  
Summary of Distributions,  $K_D$ 's

	<u>Ms-Bi</u>	<u>Ep-Hb</u>	<u>Pc-Hb</u>	<u>Pc-Ep</u>
Ti	0.56	n.o.	n.o.	n.o.
Fe <sup>+3</sup>	0.32	0.80	0.002	0.02
Al	n.o.	n.o.	n.o.	n.o.
Cr	0.28	1.2	0.05	n.d.
Fe <sup>+2</sup>	0.59	1.00	n.d.	n.d.
		1.43		
Mg	2.3	0.32	n.o.	0.03
Mn	0.62	1.74	n.o.	n.o.
Zn	0.76	$X_{Fe^{+2}}^{Hb}$	$X_{Mn}^{Hb}$	0.02
Co	7.5	24	0.8	0.03
Ni	6.9	n.o.	n.o.	0.02
Cu	11	45	0.9	n.o.
Li	2.1	n.o.	0.3	n.o.
K	n.o.	1.5	$X_{Rb}^{Pc}$	35
Na	2.9	0.79	n.o.	n.o.
Rb	0.41	n.d.	n.d.	n.d.
Ca	n.o.	n.o.	n.o.	n.o.
Sr	n.o.	20	13.3	n.o.
Ba	1.3	n.d.	n.d.	n.d.
Pb	n.o.	n.o.	n.o.	n.o.

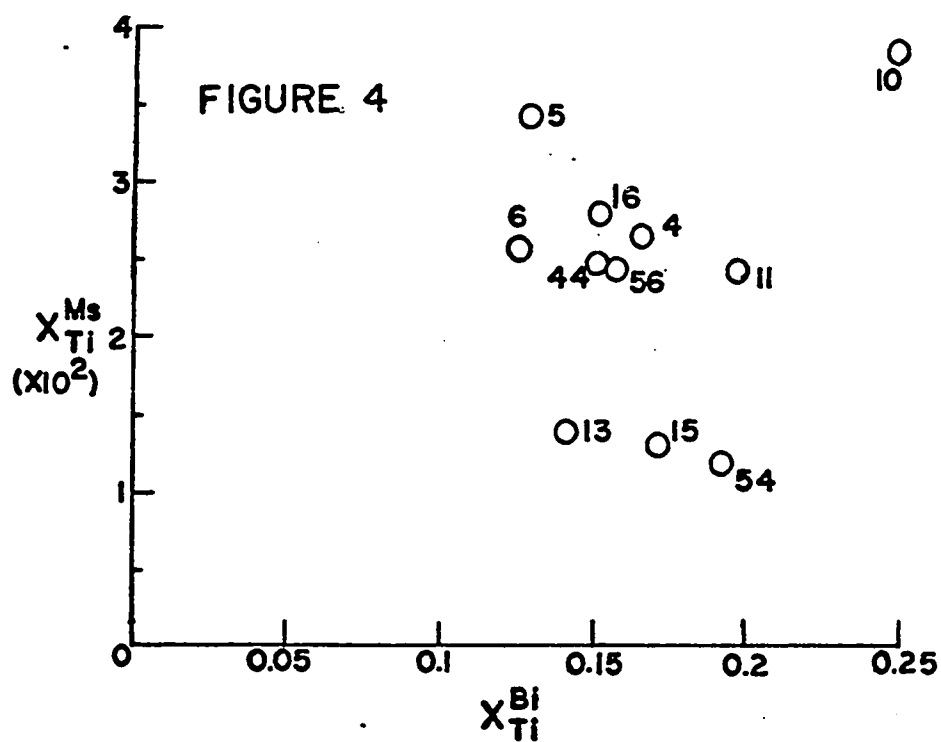
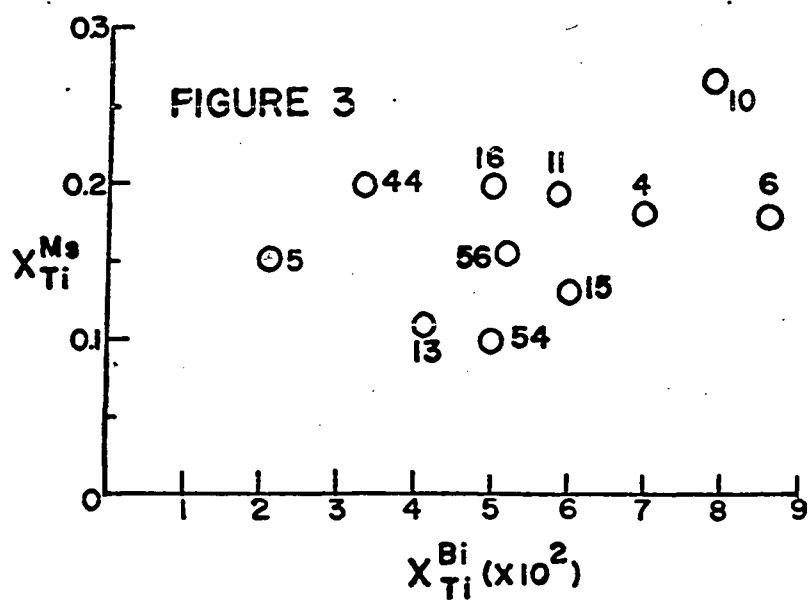
n.o.: distribution not observed

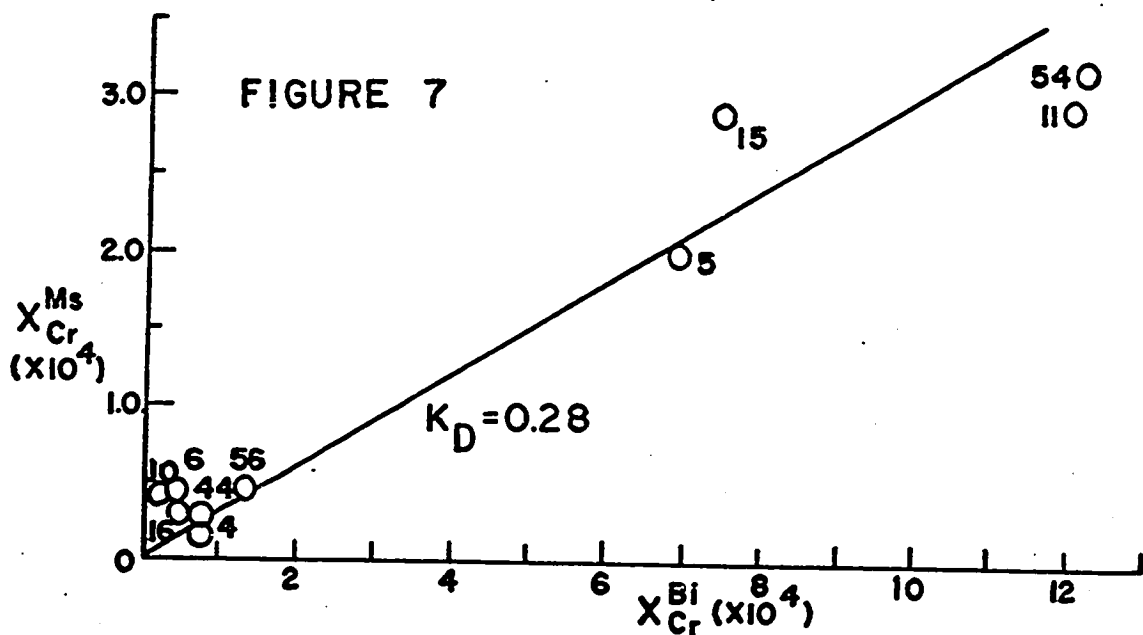
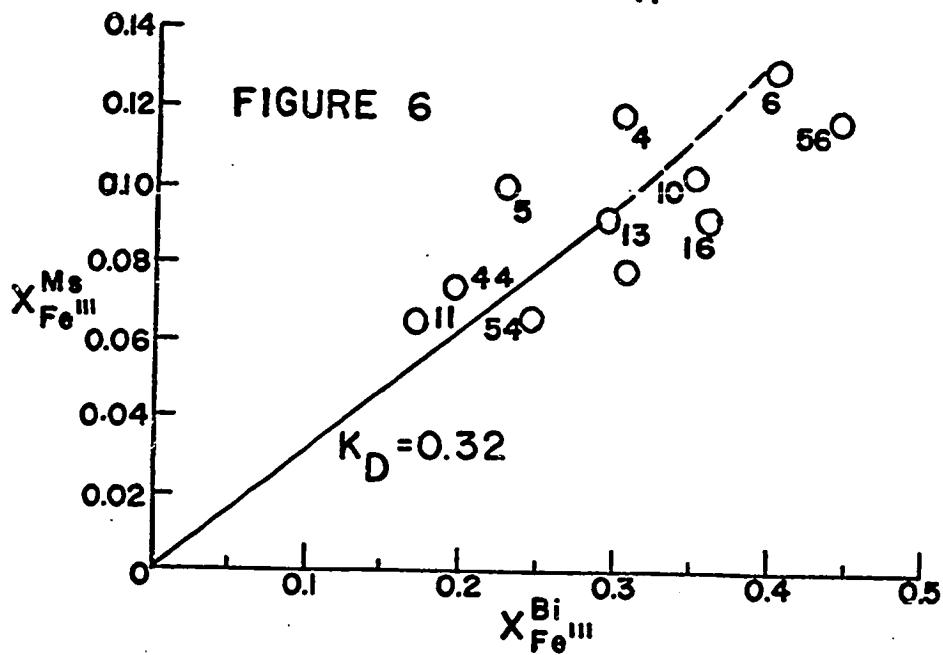
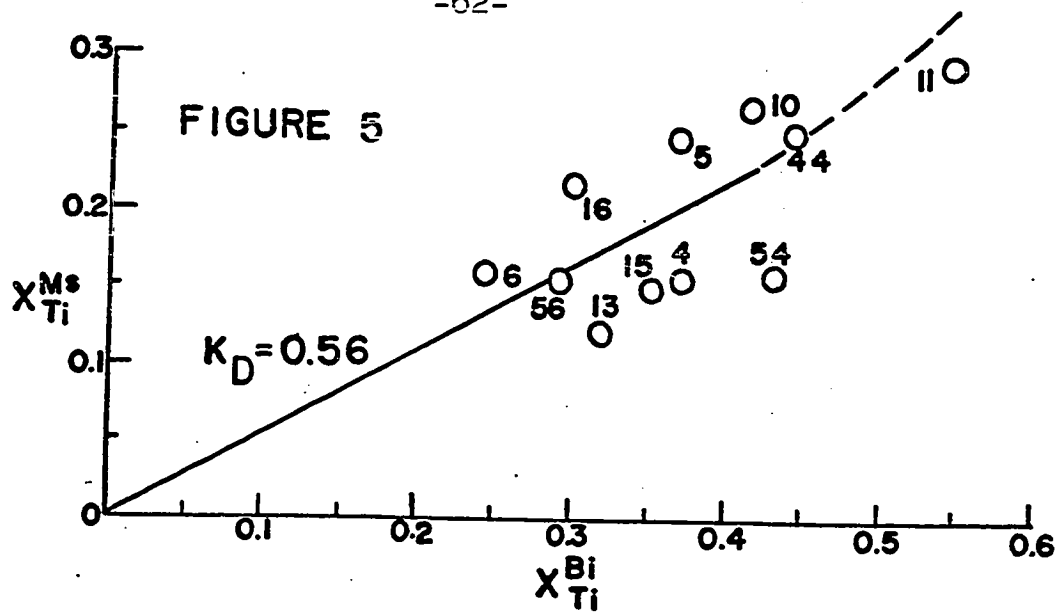
n.d.: distribution not determined

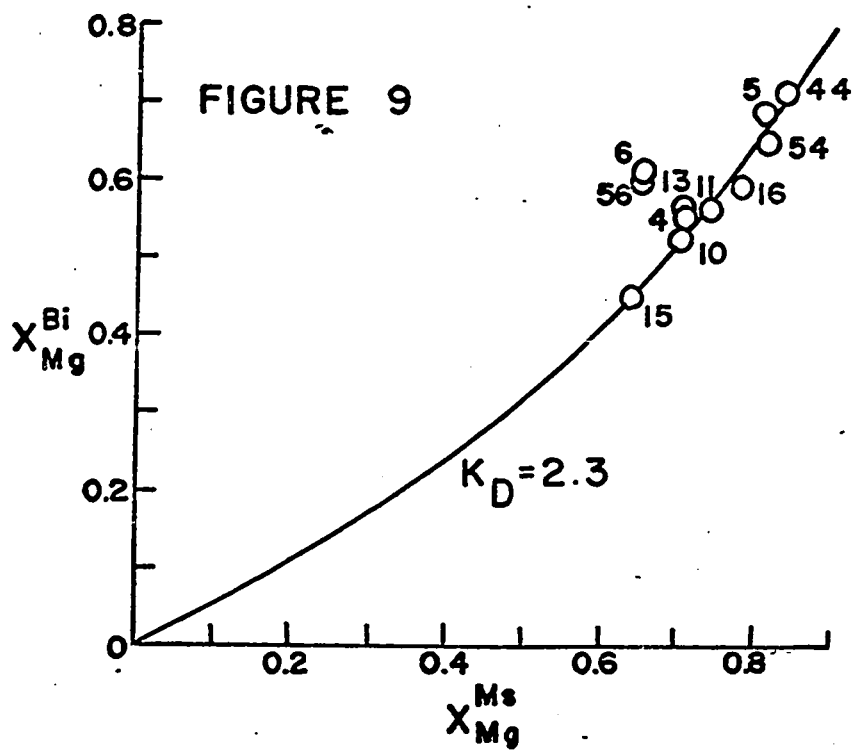
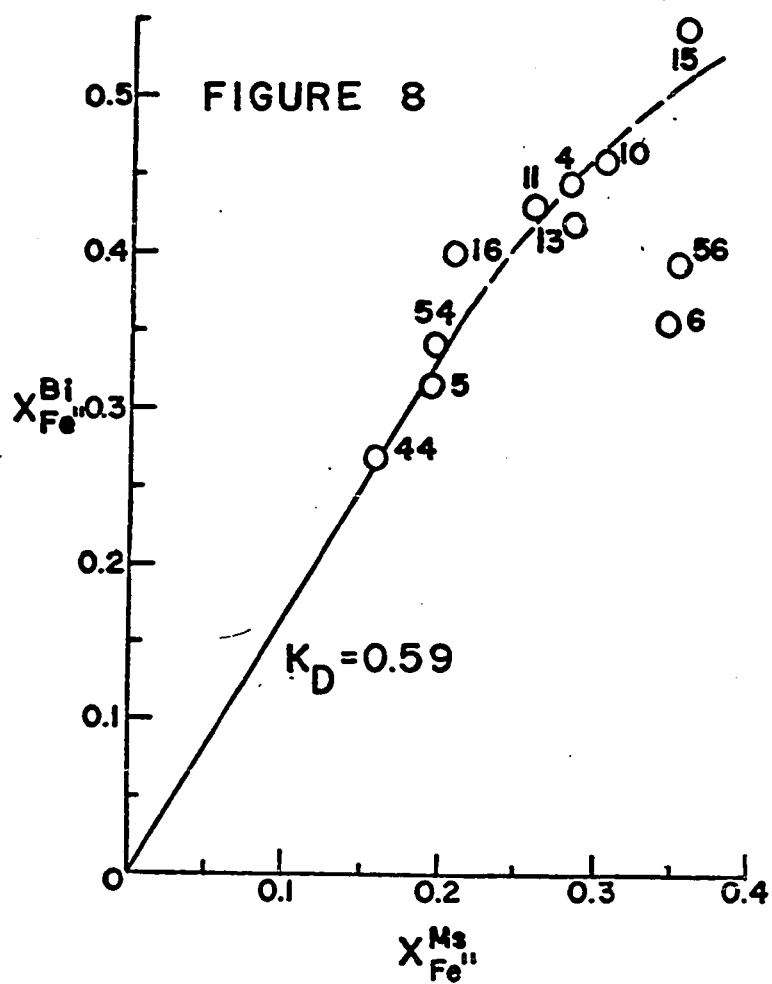
$x_A^1$  : distribution controlled by the mole fraction of  
A in phase 1

case of the micas it will be necessary to examine the distribution constant for an element as it varies with temperature by synthesizing coexisting micas at various water vapor pressures and temperatures and observing  $K_D$  as a function of temperature.

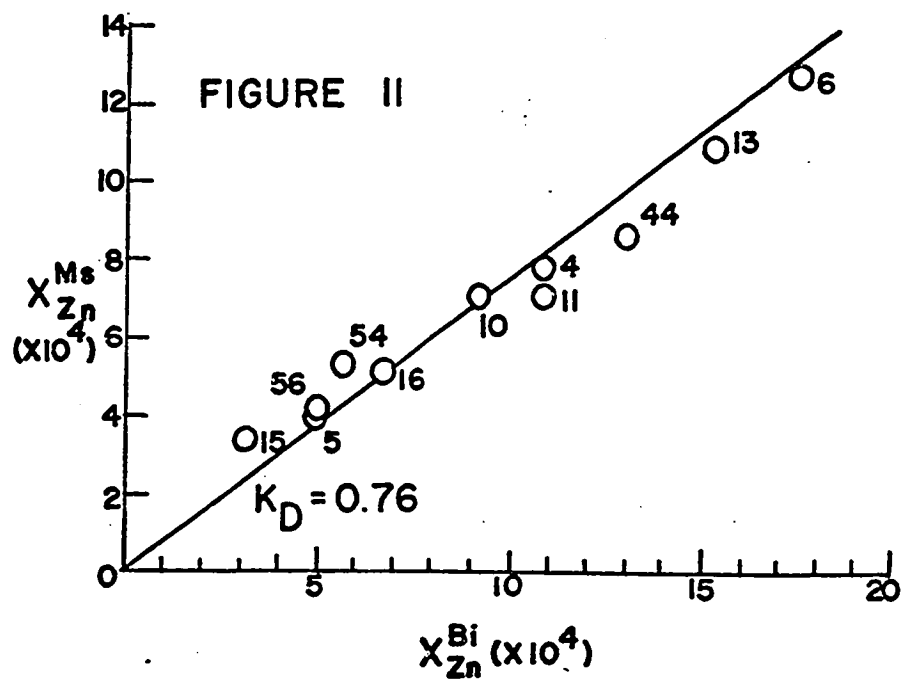
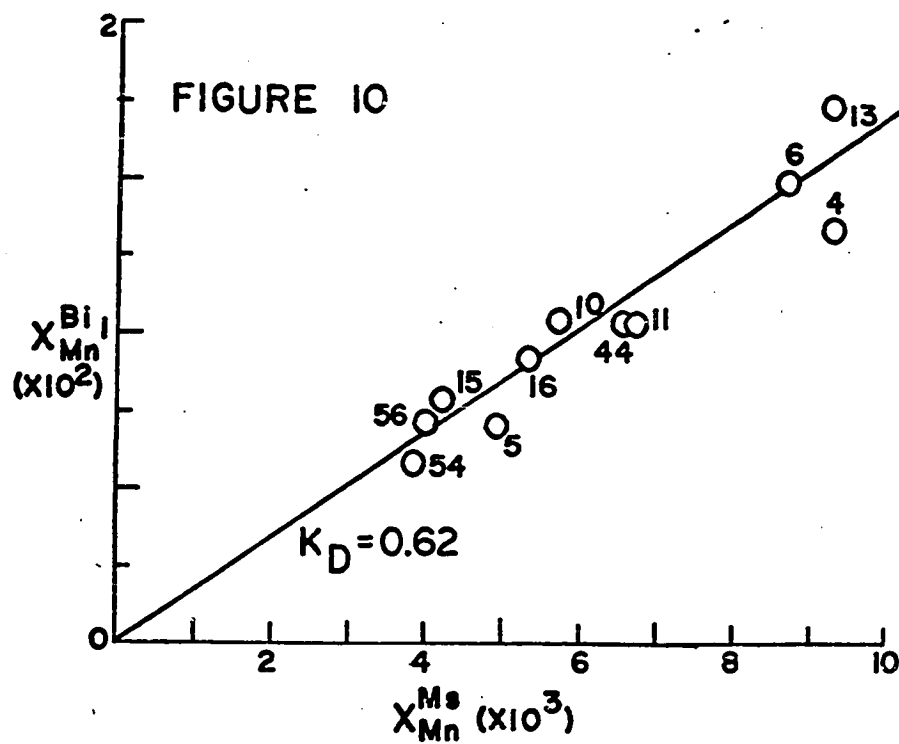
Preliminary electron probe microanalysis for Mg and Fe in the micas of samples MM 13 and WM 5 indicates that variations of more than 7% in the abundances of these two elements in biotite grains within two mm. of each other and muscovite grains within two mm. of each other do not exist.

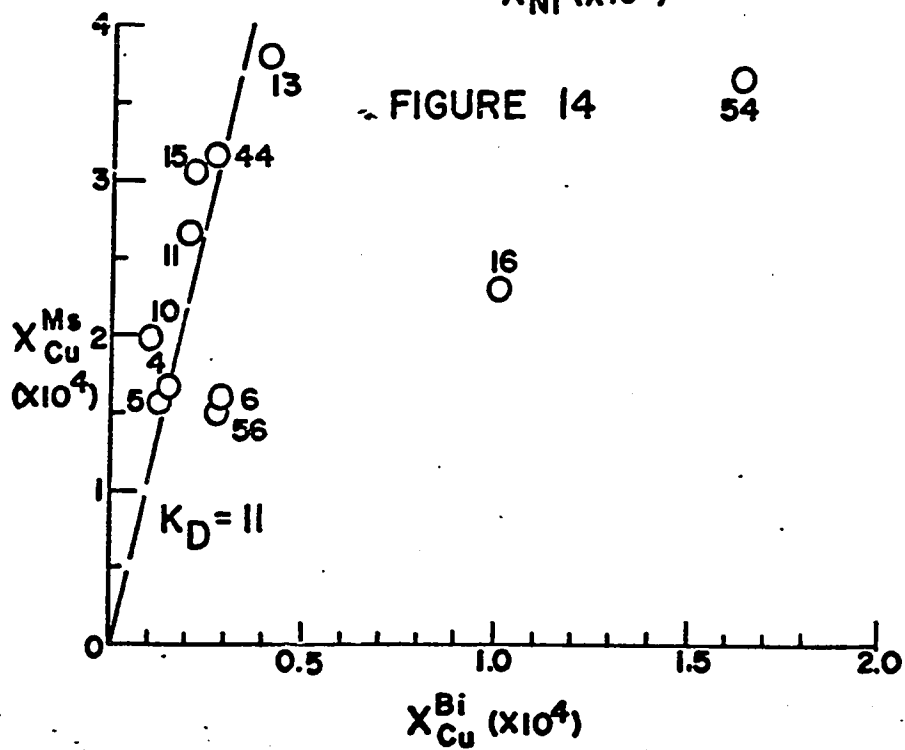
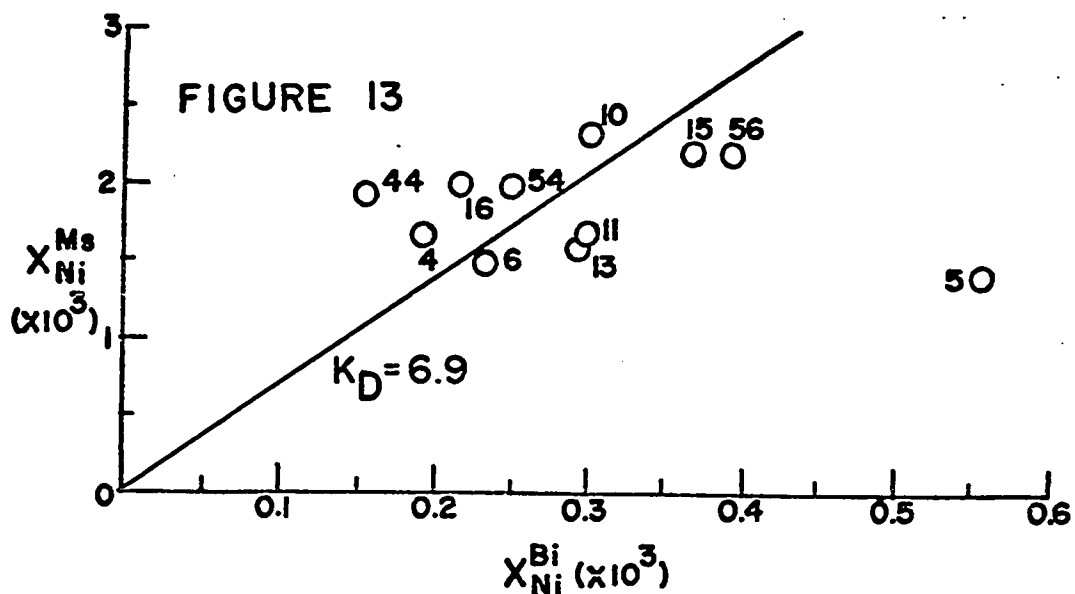
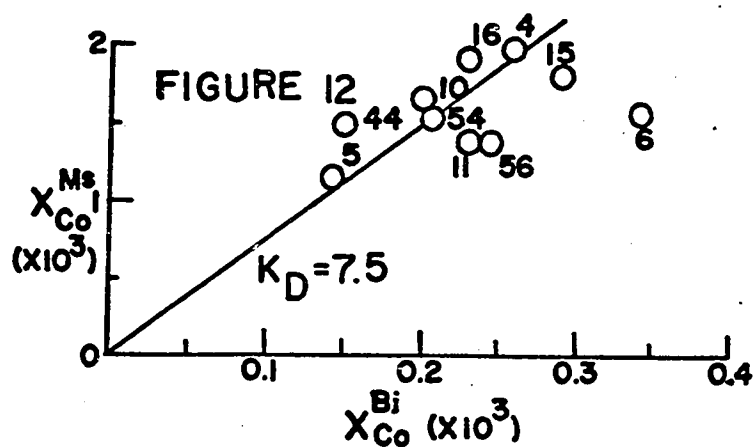


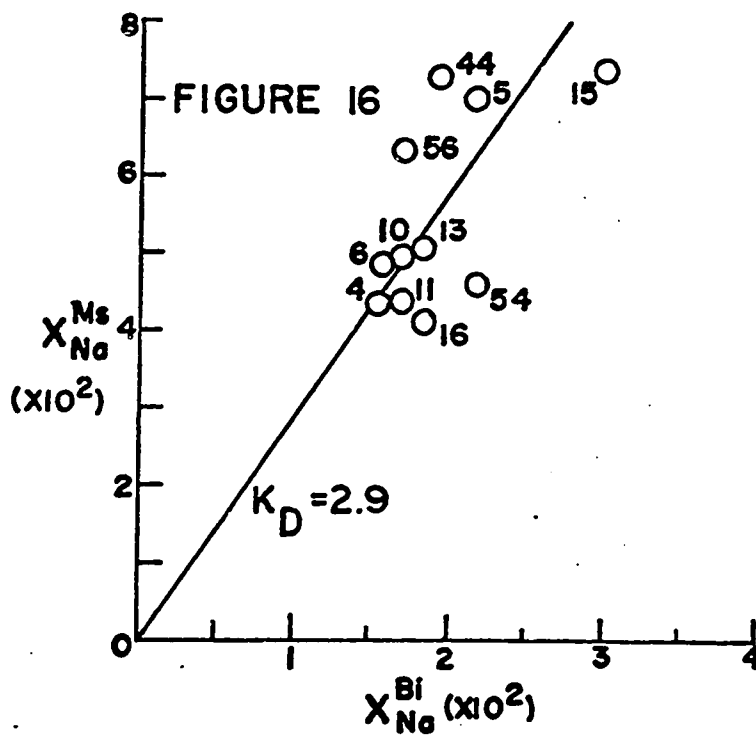
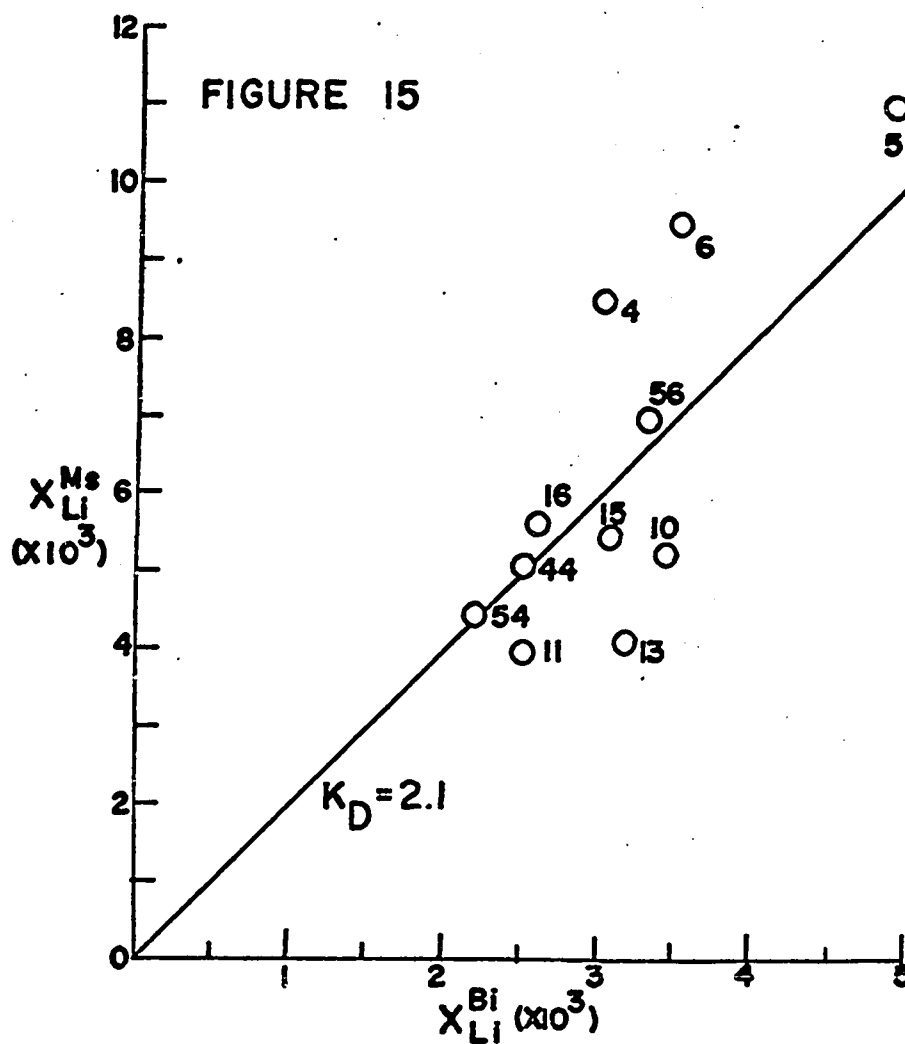


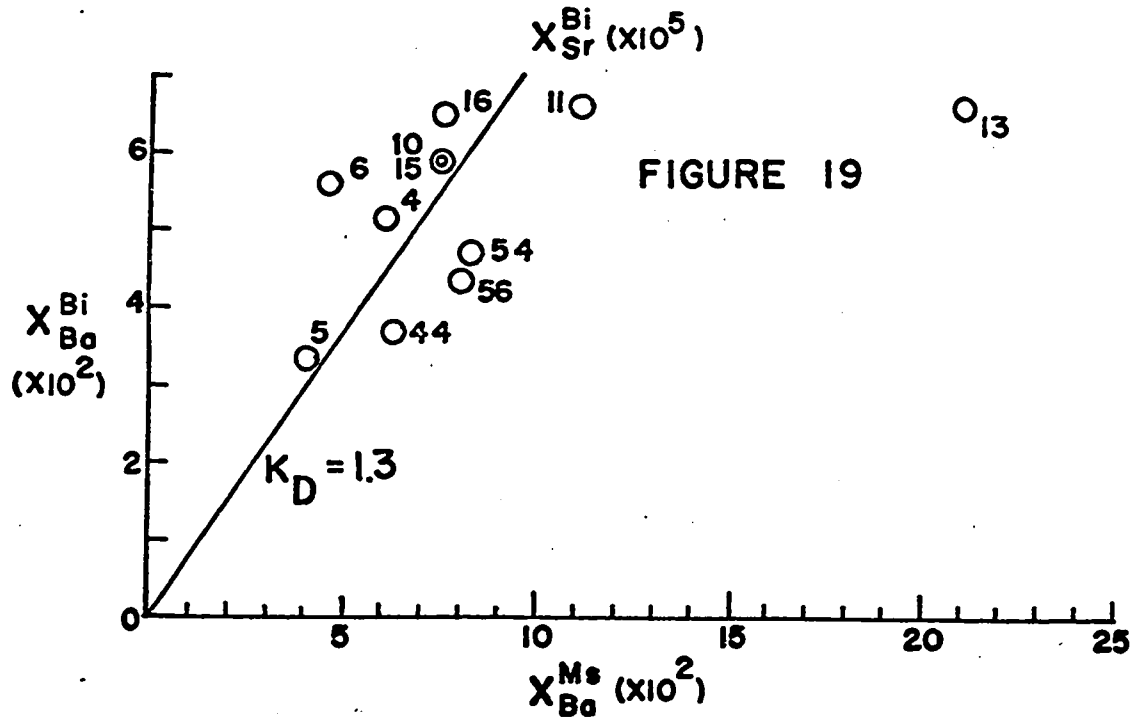
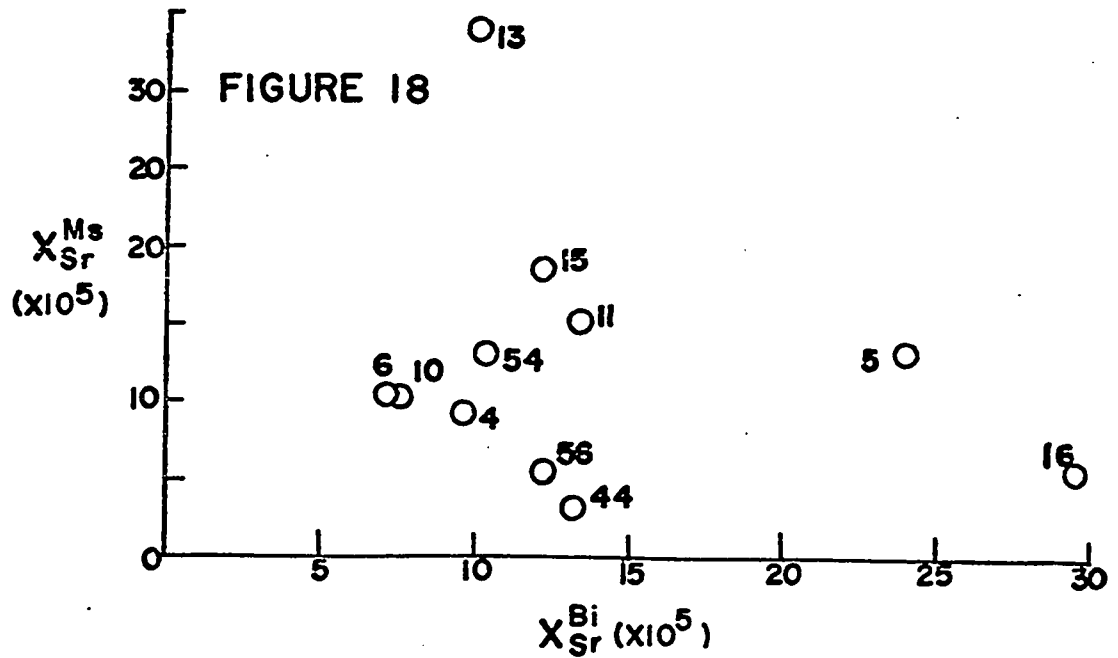
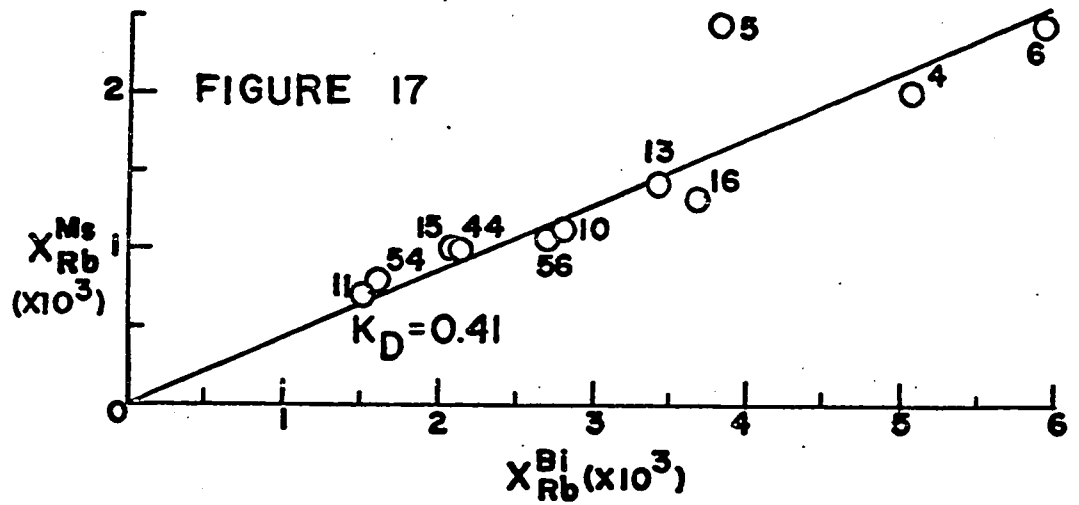


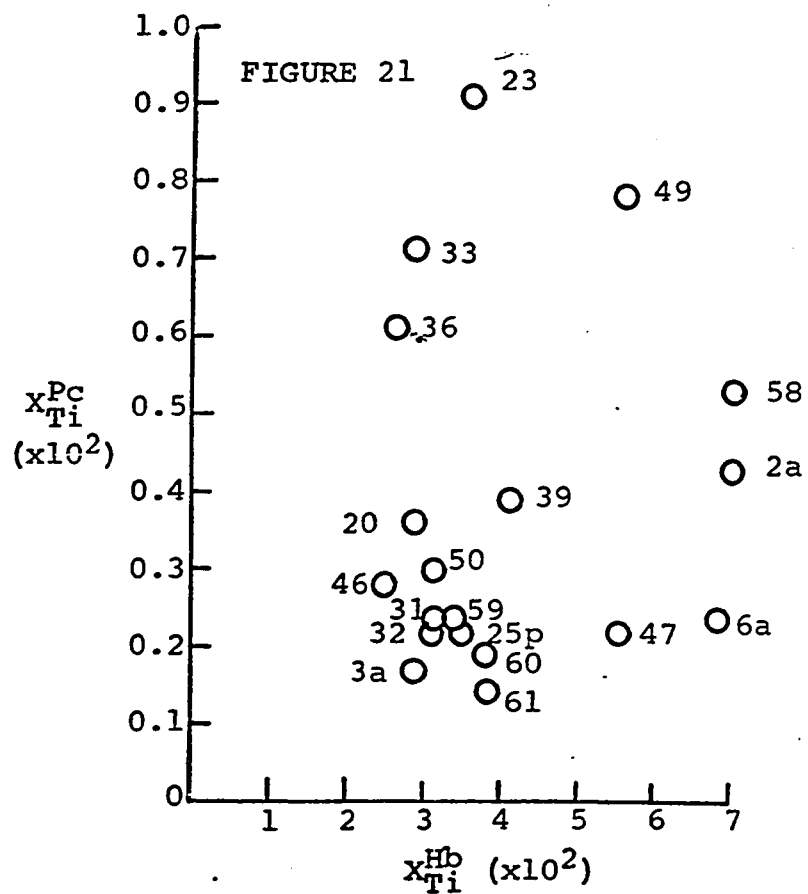
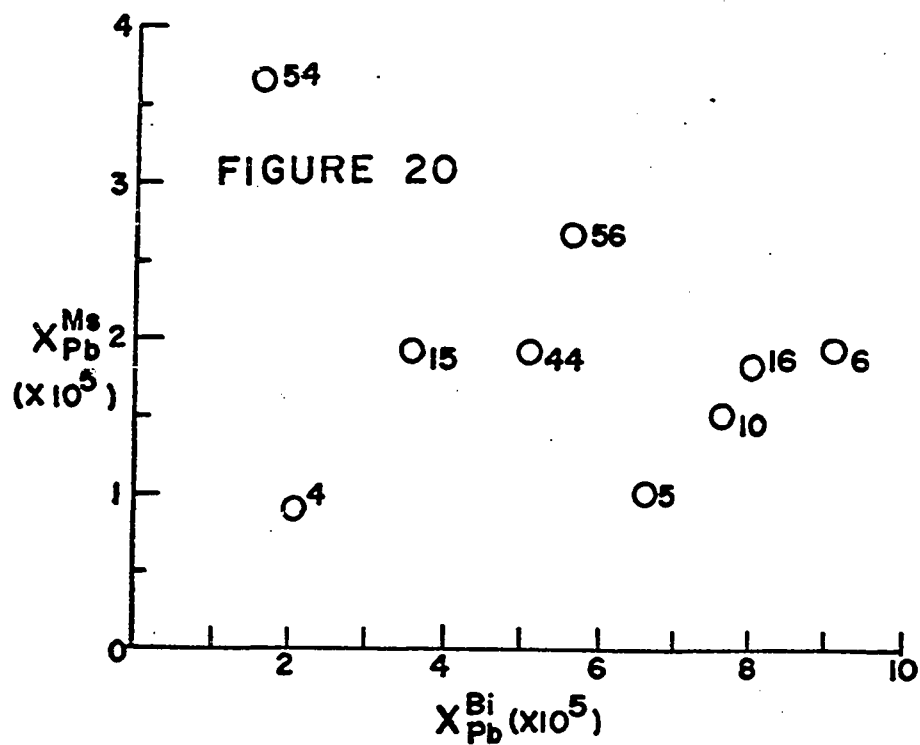


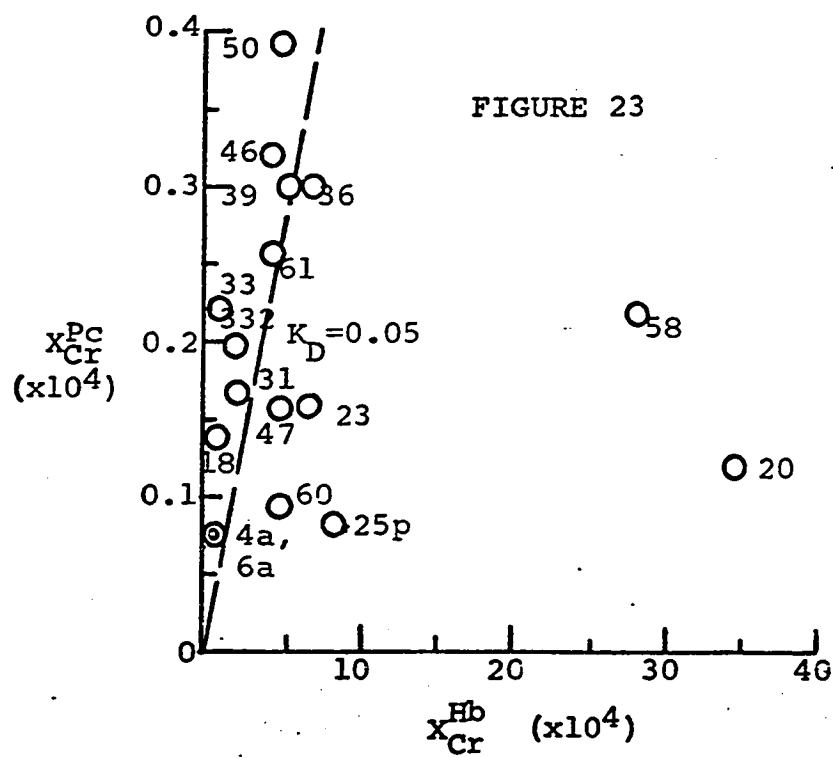
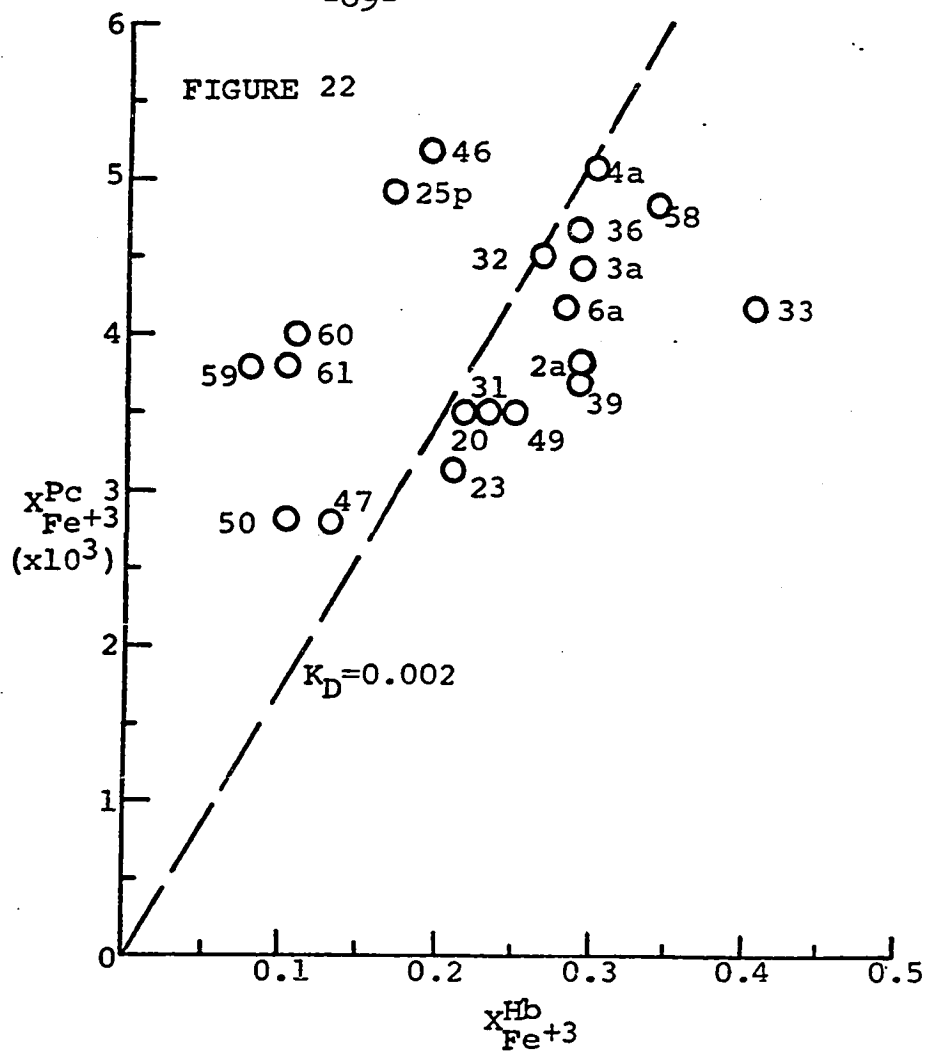


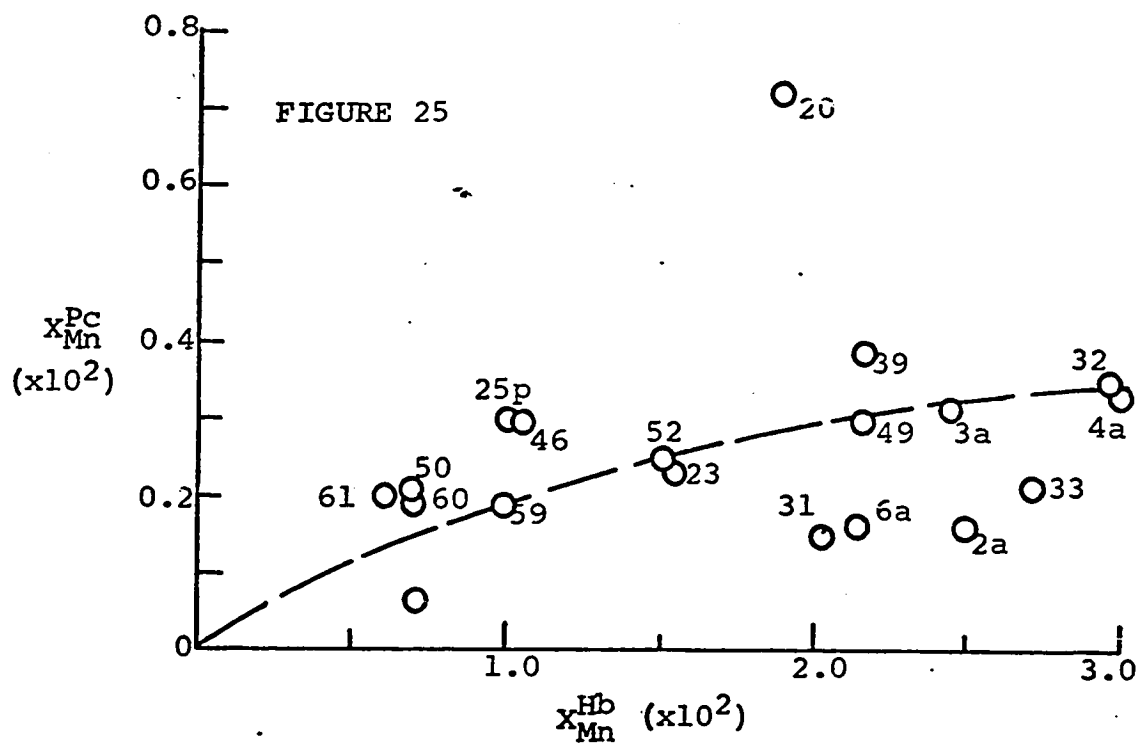
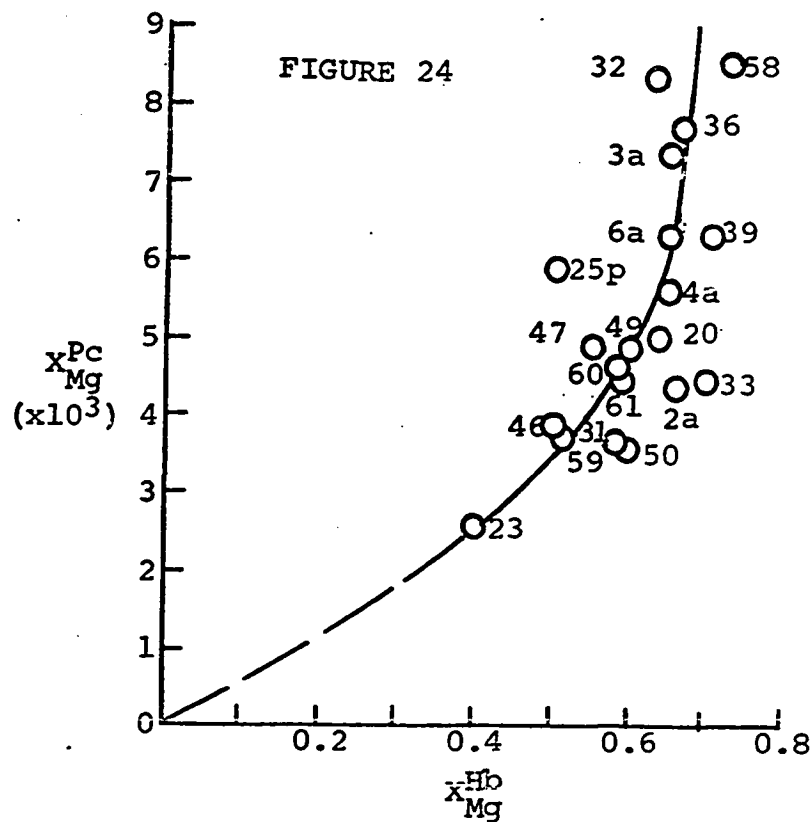


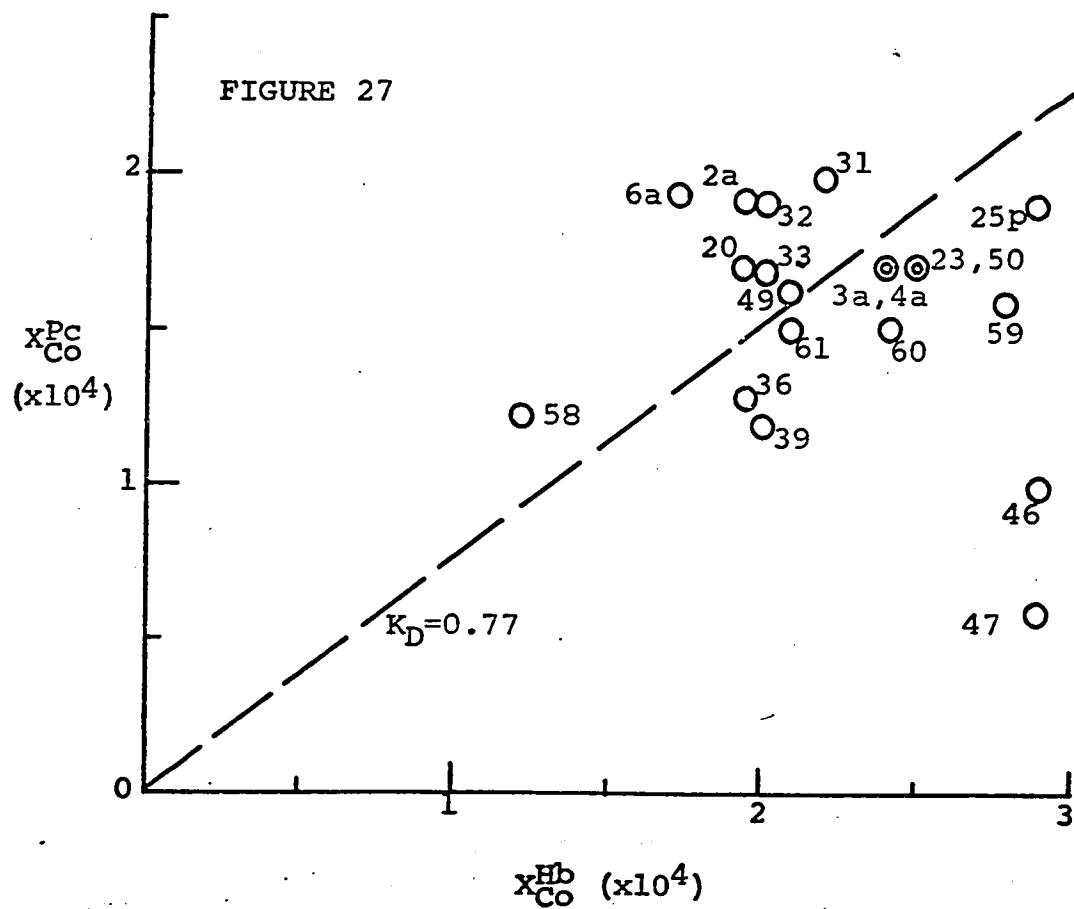
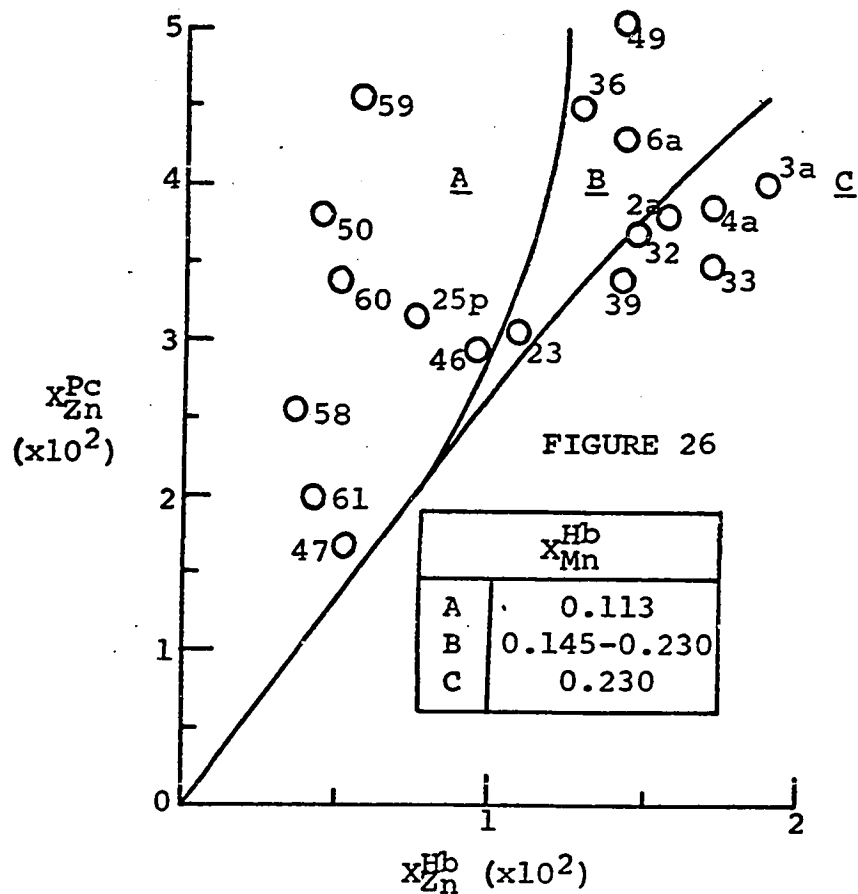






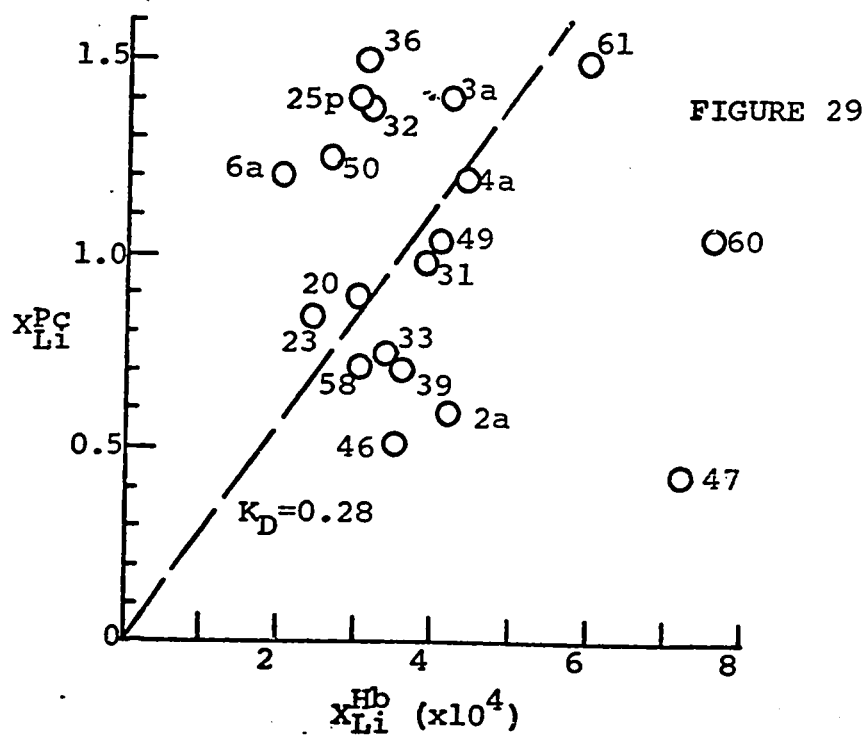
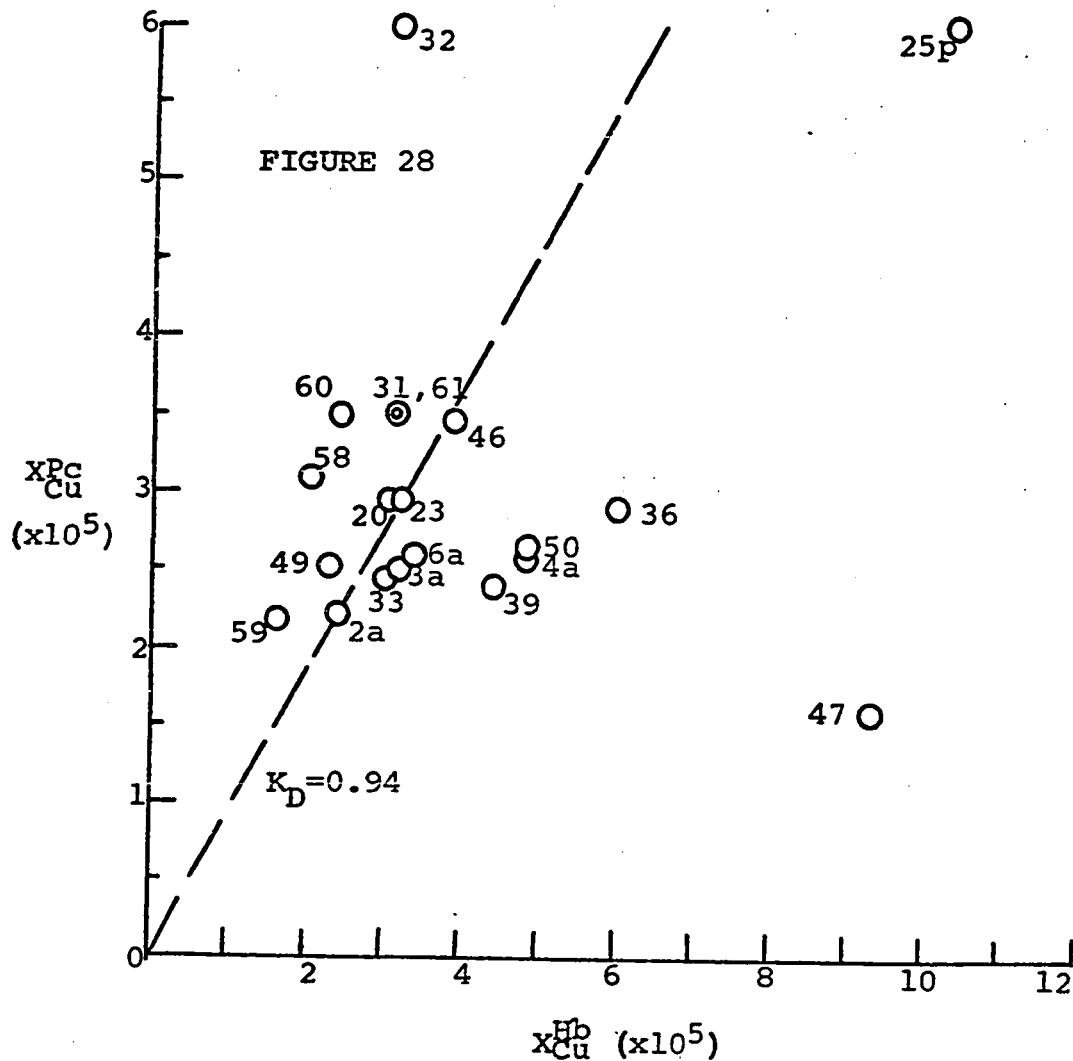


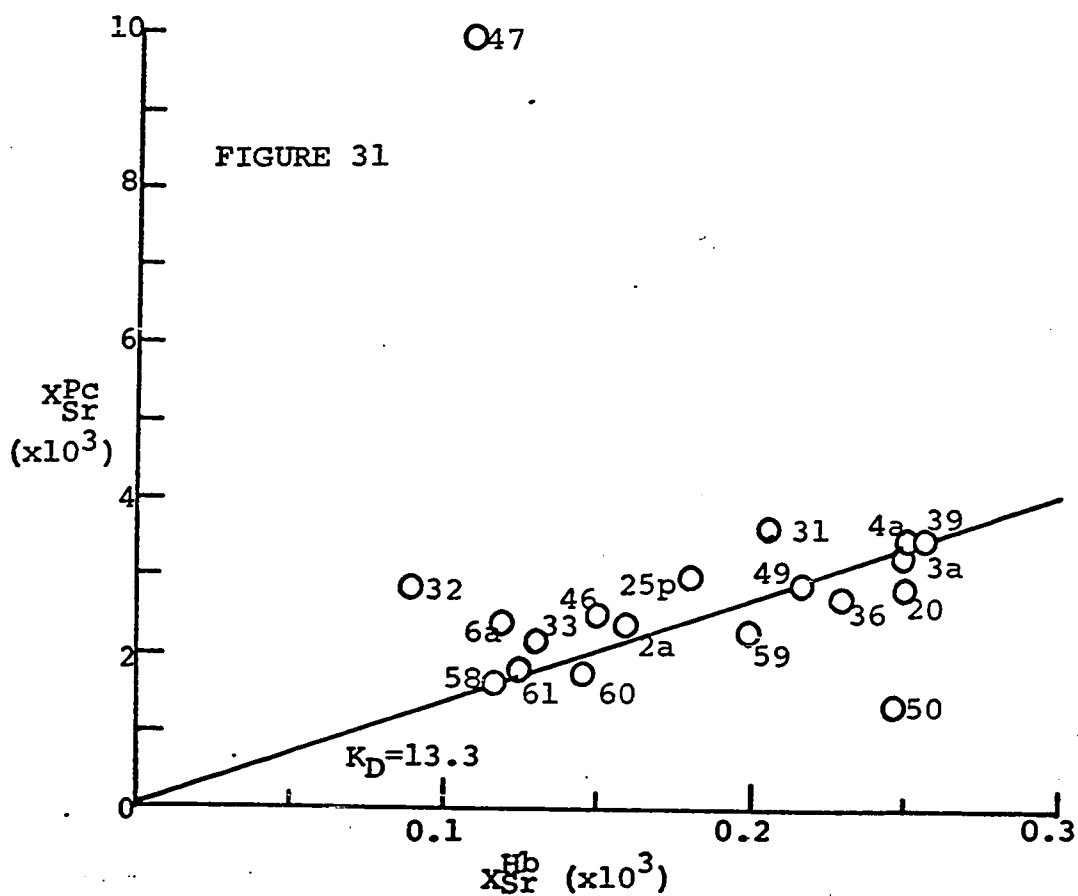
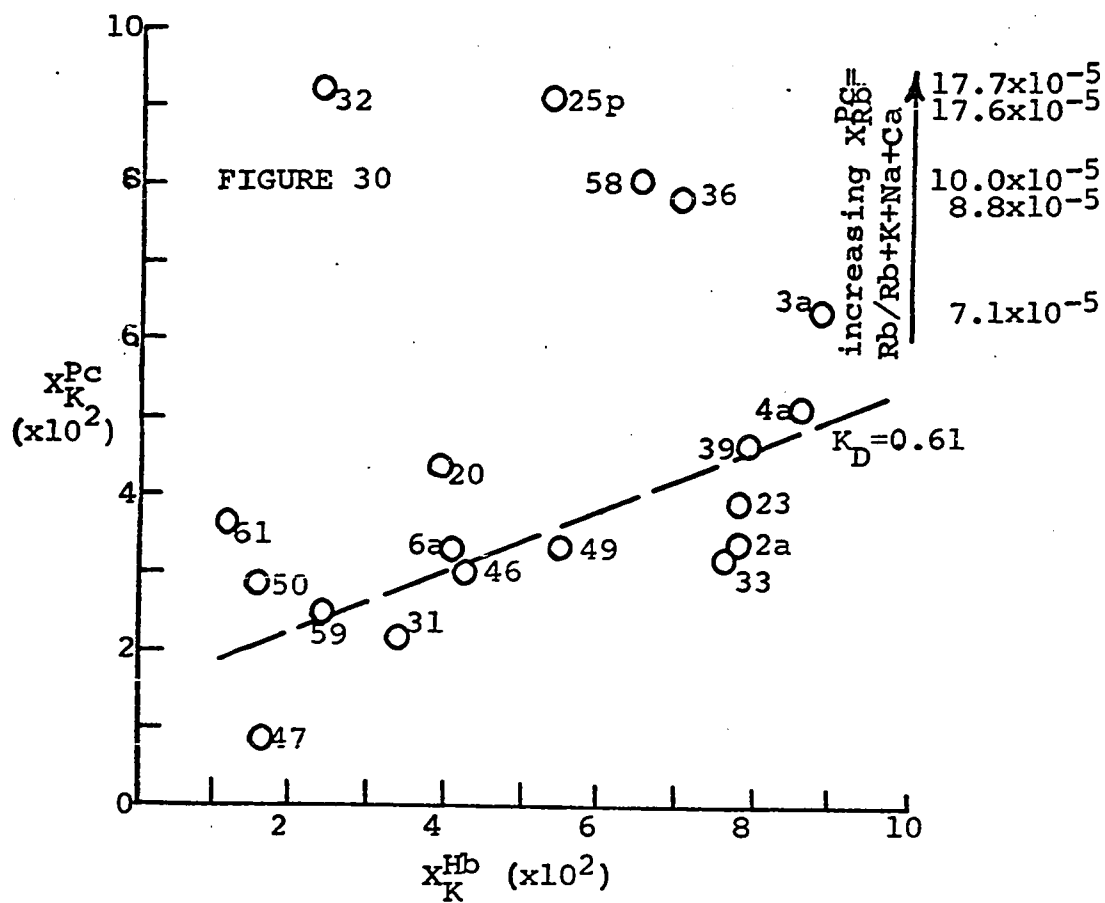


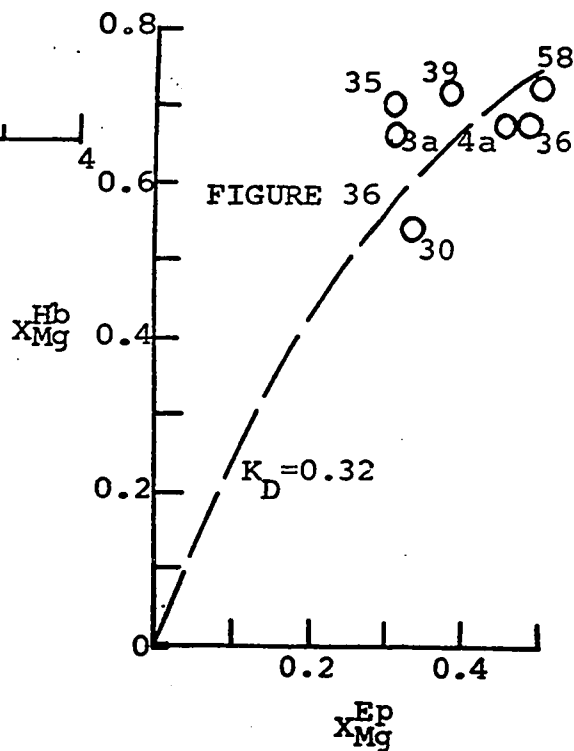
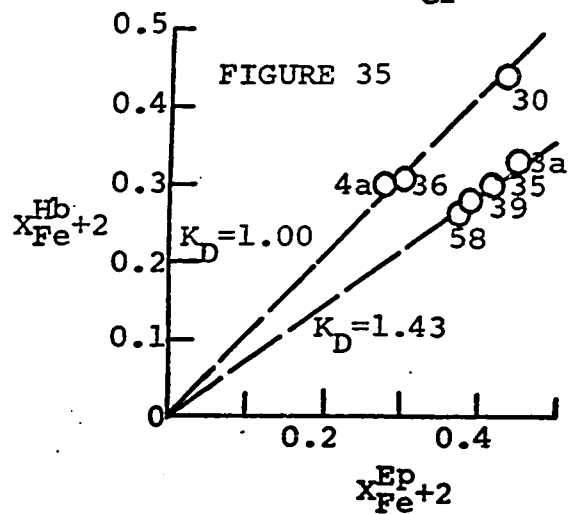
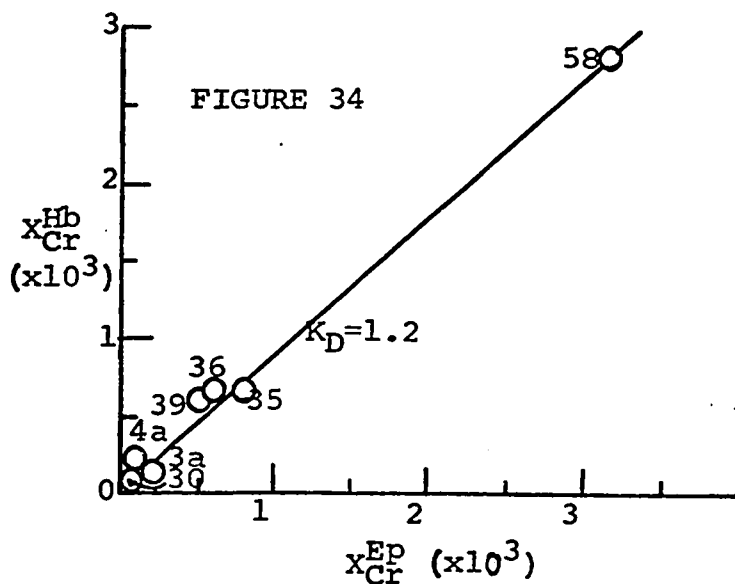
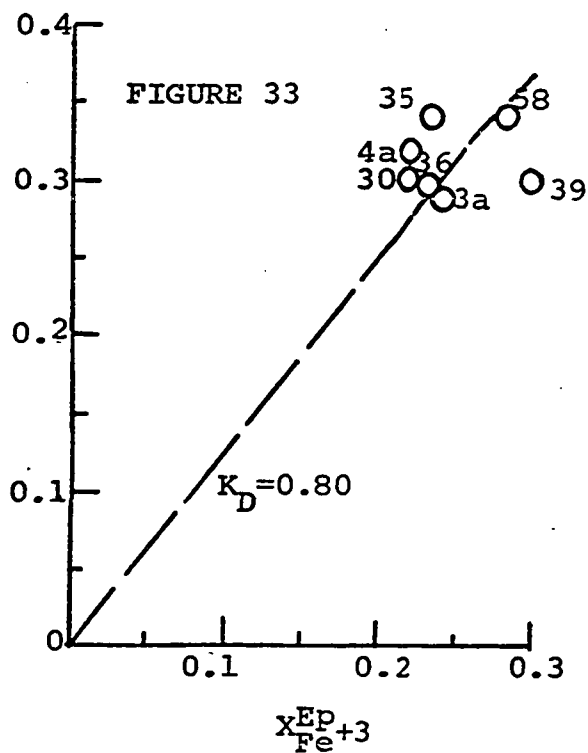
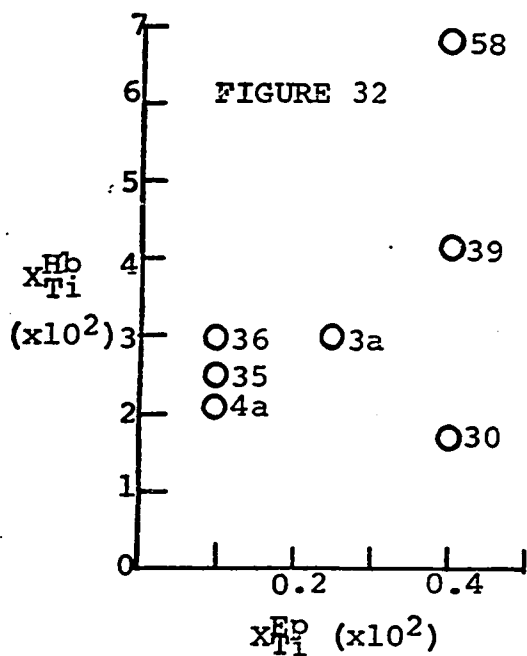




-72-







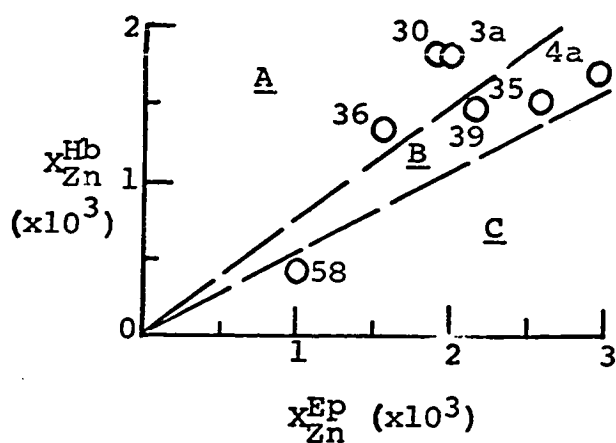
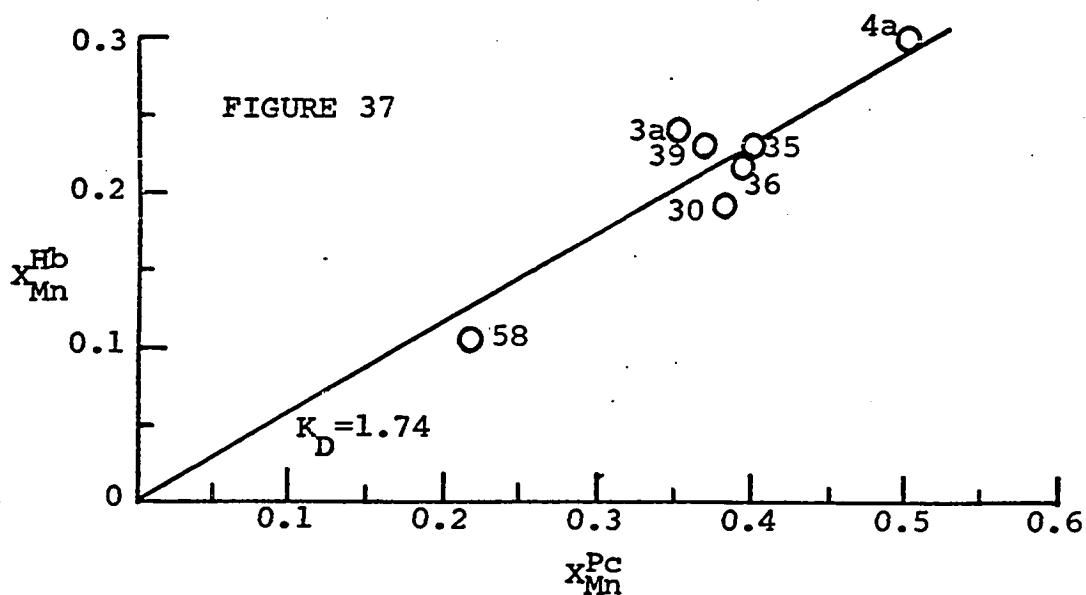
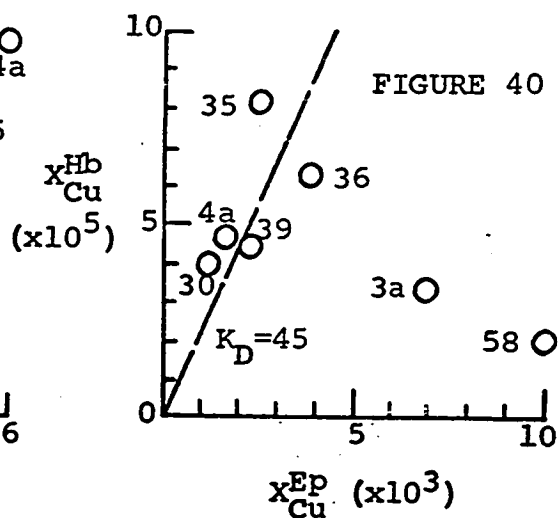
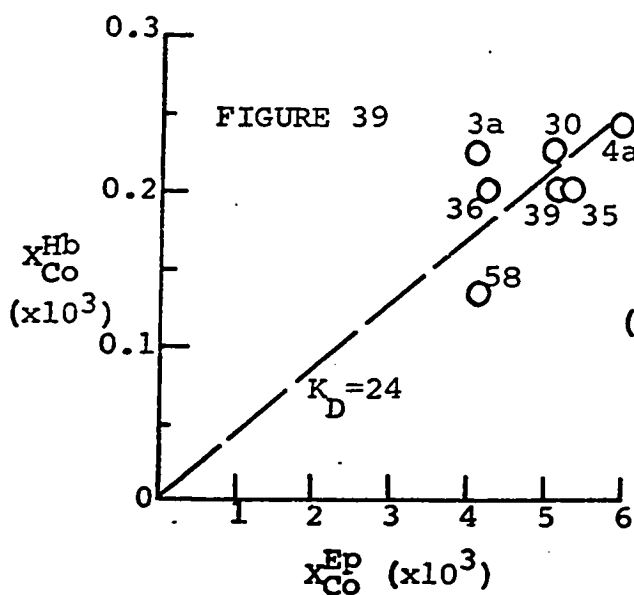
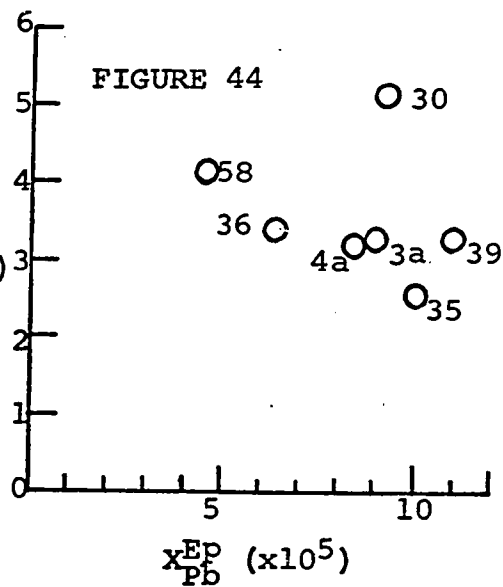
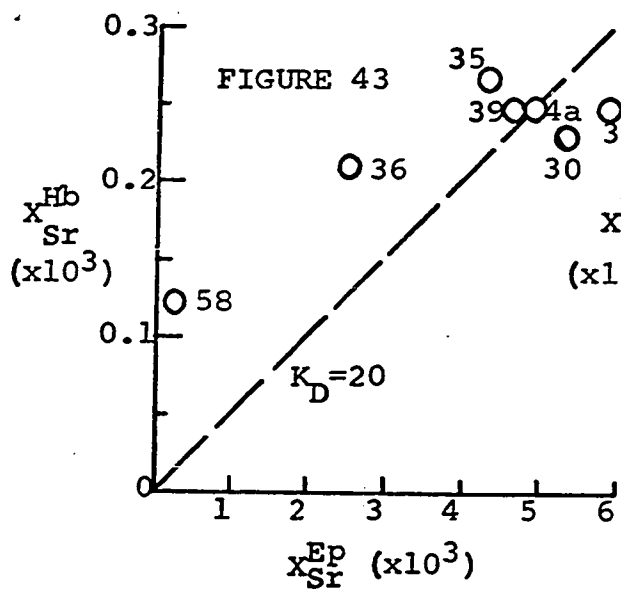
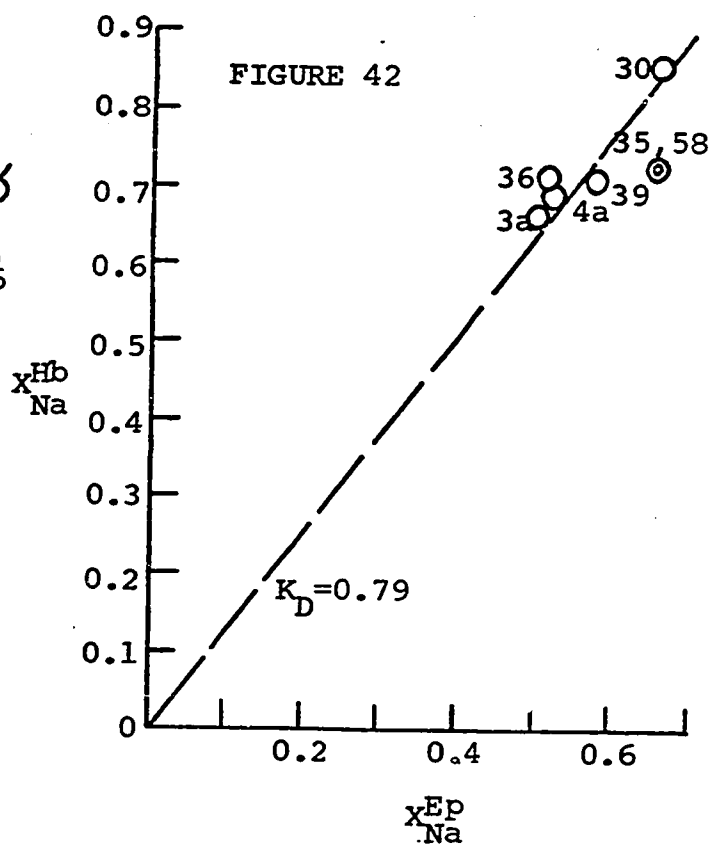
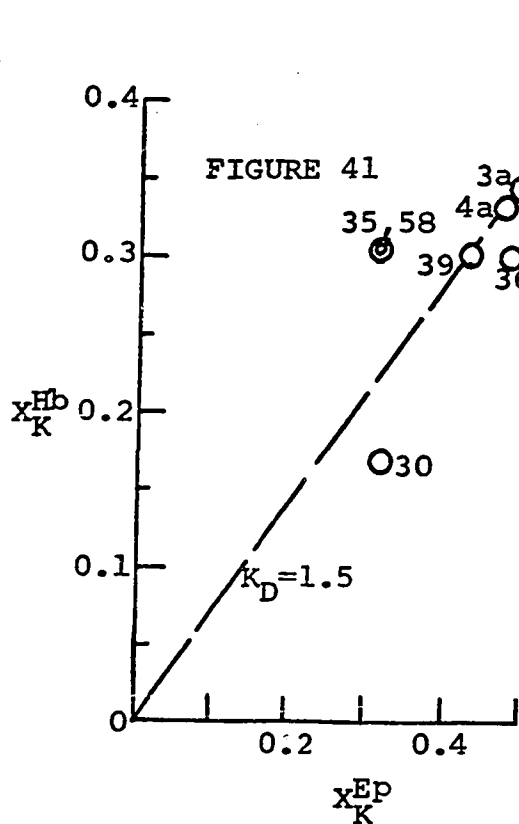
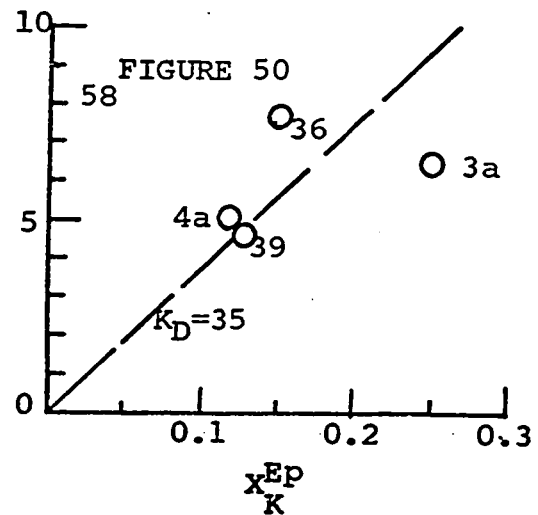
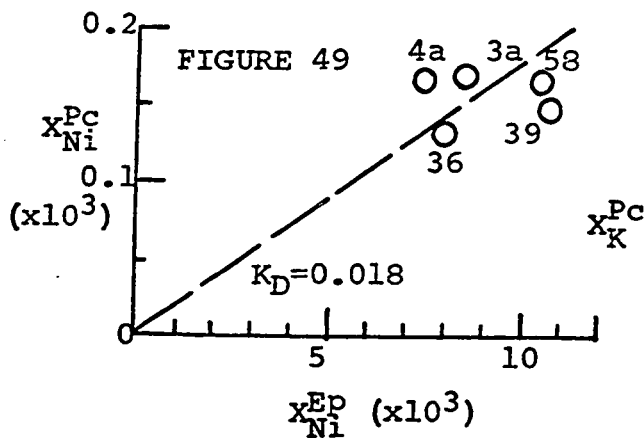
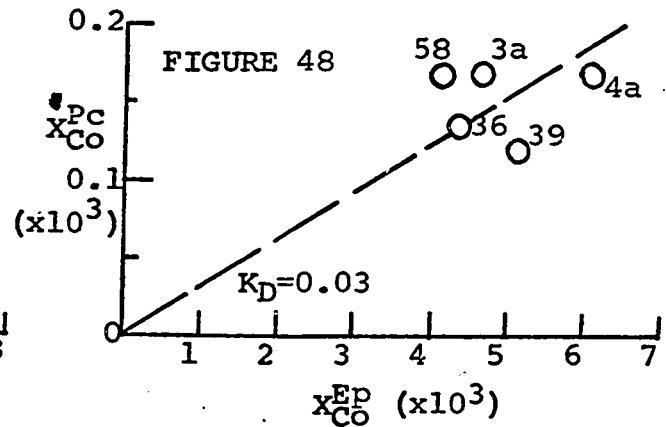
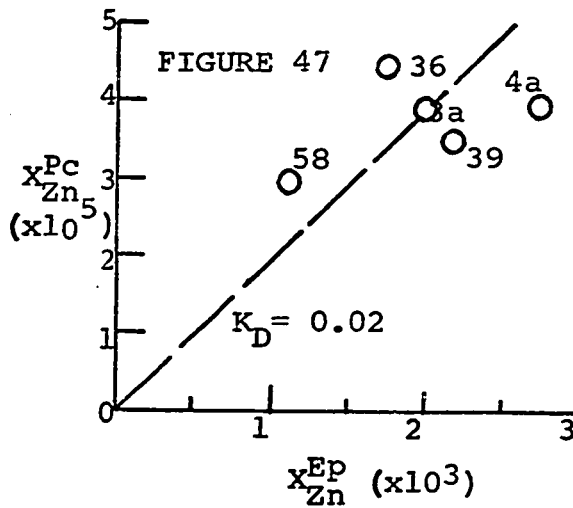
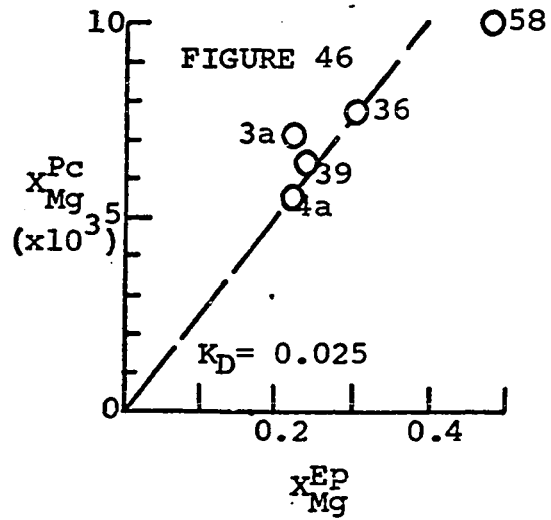
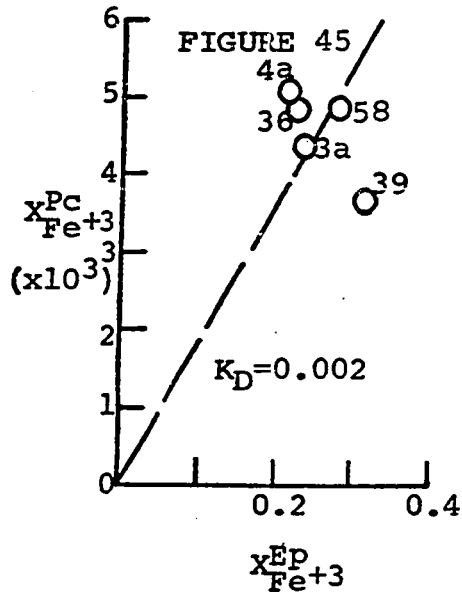


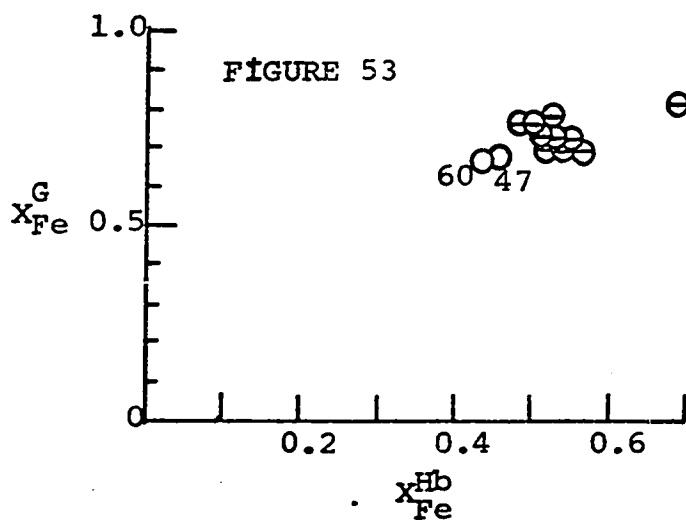
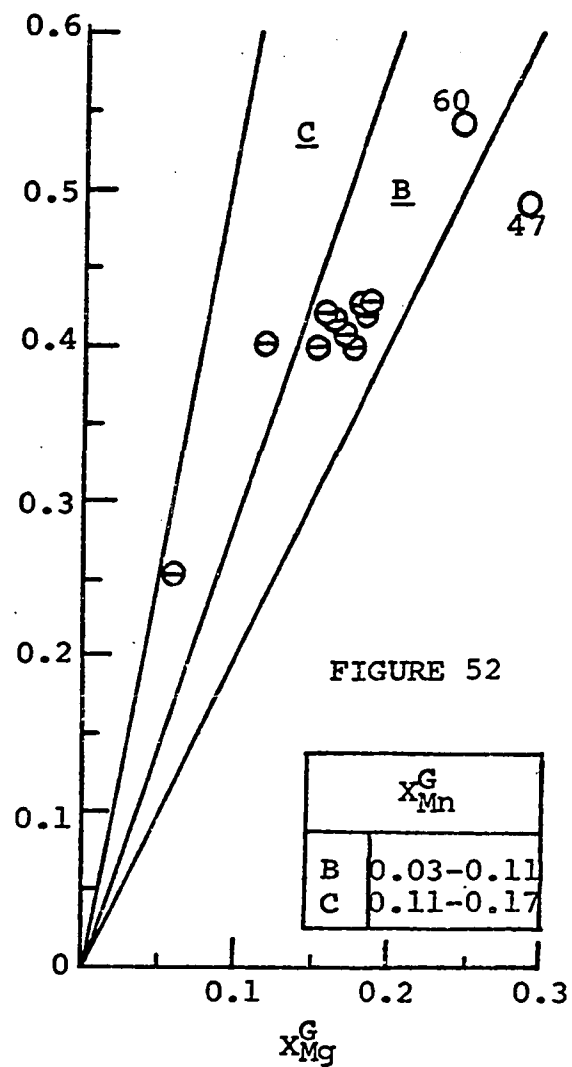
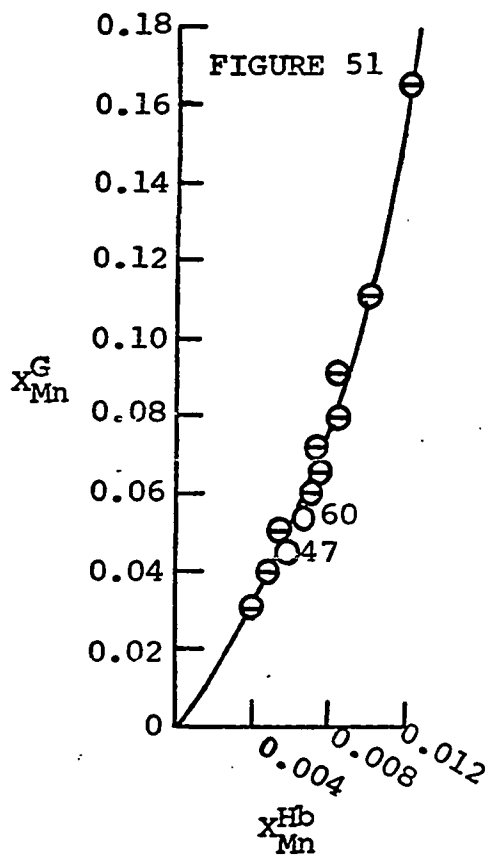
FIGURE 38

	$x_{Fe+2}^{Hb}$
A	0.31-0.44
B	0.28-0.30
C	0.26









⊖ KRETZ (1959)  
○ THIS INVESTIGATION

- Albee, A.L., 1965a, Distribution of Fe, Mg, and Mn between garnet and biotite in natural mineral assemblages: Jour. Geol. 73: 155-164.
- Albee, A.L., et al., 1965b, Phase equilibria in three assemblages of kyanite-zone pelitic schists: Lincoln Mountain Quadrangle, central Vermont: Jour. Pet. 6: 246-301.
- Ball, T.K. and R.H. Filby, 1965, The zinc contents of some geochemical standards by neutron activation and X-ray fluorescence analysis: Geochim. et Cosmochim. Acta 29: 737-740.
- Bethke, P.M. and P.B. Barton, Jr., 1959, Trace element distribution as an indication of pressure and temperature of ore deposition: Bull. Geol. Soc. Amer. 70: 1569-1570.
- Billings, G.K., 1963, Major and trace element relationships within coexisting minerals of the Enchanted Rock batholith, Llano Uplift, Texas: Doctoral Dissertation, Rice University.
- Carstens, H., 1958, Note on the distribution of some minor elements in coexisting ortho- and clino-pyroxenes: Norsk. Geol. Tidsskr. 38: 257-260.
- Carter, J.L., 1965, The origin of olivine bombs and related inclusions in basalts: Doctoral Dissertation, Rice University.
- Chinner, G.A., 1960, Pelitic gneisses with varying ferrous/ferric ratios from Glen Clova, Angus, Scotland: Jour. Pet. 1: 178-217.
- Cotton, F.A. and G. Wilkinson, 1962, Advanced Inorganic Chemistry: Interscience Publishers, 959 p.
- Curtis, C.D., 1964, Applications of the crystal-field theory to the inclusion of trace transition elements in minerals during magmatic differentiation: Geochim. et Cosmochim. Acta 28: 389-404.
- Deer, W.A., R.A. Howie, and J. Zussman, 1962, Rock Forming Minerals, vols. 1 and 3, John Wiley and Sons, Inc.
- \_\_\_\_\_, 1963, Rock Forming Minerals, vols. 2 and 4, John Wiley and Sons, Inc.
- De Vore, G.W., 1955a, The role of absorption in the distribution and fractionation of elements: Jour. Geol. 63: 159-190.



- De Vore, G.W., 1955b, Crystal growth and the distribution of elements: Jour. Geol. 63: 471-494.
- \_\_\_\_\_, 1957, The association of strongly polarizing cations as a major influence in element distribution, mineral composition, and crystal growth: Jour. Geol. 65: 178-195.
- Edwards, A.B., 1957, Amphibolites from the Broken Hill District: Jour. Geol. Soc. Australia 5: 1-32.
- Engel, A.E.J. and C.G. Engel, 1962a, Progressive metamorphism of amphibolite, northwest Adirondack Mountains, New York, from Petrologic Studies, pp. 37-82, Buddington Vol., Geol. Soc. Amer., 660 p.
- \_\_\_\_\_, 1962b, Hornblendes formed during progressive metamorphism of amphibolites, northwest Adirondack Mountains, New York, Bull. Geol. Soc. Amer. 73: 1499-1514.
- \_\_\_\_\_, and R.G. Havens, 1964, Mineralogy of amphibolite layers in the gneiss complex, northwest Adirondack Mountains, New York: Jour. Geol., 72: 131-156.
- Ernst, W.G., 1964, Petrochemical study of coexisting minerals from low-grade schists, eastern Shikoku, Japan: Geochim. et Cosmochim. Acta 28: 1631-1688.
- Evans, B.W. and B.E. Leake, 1960, The composition and origin of the striped amphibolites of Connemara, Ireland: Jour. Pet. 1: 337-363.
- Ewell, W.T. and J.A.F. Gidley, 1963, Atomic Absorption Spectrometry: The Macmillan Co.
- Fairbairn, H.W., L.H. Ahrens, and L.G. Garfinkle, 1953, Minor element content of Ontario diabase; Geochim. et Cosmochim. Acta 3: 34-46.
- Filby, R.H., 1964, The contents of several trace elements in some standard rock samples: Geochim. et Cosmochim. Acta 28: 265-267.
- Fleisher, M., 1965, Summary of new data on rock samples G-1 and W-1, 1962-1965: Geochim. et Cosmochim. Acta 29: 1263-1284.
- Francis, G.H., 1958, The amphibolite of Doir'a 'Chatha (Durcha), Sutherland: Geol. Mag. 95: 25-40.
- Fredrickson, A.F., 1962, Partition coefficients - new tool for studying geologic problems: Bull. Amer. Assn. Petrol. Geol. 46: 518-534.

- Frost, M.J., 1962, Metamorphic grade and the Fe-Mg distribution between coexisting garnet-biotite and garnet-hornblende: *Geol. Mag.* 99: 427-438.
- Fyfe, W.S., F.J. Turner, and J. Verhoogen, 1958, Metamorphic Reactions and Metamorphic Facies: *Geol. Soc. Amer. Memoir* 73, 259 p.
- Goldschmidt, V.M., 1937, The principles of distribution of chemical elements in minerals and rocks: *Jour. Chem. Soc.* 1937, 655.
- Green, J.C., 1963, High-level metamorphism of pelitic rocks in northern New Hampshire: *Amer. Min.* 48: 991-1023.
- Greenwood, H.J., B.R. Doe, and W.C. Phinney, 1964, A discussion. Phase equilibria in the metamorphic rocks of St. Paul Island and Cape North, Nova Scotia: *Jour. Pet.* 5: 189.
- Hall, R.N., 1957, Variation of the distribution coefficient and solid solubility with temperature: *Jour. Phys. Chem. Solids* 3: 63-73.
- Hamilton, E.I., 1965, *Applied Geochronology*, Academic Press, 267 p.
- Harker, A., 1893, On the migration of material during the metamorphism of rock masses: *Jour. Geol.* 1: 574-578.
- Harriss, R.C. and J.A.S. Adams, 1966, Geochemical and mineralogical studies on the weathering of granitic rocks: *Amer. Jour. Sci.* 264: 146-173.
- Hay-Roe, Hugh, 1957, *Geology of Wylie Mountains and vicinity, Culberson and Jeff Davis Counties, Texas: Geologic Quadrangle Map No. 21, Bureau of Economic Geology, University of Texas.*
- Hill, A.E., G.S. Durham, and J.E. Ricci, 1940, Distribution of isomorphous salts in solubility equilibrium between liquid and solid phases: *Jour. Amer. Chem. Soc.* 62: 2723-2732.
- Kaye, M.J., 1965, X-ray fluorescent determinations of several trace elements in some standard geochemical samples: *Geochim. et Cosmochim. Acta* 29: 139-141.
- King, P.B. and P.T. Flawn, 1953, *Geology and Mineral Deposits of Pre-Cambrian Rocks of the Van Horn Area, Texas: University of Texas Publication*, 218 p.

- Kretz, R., 1959, Chemical study of garnet, biotite, and hornblende from gneisses of southwestern Quebec, with emphasis on distribution of elements in coexisting minerals: Jour. Geol. 67: 371-402.
- \_\_\_\_\_, 1960, Distribution of certain elements among coexisting calcic amphibole, and biotite in skarns: Geochim. et Cosmochim. Acta 20: 161-191.
- \_\_\_\_\_, 1961, Some applications of thermodynamics to coexisting minerals of variable composition: Jour. Geol. 69: 361-387.
- \_\_\_\_\_, 1964, Analysis of equilibrium in garnet-biotite-sillimanite gneisses from Quebec: Jour. Pet. 5: 1-20.
- McClure, D.S., 1957, The distribution of transition metal cations in spinels: Jour. Phys. Chem. Solids 3: 311-317.
- McIntire, W.L., 1963, Trace element partition coefficients - a review of theory and applications to geology: Geochim. et Cosmochim. Acta 27: 1209-1264.
- McKay, D.S., 1964, A chemical study of coexisting metamorphic muscovite and biotite from eastern New York and western Connecticut: Doctoral Dissertation, Rice University.
- Miyashiro, A., 1953, Ca-poor garnet in relation to metamorphism: Geochim. et Cosmochim. Acta 4: 179-200.
- \_\_\_\_\_, 1956, Garnet-biotite equilibrium in some metamorphic rocks of the Ryoke zone: Jour. Geol. Soc. Japan 62: 700-702.
- \_\_\_\_\_, 1957, The chemistry, optics, and genesis of the alkali-amphiboles: Jour. Fac. Sci., Univ. of Tokyo, Sec. II, 11, pt. 1, 57-83.
- Mueller, R.F., 1960, Compositional characteristics and equilibrium relations in mineral assemblages of a metamorphosed iron formation: Amer. Jour. Sci. 258: 449-497.
- \_\_\_\_\_, 1961, Analysis of relations among Mg, Fe, and Mn in certain metamorphic minerals: Geochim. et Cosmochim. Acta 25: 267-296.
- \_\_\_\_\_, 1962, Energetics of certain silicate solid solutions: Geochim. et Cosmochim. Acta 26: 581-598.
- Neumann, H., J. Mead, and C.J. Vitaliano, 1954, Trace element variation during fractional crystallization as calculated from the distribution law: Geochim. et Cosmochim. Acta 6: 90-99.

- Nockolds, S.R., 1966, The behavior of some elements during fractional crystallization of some magma: *Geochim. et Cosmochim. Acta* 30: 267-278.
- Nockolds, S.R. and R.L. Mitchell, 1948, The geochemistry of some Caledonian rocks: A study in the relationship between the major and trace elements in igneous rocks and their minerals: *Trans. Roy. Soc. Edinb.* 61: 533-575.
- Phinney, W.C., 1963, Phase equilibrium in the metamorphic rocks of St. Paul and Cape North, Nova Scotia: *Jour. Pet.* 4: 90-103.
- Radoslovich, E.W., 1963a, The cell dimensions and symmetry of layer lattice silicates IV, Interatomic forces: *Amer. Min.* 48: 76-99.
- , 1963b, The cell dimensions and symmetry of layer lattice silicates V, Composition limits: *Amer. Min.* 48: 348-367.
- Ramberg, H. and G.W. De Vore, 1951, The distribution of  $\text{Fe}^{+2}$  and  $\text{Mg}^{+2}$  in coexisting olivines and pyroxenes: *Jour. Geol.* 59: 193-210.
- Ringwood, A.E., 1955, The principles governing trace element distribution during magmatic crystallization: *Geochim. et Cosmochim. Acta* 7: 189-202.
- Shapiro, L., 1960, A spectrophotometric method for determining the FeO in rocks: U.S. Geol. Survey Prof. Paper no. 400, B496-B497.
- and W.W. Brannock, 1962, Rapid analysis of silicate, carbonate, and phosphate rocks: *Geol. Survey Bull.* 1144-A, 55 p.
- Shaw, D.M., 1953, The camouflage principle and trace element distribution in magmatic minerals: *Jour. Geol.* 61: 142-151.
- Smith, F.G., 1963, *Physical Geochemistry*: Addison-Wesley Pub. Co., 624 p.
- Solodov, N.A., 1960, Distribution of alkali metals and minerals of a zoned pegmatite in the Mongolian Altai: *Geokhimiya*, 1960, no. 8, 874-885.
- Stevens, R.E., 1946, A system for calculating analyses of micas and related minerals to end members: *U.S. Geol. Survey Bull.* 950, 101-119.

- Stewart, F.H., 1942, Chemical data on a silica-poor argillaceous hornfels and its constituent minerals: *Min. Mag.* 26: 260-266.
- Stow, S.H., 1965, A radiometric and chemical study of the binary Fitzwilliam granite of New Hampshire: Master's Dissertation, Rice University.
- Strens, R.G.J., 1966, Stability and relations of the Fe-Al epidotes: *Min. Mag.* 36: 464-475.
- Stubicon, U. and R. Roy, 1961, Isomorphous substitution and infrared spectra of the layer lattice silicates: *Amer. Min.* 46: 32-51.
- Sturt, B.A., 1962, The composition of garnets from pelitic schists in relation to the grade of regional metamorphism: *Jour. Pet.* 3: 181-191.
- Taylor, S.R., 1955, The origin of some New York metamorphic as shown by their major and trace element abundances: *Geochim. et Cosmochim. Acta* 8: 182-197.
- \_\_\_\_\_ and P. Kolbe, 1964, Geochemical standards: *Geochim. et Cosmochim. Acta* 28: 447-454.
- Thompson, J.B., Jr., 1955, The thermodynamic basis for the mineral facies concept: *Amer. Jour. Sci.* 253: 65-103.
- \_\_\_\_\_, 1957, The graphical analysis of mineral assemblages in pelitic schists: *Amer. Min.* 42: 842-858.
- Trumbore, F.A., C.R. Isenberg, and E.M. Porbansky, 1958, On the temperature dependence of the distribution coefficient: *Jour. Phys. Chem. Solids* 9: 60-69.
- Turekian, K.K. and W.C. Phinney, 1962, The distribution of Ni, Co, Cr, Cu, Ba, and Sr between biotite-garnet pairs in a metamorphic sequence: *Amer. Min.* 47: 1434-1441.
- Turner, F.J. and J. Verhoogen, 1960, *Igneous and Metamorphic Petrology*: McGraw-Hill, 694 p.
- Twiss, P.C., 1959, *Geology of Van Horn Mountains, Texas: Geologic Quadrangle Map no. 23*, Bureau of Economic Geology, University of Texas.
- Wager, L.R. and R.L. Mitchell, 1951, Distribution of trace elements during strong fractionation of basic magma - a further study of the Skaergaard intrusion: *Geochim. et Cosmochim. Acta* 1: 129-208.

Webber, G.R., 1965, Second report of analytical data for CAAS syenite and sulphide standards: *Geochim. et Cosmochim. Acta* 29: 229-248.

Weill, D.F. and W.S. Fyfe, 1964, A discussion of the Korzhinskii and Thompson treatment of thermodynamic equilibrium in open systems: *Geochim. et Cosmochim. Acta* 28: 565-576.

Yoder, H.S., 1952, The  $MgO-Al_2O_3-SiO_2-H_2O$  system and the related metamorphic facies: *Amer. Jour. Sci.*, Bowen Vol., 569-527.

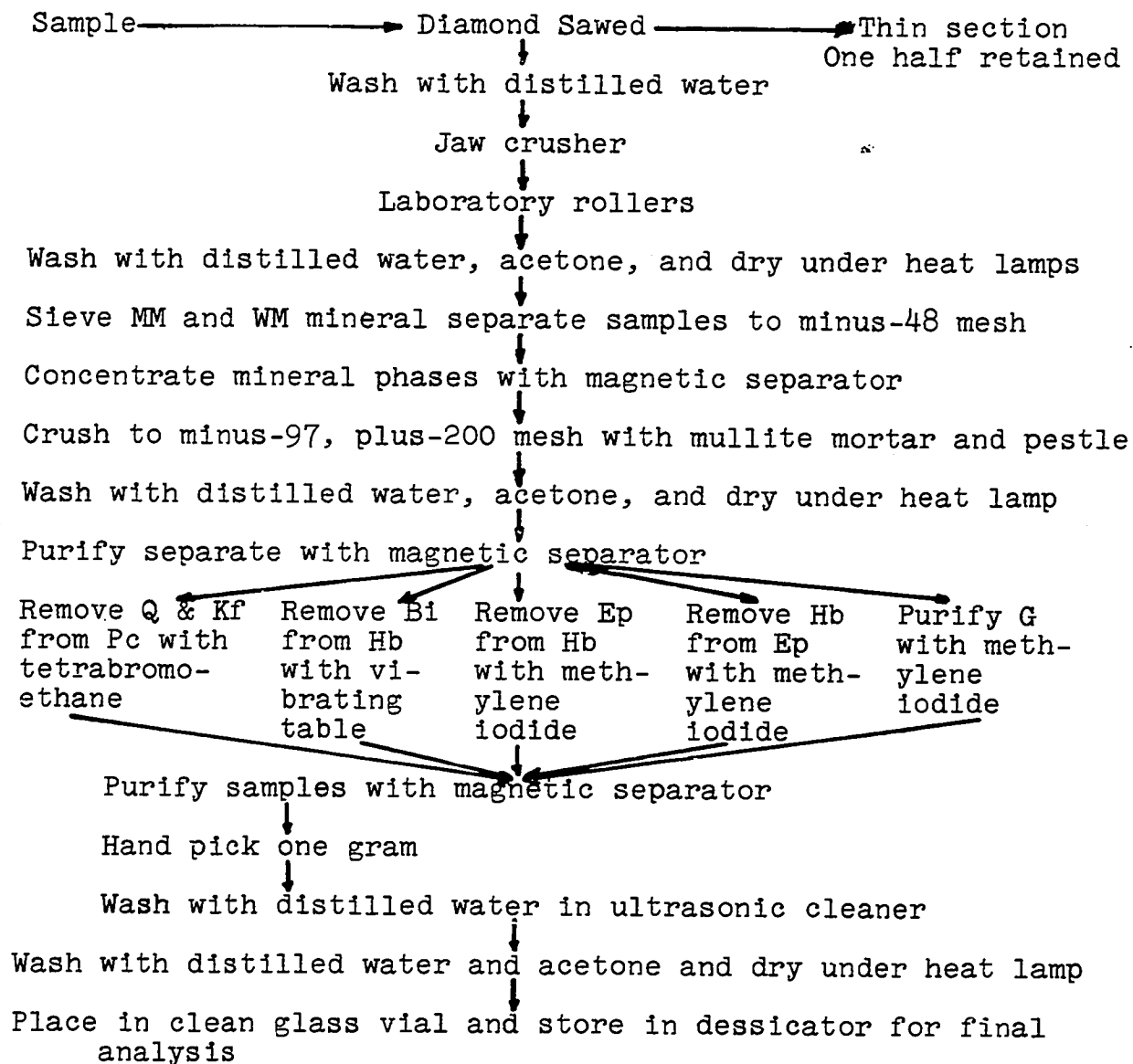
Zartman, R.E., 1965, Rubidium-strontium age of some metamorphic rocks from the Llano Uplift, Texas: *Jour. Pet.* 6: 28-36.

## APPENDIX

### SAMPLE PREPARATION

All samples for this investigation were collected during the spring and summer of 1965, and were generally two to three pounds in size. The original piece was cut by means of a diamond saw into two smaller pieces, one for sample preparation and one for reference (see Fig. 54). A slab was also cut in order that a thin section might be prepared. The portion for analysis was trimmed to remove the outer weathered material, and the weight recorded (Table 4). All samples were broken by means of  $3\frac{1}{4}$  by  $4\frac{1}{2}$  inch Denver jaw crusher to one-half inch pieces and then crushed further with a Sturtevant laboratory roll. The pulverized samples from which mineral separates were to be prepared were washed with distilled water and reagent grade acetone to remove the fine dust particles in order that the magnetic separator might be used.

In order that the Frantz Isodynamic separator might be used more efficiently, it was necessary to wash the ground sample as described above and remove all grains larger than 48 mesh. The minus-48 mesh portion was run through the magnetic separator and the various mineral phases concentrated to about 90% purity. In most cases about 15 to 30 grams of each phase was retained for further purification, and this portion was ground in a mullite mortar and pestle to pass a 97-mesh nylon screen and fall onto a 200-mesh screen,



Flow Diagram for Sample Preparation

Figure 54



Table 4  
Sample Weights

<u>Sample</u>	<u>Wt.-gms.</u>	<u>Sample</u>	<u>Wt.-gms.</u>
MM 2a	155	MM 33	295
MM 3a	100	MM 35	275
MM 4a	360	MM 36	300
MM 6a	200	MM 39	280
MM 4	250	MM 44	270
MM 6	140	MM 45	320
MM 10	390	MM 46	260
MM 11	300	MM 47	275
MM 13	80	MM 49	298
MM 15	250	MM 50	320
MM 16	350	MM 51	255
MM 18	120	MM 54	286
MM 20	260	MM 55	300
MM 23	200	MM 56	320
MM 25h	70	MM 58	310
MM 25p	220	MM 59	285
MM 30	365	MM 60	245
MM 31	293	MM 61	315
MM 32	285	WM 5	285

washed with distilled water and reagent grade acetone and dried under heat lamps. Further purification was carried out on samples by repeated passes through the isodynamic separator to remove phases of greatly different magnetic susceptibility from the mineral under consideration. In this fashion acidic phases such as quartz and feldspar could be quite efficiently separated from the basic minerals such as hornblende, anthophyllite, epidote, biotite, and almandine. The separation of muscovite from biotite, feldspar, and quartz was almost 100% efficient by means of the magnetic separator, but separations within the acidic and basic groups proved to be less efficient and more difficult. In samples containing potassium feldspar and/or quartz in addition to plagioclase, magnetic means could not be used. It was found that tetrabromoethane diluted with acetone, and extensive hand picking were the best methods.

As mentioned above, the purification of muscovite and biotite by magnetic means was relatively simple, but the complete removal of epidote and biotite from hornblende was quite frustrating. Magnetic separation means proved to be only about 90% effective in the separation of hornblende and epidote and had little effect on the removal of biotite from hornblende. Biotite was effectively removed employing a tilted shaking table and collecting the hornblende grains which rolled off the glazed paper top while the biotite flakes were retained. Owing to the overlap in densities of the biotite and hornblende, heavy liquids could not be used as they were

for the removal of epidote from hornblende. Little biotite appeared in the epidote samples because of its original concentration with the hornblende during the initial magnetic separation. Use of methylene iodide coupled with hand picking was effective in the final purification of hornblende and epidote samples.

Purification of the few almandine and anthophyllite phases was not excessively difficult and was performed coupling the use of methylene iodide with magnetic means.

Final hand picking of about one gram of each sample was performed at 40 power magnification employing a binocular microscope and a small moist brush. This portion was washed for about one hour with a Bendix Model SEC-48 ultrasonic cleaner by placing the sample in a one-inch diameter test-tube and suspending the tube in the sonic bath. After the cleaning period, the pure mineral separate was washed with distilled water and acetone and dried under a heat lamp for one hour. The dried sample was finally placed in a clean, dry glass vial and stored in a dessicator.

Grain counts of the clean separates indicated most of the samples to be at least 99.9% pure. Hand picking of contaminating epidote grains from the hornblende and plagioclase samples was 100% effective owing to the definite color differences among the phases. Most remaining biotite could be distinguished and removed from the hornblende, and never remained in excesses of one grain in 1,000. Epidote separates were often contaminated with about 0.1 to 0.5% hornblende,

but always in the form of composite grains. Contamination of plagioclase with quartz and potassium feldspar was estimated to range up to 0.5% in some cases because of the difficulty in distinguishing among these minerals under the binocular microscope. Muscovite and biotite always approached 100% purity. Any contamination of the muscovite was in the form of composite grains with biotite. Anthophyllite was at least 99.9% pure, but contamination of the almandine by composite hornblende grains was about 0.5%.

#### CHEMICAL PREPARATION, PRECISION, SENSITIVITY, AND ANALYSIS

In most cases 100-fold stock solutions were prepared for further dilution and analysis by dissolving a  $0.5000 \pm 0.0010$  gram portion of the cleaned dry mineral separate in hydrofluoric and nitric acids and diluting to 50.0 mls. In some cases a  $0.2500 \pm 0.0010$  gram sample was used and the final dilution was made to 25 mls.

The sample was weighed onto a small piece of drafting linen and transferred to a 100 ml. FEP teflon beaker, at which time 10 mls. of concentrated reagent grade  $\text{HNO}_3$  were added and the beaker, covered with a teflon watch glass, was heated under a heat lamp for 1.5 hours. Six mls. of concentrated HF were added and the covered beaker allowed to heat for one hour after which the cover was removed and the solution was evaporated to dryness. When the sample had dried, five mls. of concentrated  $\text{HNO}_3$  and two mls. of HF

were added and the solution taken to dryness a second time. The residue on drying was not allowed to turn dark brown (owing to the formation of iron oxide), but was removed when it became white and quite flaky. For the final redissolving two mls. of concentrated  $\text{HNO}_3$  and about 90 mls. of distilled water were added to the beaker which was then covered with the teflon watch glass and heated with the heat lamps for 10 to 12 hours. In most cases the sample would be completely in solution after this treatment, but, if a residue remained, more water was added and further heating was required. Elemental blank contributions from the water were negligible. When the residue (shown by X-ray analysis to be calcium and/or magnesium fluoride) was observed to be dissolved, the cover was removed and the volume of the solution reduced to about 25 mls. by evaporation, then cooled and transferred to a 50-ml. volumetric flask and diluted to volume. This 100-dilution stock was poured into a 60-ml. polyethylene bottle and kept for further dilutions and analyses. From the stock solutions 50-fold (5000x) dilutions were prepared for all samples. Dilutions of 15000x were prepared for most samples. In the case of the muscovite, 25000x dilutions were found more useful. In addition to the 5000x and 15000x, a 50,000x dilution was prepared for the two almandine samples. A detailed list of the dilution ranges used for the elemental analyses in the various phases is found in Table 5. The exact dilution for each sample is of course dependent upon the exact sample weight.

Analyses for all elements except  $\text{Fe}^{+2}$  and Ti were carried out by means of a Perkin-Elmer Model 214 atomic absorption flame spectrophotometer. Elwell and Gidly (1962) discuss the theory and operation of the flame photometer, and the reader is referred to Billings (1963), McKay (1964), Harriss and Adams (1966), Carter (1965), and Stow (1965) for readings involving applications of flame photometry to geologic problems. All analyses done by this method could be carried out directly on the appropriately diluted solution (see Table 5) with the exception of Mg, Ca, Sr, and Ba. It was found that a spike of 60,000 p.p.m. La solution (prepared by dissolving 93.6 grams of  $\text{La}(\text{NO}_3)_3$  in one liter of distilled water) had to be added to the appropriately diluted sample in order to complex the Al ions in solution which interfere in the flame with the alkaline earths. When the 100x range was used, two mls. of the La spike were added to four mls. of the sample, and when the 5000x range was used, one ml. was added to 10 mls. of sample. For the 15,000x and 25,000x solutions, 0.5 ml. of La solution was added to 10 mls. of sample. Standards were treated in the same way. Aluminum was determined by flame photometry employing a  $\text{N}_2\text{O}$ -acetylene flame and a high temperature burner.

Titanium was studied using the method of Shapiro and Brannock (1962). The procedure was followed exactly except that the sample solution was that obtained from the  $\text{HF-HNO}_3$  opening and not the solution B recommended in the published procedure. Ferrous ion was determined in accordance with the

procedure described by Shapiro (1960).

Throughout the investigation a wide variety of primary and secondary standards were employed. Where disagreement existed among the standards, the primary standards were considered more important and more accurate. The primary standards used included G-1, W-1, Sy-1, Sul-1, and NBS standard Fld-99. Secondary standards included CRB-788, T-1, Pomona 2,3,5,7,9, 13,15, and 16, and a series of artificial mineral standards prepared from reagent grade nitrates, carbonates, and metals. Salt solutions were used only to determine linearity of the flame photometer, and reproducibility of peak and absorption readings. All working curves were drawn in accord with primary (and secondary) rock standard absorption and peak height readings.

Although all of the above mentioned standards could be used for major elements, only the primary standards, CRB-788, and an artificial biotite, AB-1 spiked with trace elements, could be employed in defining the working curves for trace elements.

For the determination of  $\text{Fe}^{+2}$ , W-1, Sy-1, and G-1 were consistently used.

Table 6 indicates the precision and sensitivity in solution determined throughout this investigation. Precision was determined by a triplicate opening of sample CM-1, and comparison of the elemental concentrations determined in the three openings. The sensitivity in solution is defined as the amount of metal present at 1% absorption.

Table 5  
Dilution Ranges for Analysis

	Bi	Ms	Hb	Pc	Ep	At	G
Al	100x	100x	100x	100x	100x	100x	100x
Ti	5,000	100	100	100	100	100	100
Fe	15,000	5,000	15,000	100	15,000	15,000	50,000
Ca	100	100	15,000	5,000	15,000	5,000	15,000
Mg	15,000	5,000	15,000	5,000	15,000	15,000	5,000
Na	5,000	5,000	5,000	15,000	100	5,000	100
K	15,000	25,000	5,000	5,000	100	100	100
Mn	5,000	100	5,000	5,000	5,000	5,000	15,000
Ba	100	100	nd	nd	nd	nd	nd
Co	100	100	100	100	100	100	100
Cr	100	100	100	100	100	100	100
Cu	100	100	100	100	100	100	100
Li	100	100	100	100	100	100	100
Ni	100	100	100	100	100	100	100
Pb	100	100	100	100	100	100	100
Rb	100	100	100	100	100	100	100
Sr	100	100	100	100	100	100	100
Zn	100	100	100	100	100	100	100

nd = not determined



Table 6

Precision and Sensitivity of Analyses

	<u>CM 1-1</u>	<u>CM 1-2</u>	<u>CM 1-3</u>	<u>Avg.</u>	<u>Pre- cision*</u>	<u>Sensi- tivity**</u>
SiO <sub>2</sub> %	52.80	51.63	52.56	52.3	±5 %	
Al <sub>2</sub> O <sub>3</sub>	17.20	17.80	17.00	17.3	3	
TiO <sub>2</sub>	0.52	0.50	0.58	0.53	8	
Fe <sub>2</sub> O <sub>3</sub>	0.97	0.92	0.97	0.95	3.2	
FeO	8.61	8.75	8.68	8.68	0.8	
CaO	8.91	9.24	9.35	9.16	2.7	
MgO	7.57	7.69	7.53	7.61	1.0	
K <sub>2</sub> O	1.06	1.04	1.04	1.05	1.0	
Na <sub>2</sub> O	2.22	2.24	2.22	2.23	0.5	
MnO	0.142	0.143	0.141	0.142	0.7	
Al %	9.10	9.40	9.00	9.2	2 %	1.0 p.p.m.
Ti	0.31	0.30	0.35	0.33	9	
Fe <sup>+3</sup>	0.68	0.64	0.68	0.67	4.5	0.5
Fe <sup>+2</sup>	6.70	6.81	6.76	6.75	0.9	0.1 %
Ca	6.40	6.60	6.68	6.56	3.1	0.05 p.p.m.
Mg	4.57	4.64	4.54	4.58	1.3	0.1
K	0.88	0.86	0.86	0.86	2.3	0.1
Na	1.65	1.66	1.65	1.65	0.6	0.1
Mn	0.110	0.111	0.109	0.110	0.9	0.08
Ba p.p.m.	260	220	200	227	15	1.5
Co	60	60	65	62	5	0.5
Cr	88	93	97	93	10	0.4
Cu	38	37	37	37	3	0.1
Li	19	20	20	20	5	0.2
Ni	150	145	145	147	2	0.8
Pb	15	20	15	17	18	2.0
Rb	15	15	14	15	6	0.5
Sr	400	420	420	413	2	0.3
Zn	55	60	60	58	5	0.1

\* Reproducibility of any reading

\*\* Amount of metal present at 1% absorption

Table 7

Chemical Analyses

(see Table 6 for accuracy and precision)

	Bi 4	Bi 6	Bi 10	Bi 11	Bi 13	Bi 15
SiO <sub>2</sub> %	38.6	41.0	34.3	36.7	36.7	36.0
Al <sub>2</sub> O <sub>3</sub>	19.1	18.3	19.1	19.3	18.7	19.1
TiO <sub>2</sub>	2.47	2.50	3.13	2.38	1.65	2.25
Fe <sub>2</sub> O <sub>3</sub>	4.28	7.92	4.32	1.99	3.40	4.25
FeO	12.97	8.45	15.20	14.80	14.47	16.78
CaO	0.12	0.13	0.01	0.01	0.04	0.06
MgO	9.20	8.20	9.77	10.77	10.69	8.04
Na <sub>2</sub> O	0.108	0.101	0.118	0.115	0.124	0.229
K <sub>2</sub> O	9.75	9.08	9.73	9.60	9.63	9.07
MnO	0.388	0.340	0.348	0.384	0.604	0.259
Al %	10.1	9.7	10.1	10.2	9.9	10.1
Ti	1.48	1.50	1.88	1.43	0.99	1.35
Fe <sup>+3</sup>	2.99	5.54	3.02	1.39	2.38	2.97
Fe <sup>+2</sup>	10.09	6.56	11.81	11.50	11.25	13.03
Ca	0.087	0.091	0.010	0.008	0.028	0.046
Mg	5.55	4.95	5.90	6.50	6.45	4.85
Na	0.080	0.075	0.088	0.086	0.092	0.170
K	8.10	7.53	8.07	7.96	7.99	7.52
Mn	0.300	0.263	0.269	0.297	0.467	0.200
Ba ppm	1600	1600	1800	2000	2000	1700
Co	65	65	75	65	75	75
Cr	8	6	8	93	8	65
Cu	4	6	5	6	12	6
Li	82	80	109	81	104	96
Mn	3002	2625	2690	2968	4670	2000
Ni	45	50	80	85	80	95
Pb	10	40	35	35	45	15
Rb	960	1060	520	280	660	400
Sr	18	10	14	26	18	22
Zn	295	370	275	335	500	95

Table 7 (Continued)

	MM 16 B1	MM 44 B1	MM 45 B1	MM 54 B1	MM 56 B1	WM 5 B1
SiO <sub>2</sub> %	37.7	41.4	38.9	38.6	36.8	40.7
Al <sub>2</sub> O <sub>3</sub>	18.3	16.6	18.9	17.8	16.4	14.7
TiO <sub>2</sub>	1.97	1.45	1.03	2.17	1.97	1.02
Fe <sub>2</sub> O <sub>3</sub>	5.08	1.82	1.50	2.89	5.52	1.75
FeO	11.90	9.71	12.12	11.90	12.68	12.63
CaO	0.13	0.17	0.03	0.39	0.31	0.01
MgO	11.23	14.67	13.90	12.68	10.93	14.91
Na <sub>2</sub> O	0.121	0.116	0.417	0.157	0.108	0.144
K <sub>2</sub> O	9.22	9.66	8.95	9.18	9.04	9.90
MnO	0.309	0.413	0.259	0.218	0.221	0.286
Al %	9.7	8.8	10.0	9.4	8.7	7.8
Ti	1.18	0.87	0.62	1.30	1.18	0.61
Fe <sup>+3</sup>	3.55	1.27	1.05	2.02	3.86	1.22
Fe <sup>+2</sup>	9.25	7.55	9.43	9.25	9.86	9.82
Ca	0.094	0.120	0.024	0.280	0.220	0.009
Mg	6.78	8.85	8.40	7.65	6.60	9.00
Na	0.090	0.086	0.309	0.117	0.080	0.107
K	7.65	8.01	7.43	7.62	7.50	8.22
Mn	0.239	0.319	0.200	0.169	0.171	0.221
Ba ppm	1900	1100	2500	1400	1100	1000
Co	65	45	60	70	65	55
Cr	5	6	6	96	12	35
Cu	30	9	5	50	8	4
Li	87	88	75	75	104	181
Mn	2391	3193	1996	1692	1705	2212
Ni	60	45	50	70	50	50
Pb	35	25	8	8	25	30
Rb	690	420	310	310	490	730
Sr	54	26	25	20	22	46
Zn	210	425	215	180	140	180

Table 7 (Continued)

	MM 4 Ms	MM 6 Ms	MM 10 Ms	MM 11 Ms	MM 13 Ms	MM 15 Ms
SiO <sub>2</sub> %	51.1	50.4	52.9	50.4	50.8	54.5
Al <sub>2</sub> O <sub>3</sub>	25.3	26.1	24.6	28.6	26.6	27.4
TiO <sub>2</sub>	0.82	0.88	1.33	0.87	0.43	0.45
Fe <sub>2</sub> O <sub>3</sub>	4.88	4.38	3.60	2.23	3.24	2.53
FeO	0.94	1.21	0.77	0.87	0.90	0.96
CaO	0.003	0.010	0.000	0.000	0.06	0.01
MgO	1.28	1.34	1.24	1.36	1.31	0.994
Na <sub>2</sub> O	0.326	0.385	0.398	0.380	0.489	0.600
K <sub>2</sub> O	10.85	10.62	10.65	10.82	10.67	10.37
MnO	0.030	0.031	0.018	0.022	0.039	0.012
Al %	13.4	13.8	13.0	15.1	14.1	14.5
Ti	0.49	0.53	0.80	0.52	0.26	0.27
Fe <sup>+3</sup>	3.41	3.06	2.52	1.56	2.27	1.77
Fe <sup>+2</sup>	0.73	0.94	0.60	0.68	0.70	0.76
Ca	0.002	0.01	0.00	0.00	0.044	0.009
Mg	0.775	0.810	0.750	0.820	0.788	0.600
Na	0.242	0.286	0.295	0.282	0.363	0.445
K	9.00	8.82	8.83	8.98	8.85	8.60
Mn	0.023	0.024	0.014	0.017	0.030	0.009
Ba ppm	2100	1800	2600	4500	9000	2600
Co	60	55	50	45	nd	65
Cr	4	10	10	67	nd	63
Cu	5	5	6	8	11	8
Li	28	31	17	13	13	15
Mn	227	237	134.5	168.5	296	92.5
Ni	45	45	60	45	40	50
Pb	5	10	8	nd	nd	10
Rb	440	480	270	155	370	210
Sr	18	25	25	37	90	40
Zn	23	44	21	22	33	9

Table 7 (Continued)

	MM 16 Ms	MM 44 Ms	MM 54 Ms	MM 56 Ms	WM 5 Ms	MM 2a Hb
SiO <sub>2</sub> %	51.9	53.2	54.0	53.0	54.3	48.3
Al <sub>2</sub> O <sub>3</sub>	26.1	25.9	25.5	24.0	23.4	6.50
TiO <sub>2</sub>	0.95	0.87	0.42	0.80	0.92	0.67
Fe <sub>2</sub> O <sub>3</sub>	3.16	2.58	2.24	3.82	2.69	4.54
FeO	0.71	0.50	0.63	1.33	0.81	10.20
CaO	0.00	0.00	0.00	0.004	0.00	12.39
MgO	1.48	1.49	1.54	1.33	1.95	11.93
Na <sub>2</sub> O	0.348	0.586	0.343	0.516	0.539	1.56
K <sub>2</sub> O	10.88	10.40	10.83	10.70	10.24	1.09
MnO	0.018	0.021	0.013	0.014	0.021	0.822
Al %	13.8	13.7	13.5	12.7	12.4	3.45
Ti	0.57	0.52	0.25	0.48	0.55	0.67
Fe <sup>+3</sup>	2.21	1.80	1.57	2.67	1.88	3.24
Fe <sup>+2</sup>	0.55	0.39	0.49	1.03	0.63	7.94
Ca	0.00	0.00	0.00	0.003	0.00	8.85
Mg	0.890	0.900	0.930	0.800	1.175	7.20
Na	0.258	0.435	0.254	0.383	0.400	1.16
K	9.02	8.64	8.99	8.88	8.50	0.90
Mn	0.014	0.016	0.010	0.011	0.016	0.635
Ba ppm	2700	2300	2900	3000	1300	nd
Co	50	55	50	55	50	50
Cr	7	6	71	10	35	12
Cu	7	9	11	5	6	7
Li	19	16	15	25	49	13
Mn	143.5	163	99.8	114	155.5	6350
Ni	55	50	55	65	50	50
Pb	10	10	20	15	5	20
Rb	290	220	170	260	510	48
Sr	12	6	30	12	5	42
Zn	16	25	17	13	16	475

Table 7 (Continued)

	MM 3a Hb	MM 4a Hb	MM 6a Hb	MM 18 Hb	MM 20 Hb	MM 23 Hb
SiO <sub>2</sub> %	47.1	46.4	47.7	40.8	47.2	40.4
Al <sub>2</sub> O <sub>3</sub>	7.8	7.9	7.0	11.4	9.7	12.8
TiO <sub>2</sub>	0.53	0.42	1.13	0.78	0.58	0.97
Fe <sub>2</sub> O <sub>3</sub>	5.21	5.69	4.72	7.44	4.56	5.51
FeO	10.25	9.72	10.48	14.75	10.48	17.10
CaO	12.29	12.39	12.08	11.55	11.96	11.55
MgO	11.31	11.18	11.69	8.45	10.94	6.46
Na <sub>2</sub> O	1.55	1.59	1.71	1.61	1.51	1.69
K <sub>2</sub> O	1.24	1.21	0.543	0.801	0.500	1.04
MnO	0.726	0.901	0.750	0.437	0.582	0.445
Al %	4.15	4.20	3.68	6.05	5.13	6.80
Ti	0.32	0.25	0.68	0.47	0.35	0.58
Fe <sup>+3</sup>	3.64	3.98	3.30	5.20	3.19	3.85
Fe <sup>+2</sup>	7.98	7.56	8.15	11.48	8.15	13.30
Ca	8.78	8.85	8.63	8.25	8.55	8.25
Mg	6.83	6.75	7.05	5.10	6.60	3.90
Na	1.15	1.18	1.27	1.19	1.12	1.25
K	1.025	1.000	0.450	0.675	0.415	0.865
Mn	0.561	0.697	0.580	0.338	0.450	0.344
Co ppm	60	60	45	55	45	60
Cr	12	10	15	10	450	125
Cu	9	13	10	42	8	8
Li	12.5	13	6	4.5	15	7
Mn	5609	6968	5800	3383	4500	3440
Ni	35	35	30	45	145	60
Pb	20	20	8	25	20	40
Rb	8	8	8	8	8	8
Sr	64	66	30	50	60	48
Zn	500	475	395	215	nd	290

Table 7 (Continued)

	MM25h Hb	MM25p Hb	MM 30 Hb	MM 31 Hb	MM 32 Hb	MM 33 Hb
SiO <sub>2</sub> %	44.4	42.9	44.4	46.0	48.6	48.8
Al <sub>2</sub> O <sub>3</sub>	11.7	12.5	9.6	9.7	7.9	5.8
TiO <sub>2</sub>	0.93	0.87	0.38	0.63	0.55	0.48
Fe <sub>2</sub> O <sub>3</sub>	4.39	4.32	6.75	4.68	4.94	7.31
FeO	14.21	14.97	12.98	11.68	10.43	8.22
CaO	11.96	11.87	11.97	11.97	11.54	12.18
MgO	7.95	8.20	8.95	10.58	11.08	11.93
Na <sub>2</sub> O	1.43	1.43	1.62	1.70	1.82	1.51
K <sub>2</sub> O	0.723	0.675	0.513	0.439	0.301	1.02
MnO	0.284	0.282	0.873	0.632	0.882	0.799
Al %	6.18	6.64	5.10	5.15	4.21	3.08
Ti	0.56	0.52	0.23	0.38	0.33	0.29
Fe <sup>+3</sup>	3.07	3.02	4.72	3.27	3.45	5.11
Fe <sup>+2</sup>	11.06	11.65	10.10	9.09	8.12	6.39
Ca	8.55	8.48	8.55	8.55	8.25	8.70
Mg	4.80	4.95	5.40	6.38	6.68	7.20
Na	1.06	1.06	1.20	1.26	1.35	1.12
K	0.600	0.560	0.425	0.365	0.250	0.850
Mn	0.220	0.218	0.675	0.489	0.682	0.618
Co ppm	60	70	55	55	50	50
Cr	225	135	15	28	23	10
Cu	18	30	10	9	7	8
Li	7.5	9	11.5	12	10	10
Mn	2197	2176	6750	4885	6820	6180
Ni	65	90	60	60	50	45
Pb	35	30	30	35	25	20
Rb	8	8	8	8	8	8
Sr	60	42	58	50	22	32
Zn	230	230	480		440	475

Table 7 (Continued)

	MM 35 Hb	MM 36 Hb	MM 39 Hb	MM 46 Hb	MM 47 Hb	MM 49 Hb
SiO <sub>2</sub> %	47.7	47.1	47.2	43.0	42.8	43.6
Al <sub>2</sub> O <sub>3</sub>	7.2	7.9	8.3	12.7	13.6	10.9
TiO <sub>2</sub>	0.53	0.47	0.82	0.63	1.42	1.37
Fe <sub>2</sub> O <sub>3</sub>	5.85	5.39	5.60	4.88	3.36	6.01
FeO	9.43	9.87	8.55	14.38	13.30	11.06
CaO	12.18	12.49	11.96	11.66	10.71	12.18
MgO	11.90	11.68	12.17	8.34	9.20	9.70
Na <sub>2</sub> O	1.46	1.49	1.62	1.58	1.50	1.82
K <sub>2</sub> O	1.05	0.952	1.07	0.543	0.18	0.75
MnO	0.679	0.705	0.705	0.314	0.193	0.655
Al %	3.80	4.20	4.37	6.70	7.20	5.75
Ti	0.32	0.28	0.49	0.38	0.85	0.82
Fe <sup>+3</sup>	4.09	3.77	3.91	3.41	2.35	4.20
Fe <sup>+2</sup>	7.33	7.68	6.65	11.49	10.35	8.60
Ca	8.70	8.92	8.55	8.33	7.65	8.70
Mg	7.18	7.05	7.35	5.03	5.55	5.85
Na	1.08	1.10	1.20	1.17	1.11	1.35
K	0.870	0.790	0.885	0.450	0.150	0.620
Mn	0.526	0.545	0.545	0.243	0.150	0.507
Co ppm	50	50	50	70	70	50
Cr	80	83	81	70	77	22
Cu	23	17	12	10	25	6
Li	10	10	10.5	12	21	11.5
Mn	5260	5446	5447	2430	1498	5070
Ni	95	95	60	90	100	60
Pb	15	20	20	25	5	25
Rb	8	8	8	8	8	8
Sr	66	60	62	36	28	58
Zn	415	380	395	175	150	380



Table 7 (Continued)

	MM 50 Hb	MM 55 Hb	MM 58 Hb	MM 59 Hb	MM 60 Hb	MM 61 Hb
SiO <sub>2</sub> %	47.8	45.7	48.5	43.4	47.2	46.2
Al <sub>2</sub> O <sub>3</sub>	14.2	12.1	6.7	14.4	14.0	13.0
TiO <sub>2</sub>	0.78	1.22	1.25	0.87	0.95	0.90
Fe <sub>2</sub> O <sub>3</sub>	2.62	5.10	6.07	2.06	2.06	1.37
FeO	11.53	10.90	7.93	14.33	11.43	12.80
CaO	9.56	11.04	12.60	11.45	11.04	10.92
MgO	9.70	9.80	12.43	8.81	9.70	10.33
Na <sub>2</sub> O	1.49	1.56	1.36	1.60	1.49	1.49
K <sub>2</sub> O	0.16	0.18	0.87	0.30	0.14	0.14
MnO	0.192	0.414	0.338	0.299	0.021	0.019
Al %	7.5	6.4	3.6	7.6	7.4	7.3
Ti	0.47	0.73	0.75	0.52	0.57	0.54
Fe <sup>+3</sup>	1.83	3.57	4.25	1.44	1.44	0.96
Fe <sup>+2</sup>	8.97	8.48	6.17	11.15	9.89	9.96
Ca	6.83	7.88	9.00	8.18	7.88	7.80
Mg	5.85	5.92	7.50	5.32	5.85	6.23
Na	1.10	1.16	1.01	1.19	1.10	1.10
K	0.135	0.150	0.720	0.250	0.120	0.115
Mn	0.148	0.320	0.261	0.231	0.160	0.150
Co ppm	60	65	30	70	60	55
Cr	86	145	320	36	75	75
Cu	12	20	5	44	6	9
Li	7	29	10	12.5	22	18
Mn	1275	3200	2608	2307	163	150
Ni	90	90	175	95	100	100
Pb	10	10	25	25	30	15
Rb	8	8	8	8	8	8
Sr	56	44	30	46	42	28
Zn	130	120	95	145	135	125

Table 7 (Continued)

	MM 2a Pc	MM 3a Pc	MM 4a Pc	MM 6a Pc	MM 20 Pc
SiO <sub>2</sub> %	61.5	68.4	63.0	64.1	59.3
Al <sub>2</sub> O <sub>3</sub>	24.6	19.3	23.0	22.3	23.4
TiO <sub>2</sub>	0.17	0.05	nd	0.08	0.13
Fe <sub>2</sub> O <sub>3</sub>	0.147	0.134	0.184	0.149	0.130
FeO	nd	0.001	0.001	nd	nd
CaO	4.53	4.53	5.10	4.17	8.95
MgO	0.061	0.091	0.080	0.091	0.080
Na <sub>2</sub> O	8.35	6.46	7.71	8.51	6.94
K <sub>2</sub> O	0.59	0.96	0.85	0.55	0.83
MnO	0.038	0.070	0.84	0.040	0.207
Al %	13.0	10.2	12.2	11.8	12.4
Ti	0.10	0.03	nd	0.05	0.08
Fe <sup>+3</sup>	0.103	0.094	0.129	0.104	0.091
Fe <sup>+2</sup>	nd	0.001	0.001	nd	nd
Ca	3.24	3.24	3.64	2.98	6.40
Mg	0.0366	0.0562	0.0483	0.0550	0.0483
Na	6.20	4.79	5.72	6.31	5.14
K	0.490	0.780	0.710	0.458	0.690
Mn	0.029	0.054	0.065	0.031	0.160
Co ppm	40	30	35	40	40
Cr	2	2	2	2	3
Cu	5	5	6	6	7
Li	1.5	3	3	3	2.5
Mn	291	543	653	313	1600
Ni	50	30	35	30	35
Pb	10	5	5	35	10
Rb	8	22	8	8	15
Sr	780	870	1030	770	950
Zn	9	8	9	10	7

Table 7 (Continued)

	MM 23 Pc	MM25p Pc	MM 31 Pc	MM 32 Pc	MM 33 Pc
SiO <sub>2</sub> %	60.6	60.8	64.1	59.7	61.7
Al <sub>2</sub> O <sub>3</sub>	23.2	24.0	22.5	24.6	22.3
TiO <sub>2</sub>	0.33	0.08	0.08	0.08	0.25
Fe <sub>2</sub> O <sub>3</sub>	0.114	0.186	0.123	0.176	0.147
FeO	nd	nd	nd	nd	nd
CaO	7.00	6.65	4.98	7.55	7.00
MgO	0.041	0.087	0.052	0.124	0.069
Na <sub>2</sub> O	7.93	6.57	7.75	6.08	7.90
K <sub>2</sub> O	0.74	1.56	0.344	1.60	0.574
MnO	0.062	0.078	0.036	0.092	0.061
Al %	12.3	12.7	11.9	13.0	11.8
Ti	0.20	0.05	0.05	0.05	0.15
Fe <sup>+3</sup>	0.080	0.130	0.086	0.123	0.103
Fe <sup>+2</sup>	nd	nd	nd	nd	nd
Ca	5.00	4.75	3.56	5.40	5.00
Mg	0.0248	0.0523	0.0314	0.0746	0.0419
Na	5.88	4.87	5.75	4.51	5.85
K	0.610	1.298	0.285	1.324	0.475
Mn	0.048	0.060	0.028	0.071	0.047
Co ppm	40	40	40	40	40
Cr	4	2	4	5	5
Cu	7	14	8	14	6
Li	2.3	3.5	2.3	3.5	2
Mn	475	601	275	711	466
Ni	35	30	25	35	45
Pb	10	35	25	25	15
Rb	15	55	8	55	8
Sr		950	1100	940	750
Zn	8	7	2	8	9

Table 7 (Continued)

	MM 36 Pc	MM 39 Pc	MM 46 Pc	MM 47 Pc	MM 49 Pc	MM 50 Pc
SiO <sub>2</sub> %	60.2	60.9	61.6	48.8	60.7	55.8
Al <sub>2</sub> O <sub>3</sub>	22.7	21.7	19.3	24.6	23.1	24.6
TiO <sub>2</sub>	0.22	0.13	0.08	0.08	0.28	0.12
Fe <sub>2</sub> O <sub>3</sub>	0.167	0.127	0.157	0.106	0.127	0.109
FeO	0.003	0.000	nd	nd	nd	nd
CaO	8.05	8.61	12.60	9.31	7.87	14.28
MgO	0.124	0.104	0.065	0.063	0.076	0.059
Na <sub>2</sub> O	6.96	7.37	5.56	16.68	7.13	4.45
K <sub>2</sub> O	1.46	0.915	0.585	0.289	0.603	0.542
MnO	0.153	0.115	0.089	0.028	0.080	0.062
Al %	12.0	11.5	10.2	13.0	12.2	13.0
Ti	0.13	0.08	0.05	0.05	0.17	0.07
Fe <sup>+3</sup>	0.119	0.089	0.110	0.074	0.089	0.076
Fe <sup>+2</sup>	0.002	0.000	nd	nd	nd	nd
Ca	5.75	6.15	9.00	6.65	5.62	10.20
Mg	0.075	0.063	0.039	0.038	0.046	0.035
Na	5.16	5.47	4.13	12.38	5.29	3.30
K	1.21	0.760	0.485	0.240	0.500	0.450
Mn	0.118	0.089	0.069	0.022	0.062	0.048
Co ppm	30	30	25	25	35	40
Cr	7	7	6	4	4	10
Cu	7	6	9	7	6	7
Li	4	2	1.5	2.1	2.8	3.5
Mn	1180	889	685	215	624	475
Ni	30	30	30	35	40	35
Pb	5	10	15	5	25	10
Rb	30	15	15	8	15	14
Sr	950	1210	890	630	950	520
Zn	12	9	8	7	13	10

Table 7 (Continued)

	MM 51 Pc	MM 58 Pc	MM 59 Pc	MM 60 Pc	MM 61 Pc
SiO <sub>2</sub> %	60.2	60.3	64.5	58.0	59.3
Al <sub>2</sub> O <sub>3</sub>	24.8	21.9	21.7	23.2	23.0
TiO <sub>2</sub>	0.08	0.42	0.08	0.07	0.05
Fe <sub>2</sub> O <sub>3</sub>	0.262	0.159	0.124	0.163	0.136
FeO	nd	0.006	nd	nd	nd
CaO	5.60	8.25	4.61	12.45	11.75
MgO	0.352	0.141	0.054	0.076	0.067
Na <sub>2</sub> O	2.82	7.15	8.48	5.46	5.02
K <sub>2</sub> O	5.88	1.57	0.422	0.512	0.662
MnO	0.230	0.146	0.048	0.056	0.054
Al %	13.1	11.4	11.5	12.3	12.2
Ti	0.05	0.25	0.05	0.04	0.03
Fe <sup>+3</sup>	0.123	0.115	0.087	0.114	0.095
Fe <sup>+2</sup>	nd	0.004	nd	nd	nd
Ca	4.00	5.90	3.29	8.90	8.40
Mg	0.221	0.085	0.033	0.046	0.041
Na	2.09	5.30	6.29	4.05	3.72
K	4.88	1.30	0.350	0.425	0.549
Mn	0.179	0.113	0.037	0.043	0.042
Co ppm	45	35	35	35	35
Cr	2	5	2	2	6
Cu	7	8	5	9	8
Li	34	2	nd	3	4
Mn	1788	1130	364	429	424
Ni	35	35	30	40	25
Pb	10	10	20	30	30
Rb	300	35	8	nd	13
Sr	380	580	680	610	580
Zn	13	7	11	9	5

Table 7 (Continued)

	MM 3a EP	MM 4a EP	MM 30 Ep	MM 35 Ep	MM 36 EP	MM 39 Ep
SiO <sub>2</sub> %	59.5	57.5	58.8	58.5	47.8	63.2
Al <sub>2</sub> O <sub>3</sub>	16.3	17.4	16.4	16.4	16.6	11.3
TiO <sub>2</sub>	0.08	0.03	0.13	0.03	0.03	0.12
Fe <sub>2</sub> O <sub>3</sub>	7.91	7.68	7.19	7.64	7.75	8.03
FeO	0.41	0.22	0.41	0.35	0.26	0.32
CaO	13.30	14.70	14.57	14.57	25.08	14.57
MgO	0.103	0.099	0.093	0.087	0.143	0.112
Na <sub>2</sub> O	0.019	0.001	0.031	0.050	0.023	0.014
K <sub>2</sub> O	0.028	0.017	0.023	0.038	0.031	0.015
MnO	0.317	0.371	0.353	0.304	0.326	0.291
Al %	8.6	9.2	8.7	8.7	8.8	6.0
Ti	0.05	0.02	0.08	0.02	0.02	0.07
Fe <sup>+3</sup>	5.53	5.37	5.03	5.34	5.42	5.61
Fe <sup>+2</sup>	0.32	0.17	0.32	0.27	0.20	0.25
Ca	9.50	10.50	10.40	10.40	17.90	10.40
Mg	0.062	0.060	0.056	0.053	0.086	0.068
Na	0.014	0.009	0.023	0.037	0.017	0.010
K	0.024	0.014	0.019	0.031	0.026	0.013
Mn	0.245	0.287	0.273	0.235	0.252	0.225
Co ppm	30	40	40	35	30	35
Cr	34	34	38	170	125	90
Cu	56	12	10	17	29	16
Li	1.3	0.5	0.3	1	0.5	0.5
Mn	2452	2870	2728	2347	2520	2253
Ni	65	50	45	45	55	75
Pb	45	45	50	55	60	60
Rb	8	8	8	8	8	8
Sr	1210	1150	1220	1010	890	1070
Zn	16	21	16	19	12	16

Table 7 (Continued)

	MM 58 Ep	MM 50 At	MM 51 At	MM 47 G	MM 60 G
SiO <sub>2</sub> %	48.9	48.6	47.7	35.7	36.6
Al <sub>2</sub> O <sub>3</sub>	13.6	11.3	13.0	22.7	22.7
TiO <sub>2</sub>	0.12	0.13	0.10	0.47	0.42
Fe <sub>2</sub> O <sub>3</sub>	8.25	0.50	2.92	11.46	0.29
FeO	0.32	19.47	15.60	18.61	28.45
CaO	26.50	0.32	1.23	4.02	3.78
MgO	0.199	16.20	15.80	5.22	5.60
Na <sub>2</sub> O	0.007	1.02	1.28	0.010	0.010
K <sub>2</sub> O	0.005	0.029	0.064	0.003	0.003
MnO	0.144	0.414	0.362	1.847	2.122
Al %	7.2	6.0	6.9	12.0	12.0
Ti	0.07	0.08	0.06	0.28	0.25
Fe <sup>+3</sup>	5.76	0.35	2.04	8.02	0.20
Fe <sup>+2</sup>	0.25	15.13	12.11	14.48	22.10
Ca	18.90	0.23	0.88	2.87	2.70
Mg	0.120	9.75	9.53	3.15	3.38
Na	0.005	0.760	0.950	0.007	0.008
K	0.004	0.024	0.053	0.003	0.003
Mn	0.111	0.320	0.280	1.428,	1.641
Ba ppm	nd	nd	nd	nd	nd
Co	30	60	55	90	90
Cr	760	80	100	75	60
Cu	75	5	4	17	13
Li	0.6	122	130	3	3
Mn	1108	3200	2795	14280	16410
Ni	75	90	115	60	85
Pb	45	45	30	35	35
Rb	8	8	8	8	8
Sr	640	nd	nd	nd	nd
Zn	9	210	190	37	35

Table 8

Distribution of Aluminum between the Octahedral and  
Tetrahedral Sites of the Micas

Sample	% Al	% Al <sub>tet.</sub>	% Al <sub>oc</sub>
MM 4 Bi	10.1	7.3	2.8
MM 6 Bi	9.7	6.4	3.3
MM 10 Bi	10.1	8.4	1.7
MM 11 Bi	10.2	7.6	2.6
MM 13 Bi	9.9	7.6	2.3
MM 15 Bi	10.1	7.7	2.4
MM 16 Bi	9.7	7.5	2.2
MM 44 Bi	8.8	6.6	2.2
MM 54 Bi	9.4	7.2	2.2
MM 56 Bi	8.7	7.1	1.6
Wm 5 Bi	7.8	6.2	1.8
MM 4 Ms	13.4	3.8	9.6
MM 6 Ms	13.8	4.1	9.7
MM 10 Ms	13.0	3.1	9.9
MM 11 Ms	15.1	4.4	10.7
MM 13 Ms	14.1	3.8	10.3
MM 15 Ms	14.5	3.3	11.2
MM 16 Ms	13.8	3.7	10.1
MM 44 Ms	13.7	3.2	10.5
MM 54 Ms	13.5	2.8	10.7
MM 56 Ms	12.7	3.0	9.7
Wm 5 Ms	12.4	2.6	7.8



# GEOCHRONOLOGICAL CONSIDERATIONS

Age determinations were made on three mineral separates from the Mica Mine area by means of the potassium-argon procedure. Exact sample localities may be noted in Figure 2.

The samples were crushed and the mineral separates (MM 10 B1, MM 10Ms, MM 45B1) prepared by the method described in the sample preparation section of the Appendix. Grain size was minus-48 and plus-74 mesh. Potassium was determined by absorption flame photometry.

Argon was determined by means of a stainless steel Nier type mass spectrometer designed by Dr. M.B. Ward and Dr. A.C. Daughtry and built for the Humble Research Laboratory in Houston, Texas. A spike of Ar<sup>38</sup> was used and the Bern 4M muscovite (age = 19.0 m.y.) was employed as a standard. Final age determinations were calculated by an IBM 1620 data processing unit with consideration of the following inputs:

Sample	wt.-gms.	% K	% Ar <sup>40</sup> radiogenic	Age-m.y.
MM 10 Ms	0.0334	8.62	98	995
MM 45 B1	0.0642	7.31	86	978
MM 10 B1	0.0376	7.80	96	989
MM 10 B1	0.0556	7.80	98	982
MM 10 B1	0.0632	7.80	96	983
MM 10 B1	0.0610	7.80	99	958
MM 10 B1	0.0264	7.80	59	1037

$$T_{\frac{1}{2}} \text{ of } K^{40} = 1.32 \times 10^9 \text{ yrs.}$$

The five samples of MM 10 B1 were run as an estimate of mass spectrometric precision and all agree quite closely with the possible exception of the last (1037 m.y.). It is noted that only 59% of the Ar<sup>40</sup> is radiogenic in the last case versus

96 to 99% for the first four runs. In this respect the first four ages for MM 10 B1 average  $978 \pm 20$  m.y. which is in quite close agreement with the data for the other two mineral separates.

Zartman (1965), in a report on Rb-Sr age determinations on the Valley Spring Gneiss of Llano, Texas, the other pre-Cambrian occurrence in the state, reports ages of mineral separates (plagioclase, microcline, muscovite, biotite) as  $1000 \pm 15$  m.y., a figure in accord with the above data.

Future age dates from the Van Horn region would prove interesting in that more detailed relationships among the pegmatitic and dioritic intrusions, the faulting, and the various types of metamorphism would emerge.